الجمهوريـة الجزائريـة الديمقراطيـة الشعبيـة
République Algérienne Démocratique et Populaire
وزارة التعليـم العالـي والبحـث العلمـي
Ministère de l'enseignement supérieur et de la recherche scientifique

Université Mohamed Khider Biskra
Faculté des Sciences et Technologie
Département : Génie Electrique

جامعـة محمـد خيضـر بسكـرة
كليـة العلـوم والتكنولوجيـا
قسم: الـهندسة الكهربائيـة
المرجـــع:.....

Réf:.....

جامعـة محمـد خيضر بسكرة

Thèse présentée en vue de l'obtention du diplôme de

Doctorat LMD en Génie Electrique

Filière : Électrotechnique Option : Énergie Renouvelable

THEME

Gestion Optimale de l'Energie Electrique en Présence des Sources à Energies Renouvelables

Présentée par :

AROUA FATIMA ZOHRA

Soutenue le : ……

Devant le jury composé de :

Dr. MOHAMMEDIMessaoud	MCA	Président	Université de Biskra
Dr. TERKIAmel	Professeur	Examinatrice	Université de Biskra
Dr. BEN NECIB Nadjoua	Professeur	Examinatrice	Université de Constantine 1
Dr. SALHI Ahmed	Professeur	Directeur de thèse	Université de Biskra
Dr. CHARROUF Omar	Professeur	Invité	Université de Biskra
Dr. NAIMI Djemai	Professeur	Co-Directeur de thèse	Université de Biskra

Année Universitaire 2024/2025

الجمهوريـة الجزائريـة الديمقراطيـة الشعبيـة
Democratic and People's Republic of Algeria
وزارة التعليـم العالـي والبحـث العلمـي
Ministry of Higher Education and Scientific Research

Mohamed Khider Biskra University
Faculty of Science and Technology
Department:Electrical Engineering
Ref:.....

جامعـة محمـد خيضـر بسكـرة
كليـة العلـوم والتكنولوجيـا
قسم: الهندسة الكهربائيـة
المرجـــع:.....

جامعة محمد خيضر بسكرة

A thesis presented for the Diploma of

LMD Doctorate in Electrical Engineering

Field: Electrical Engineering Option: Renewable Energy

THEME

Optimal Management of Electrical Energy in the Presence of Renewable Energy Sources

Submitted by:

AROUA FATIMA ZOHRA

Supported on: …….

Before the jury composed of:

Dr. MOHAMMEDI Messaoud	MCA	Committee chairman	Biskra University
Dr. TERKI Amel	Professor	Examiner	Biskra University
Dr. BEN NECIB Nadjoua	Professor	Examiner	Constantine1 University
Dr. SALHI Ahmed	Professor	Supervisor	Biskra University
Dr. CHARROUF Omar	Professor	Invited	Biskra University
Dr. NAIMI Djemai	Professor	Co-Supervisor	Biskra University

Academic year 2024/2025

بسم الله الرحمان الرحيم

﴿ وَمَا تَوْفِيقِي إِلَّا بِاللَّهِ عَلَيْهِ تَوَكَّلْتُ وَإِلَيْهِ أُنِيبُ ﴾

سورة هود اية (88)

DEDICATION

We dedicate this work:

- ***In memory of my parents, may Allah grant them mercy and grant them paradise as their eternal home.***

- ***To my beloved family, who have supported me in difficult times throughout my studies. I dedicate this with special affection to my brother, Mostefa, and my sister, Djamila, whose encouragement has been a constant source of strength.***

- ***To all my teachers, colleagues and friends, I wish you health, happiness and a prosperous future.***

Fatima Zohra Aroua

ACKNOWLEDGEMENTS

*First, we would like to express our deepest gratitude to **ALLAH**, the Most Powerful and Most Merciful, for giving us the strength, patience, courage, and willpower to finish our thesis after years of hard work. All the praises and thanks be to **ALLAH**.*

*This thesis was completed at the Electrical Engineering Laboratory at the University of Biskra (LGEB), under my supervision, **Pr. Salhi Ahmed**, and I would like to express my deepest appreciation and gratitude to him for his complete availability to supervise me throughout my PhD studies. I am grateful for his guidance and confidence in me. I want to thank him warmly and honestly for his scientific expertise and innovative technical discussions.*

*I am very grateful to my co-supervisor, **Pr. Naimi Djaimi**, Director of the Laboratory of Electrical Engineering at the University of Biskra (LGEB), for his encouragement, wise advice, and valuable guidance in editing this thesis. I appreciate his patience with me throughout this work. I would also like to thank **Pr. Charrouf Omar** for his assistance, valuable comments, suggestions, and cooperation in preparing this project.*

*I would also like to thank **Dr. Mohammedi Messaoud** (jury chairman) and the jury members (**Pr. Terki Amel** and **Pr. Ben Necib Nadjoua** from Constantine University**)** for graciously agreeing to evaluate this work and for their valuable suggestions, which have enriched it.*

*I extend my gratitude to the faculty and staff of the Electrical Engineering Department at Mohamed Khider University, particularly **Pr. Zouzou Salah Eddine**, **Dr.Rezig Mohamed**, **Dr.Becha Habiba** and colleagues **Mimmoun Khalida**, **Bacha Marah**, and **Fettah Khaled**. I am also thankful to Mrs **Betka Faiza** and Mrs **Saadi Meriem**, engineers in the research laboratories at Biskra University, for their help, support, encouragement, and cooperation throughout my university career and research project.*

LIST OF PUBLICATIONS AND COMMUNICATIONS

The contributions related to this thesis, have been published in the articles listed below:

A. International Publications with Editorial Board

1) **F.Z. Aroua**, A. Salhi, O. Charrouf, D. Naimi, K. Fettah, "Wind energy cost evaluation based on a techno-economic assessment in the Algerian highlands," Energy for Sustainable Development. 81 (2024) 101502. Elsevier https://doi.org/10.1016/j.esd.2024.101502, indexation: Scopus.

2) **F.Z. Aroua**, A. Salhi, C. Mayouf, D. Naimi, "A Novel Nature-Inspired Meta-heuristic Algorithm for Solving the Economic and Environmental Dispatch Problems in Power System," Prz. Elektrotechniczny. (2024) 280–285. https:// doi.org /10.15199 /48.2024.07.55, indexation: scopus.

3) C. Mayouf, A. Salhi, F. Haidara, **F.Z. Aroua**, R.A. El-sehiemy, D. Naimi, C. Aya, C. Sidi, E. Kane, "Solving Optimal Power Flow Using New Efficient Hybrid Jellyfish Search and Moth Flame Optimization Algorithms," Algorithms MDPI 17.10 (2024): 438.1–25. https://doi.org/10.3390/a17100438, indexation: Scopus.

B. International communications with Editorial Board

1) **F.Z. Aroua**, A. Salhi, S. Salhi, D. Naimi, "Economic and Environmental Dispatch In Power System Using Cheetah Optimizer Algorithm." Conférence Internationale sur les Sciences Appliquées et l'Innovation (CISAI-2023). 10-11 Juillet 2023 / Sousse-Tunisie/Proceedings of Engineering & Technology-PET - Vol 76 ISSN: 1737-9334 Copyright © 2023.

2) **F.Z. Aroua**, A. Salhi, S. Salhi, D. Naimi, "A New Efficient Meta-heuristic Method for Solving the Optimal Power Flow Problem in Power System."The 2nd Electrical Engineering International Conference (EEIC'23), December 05-06, 2023, University of Bejaia.https://eeic23.sciencesconf.org.ISBN: 978-9969-9732-0-4. researchgate.net.

Abstract

The rapid increase in electricity demand over recent years has posed significant challenges for energy management and increased pressure on the modern power grids. A solution to these issues is the integration of renewable energy sources, particularly wind power, to address fossil fuel depletion and reduce greenhouse gas emissions from conventional power plants. In line with the objectives of Algeria's national program for the integration of renewable energies, which aims to install 5,010 MW of wind power, optimal management of electrical energy in the presence of wind farms is essential to improve the performance of the DZ-114 bus transmission grid. Although wind farms offer economic and environmental benefits, their integration into the grid introduces complexities in solving the optimal power flow (OPF) problem, particularly due to uncertainties associated with operational constraints. In fact, traditional methods for solving OPF are not suitable for dealing with this type of problem, which requires the use of meta-heuristic techniques. This thesis proposes an innovative method for solving the OPF problem: the Henry Gas Solubility Optimisation (HGSO) algorithm, inspired by the physical laws of gas solubility.The OPF problem is solved in two cases, with and without wind farm integration into the electricity grid. This resolution is based on a technical and economic study to determine the best unit cost of wind energy production(UCE) within the Algerian electricity grid. The best UCE values were determined in the Highlands (Djelfa, El Bayadh, Sétif), which are implemented in the OPF problems considering the integration of wind energy.The effectiveness of the HGSO method was evaluated for sixteen OPF solution cases, aiming to minimize the total cost of electricity production, total active losses, emissions, voltage deviation, and improve the voltage stability index. The optimisation cases were conducted on three electrical test networks: the IEEE 30-bus, IEEE 57-bus, and the Algerian transmission network DZ114-bus, with and without wind farm integration. Simulation results in the MATLAB environment confirm the performance of this technique (HGSO), which surpasses other well-known meta-heuristic methods in terms of robustness and efficiency for solving the OPF problem.

Keywords: Renewable energies, Wind power, Optimal management, Uncertainty constraints, Optimal Power Flow, Electrical networks, Techno-economic, Henry Gas Solubility Optimisation (HGSO), Unit Cost of Energy (UCE), Wind farms, Highlands, Total fuel cost, Total active losses, Total Gas Emission, Voltage deviation, voltage stability index.

Résumé

L'augmentation rapide de la demande d'électricité au cours des dernières années a posé des défis importants pour la gestion de l'énergie et a accru la pression sur les réseaux électriques modernes. L'une des solutions à ces défis est l'intégration des sources d'énergie renouvelables, en particulier l'énergie éolienne, afin de remédier à l'épuisement des combustibles fossiles et de réduire les émissions de gaz à effet de serre des centrales électriques conventionnelles. Conformément aux objectifs du programme national algérien pour l'intégration d'énergies renouvelables, qui visent à installer 5 010 MW d'énergie éolienne, une gestion optimale de l'énergie électrique en présence des parcs éoliens est indispensable pour améliorer les performances du réseau électrique de transmission DZ-114 bus. Bien que les parcs éoliens offrent des avantages économiques et environnementaux, leur intégration dans le réseau introduit des complexités dans la résolution du problème du flux optimal de puissance (OPF), notamment en raison des incertitudes liées aux contraintes opérationnelles. En effet, les méthodes traditionnelles de résolution de l'OPF ne sont pas aptes à traiter un tel type de problème, ce qui nécessite le recours à des techniques méta-heuristiques. Cette thèse propose une méthode innovante pour résoudre le problème OPF : l'algorithme Henry Gas Solubility

Optimisation (HGSO), inspiré des lois physiques de la solubilité des gaz. Le problème OPF est résolu dans deux cas : avec et sans intégration des parcs éoliens dans le réseau électrique. Cette résolution s'appuie sur une étude technico-économique qui vise à déterminer le meilleur Cout Unitaire de la production de l'énergie éolienne(UCE) au sein du réseau électrique algérien. Les meilleures valeurs de l'UCE ont été déterminées dans les Hauts Plateaux (Djelfa, El Bayadh, Sétif), qui sont implémentées dans les problèmes de l'OPF considérant l'intégration l'énergie éolienne. L'efficacité de la méthode (HGSO) a été évaluée pour seize cas de résolution de l'OPF, visant à minimiser le coût total de production d'électricité, les pertes actives totales, les émissions, la déviation de la tension et à améliorer l'indice de stabilité de la tension. On a considéré pour ces cas d'optimisation trois réseaux électriques de test IEEE 30-bus, IEEE 57-bus et le réseau algérien de transmission DZ114-bus, sans et avec intégration des parcs éoliens. Les résultats de la simulation sous l'environnement MATLAB confirment la performance de cette technique (HGSO) à dominer d'autres méthodes méta-heuristiques bien connues en termes de robustesse et d'efficacité pour la résolution du problème de l'OPF.

Mots-clés : Énergies renouvelables, Énergie éolienne, Gestion optimale, Contraintes d'incertitude, Flux d'énergie optimal, Réseaux électriques, Techno-économie, Algorithme d'Optimisation de la Solubilité du Gaz de Henry (HGSO), Coût Unitaire d'Énergie (UCE), Parcs éoliens, Hauts Plateaux, Coût total de production, Pertes actives totales, Émissions totales de gaz, Déviation de tension, Indice de stabilité de la tension.

ملخص

لقد فرضت الزيادة السريعة في الطلب على الكهرباء في السنوات الأخيرة تحديات كبيرة على مستوى تسيير الطاقة وزيادة الضغط على شبكات الكهرباء الحديثة. وتتمثل إحدى الحلول الفعالة لمواجهة هذه التحديات هي دمج الطاقات المتجددة، ولا سيما طاقة الرياح، لمعالجة استنفاد الوقود الأحفوري والحد من انبعاث الغازات التي تفضي الى الانحباس الحراري من محطات الطاقة التقليدية. تماشياً مع أهداف البرنامج الوطني الجزائري لإدماج الطاقات المتجددة، الذي يسعى إلى إنتاج 5010 ميغاوات من طاقة الرياح، فإن التسيير الأمثل للطاقة الكهربائية في ظل وجود مزارع الرياح تُعدّ ضرورة لتحسين أداء شبكة نقل الكهرباء الجزائرية (DZ-114 bus). وعلى الرغم من المزايا الاقتصادية والبيئية التي توفرها مزارع الرياح، إلا أن دمجها في الشبكة الكهربائية يزيد من التعقيدات لحل مسألة التدفق الأمثل للطاقة (Optimal Power Flow – OPF)، خصوصاً بسبب عدم اليقين في القيود التشغيلية. وفي الواقع، ان الأساليب التقليدية لحل مسألة OPF غير كافية لمعالجة هذا النوع من المسائل المعقدة، مما يتطلب اللجوء إلى تقنيات الإرشاد العام Meta-heuristiques. تقترح هذه الأطروحة طريقة مبتكرة لحل مسألة OPF: خوارزمية تحسين قابلية ذوبان الغاز هنري (HGSO)، المستوحاة من القوانين الفيزيائية لذوبان الغازات. ويتم حل مسألة OPF في حالتي عدم دمج ودمج مزارع الرياح في الشبكة الكهربائية. تعتمد هذه الدراسة على تحليل تقني-اقتصادي يهدف إلى تحديد أدنى تكلفة وحدة إنتاج (UCE)للطاقة الرياح ضمن الشبكة الكهربائية الجزائرية. وقد أظهرت أفضل قيم لـ UCE في مناطق الهضاب العليا (الجلفة، البيض، سطيف)، حيث تم توظيف هذه النتائج ضمن مسائل OPFالتي تأخذ بعين الاعتبار دمج طاقة الرياح في الشبكة الكهربائية. تم تقييم كفاءة خوارزمية (HGSO)من خلال ستة عشر حالة اختبارية لمسألة OPF، استهدفت تحسين عدة دوال هدف، من بينها :تقليل التكلفة الإجمالية لإنتاج الكهرباء، خفض الضياعات النشطة الكلية، الحد من انبعاثات الغازات، تحسين انحراف الجهد، وتعزيز مؤشر استقرار الجهد في الشبكة. وقد تم اختبار هذه الحالات على ثلاث شبكات كهربائية تجريبية: IEEE 30-bus و IEEE 57-bus وشبكة النقل الجزائرية DZ-bus-114، في حالتي وجود وغياب مزارع الرياح. تؤكد نتائج المحاكاة في بيئة MATLAB الاداء العالي والفعالية الكبيرة للخوارزمية المقترحة(HGSO) لتفوقها الواضح على العديد من خوارزميات تقنيات الإرشاد العام (Meta-heuristics) الأخرى المعروفة من حيث الصلابة والكفاءة في حل مسائل OPF.

الكلمات المفتاحية: الطاقة المتجددة، طاقة الرياح، الإدارة المثلى، قيود عدم اليقين، التدفق الأمثل للطاقة**(OPF)**، شبكات الكهربائية، تقنية-اقتصادية، خوارزمية تحسين ذوبان الغاز هنري(HGSO) ، وحدة تكلفة الطاقة(UCE)، مزارع الرياح، الهضاب العليا، التكلفة الإجمالية لإنتاج الكهرباء، الضياعات النشطة الكلية، انبعاثات الغازات، انحراف الجهد، مؤشر استقرار الجهد في الشبكة.

TABLE OF CONTENTS

LIST OF FIGURES

CHAPTER IV:Power Flow Optimisation Methods

CHAPTER V:Results and Simulation

APPENDIX

LIST OF TABLES

APPENDIX A

APPENDIX B

APPENDIX C

APPENDIX D

LIST OF SYMBOLS AND ABBREVIATIONS

MOALO	Multiobjective Ant Lion algorithm
X_{min}, X_{max}	Bounds of the problem
Min, Max	Maximum and minimum values
$\nabla_{sol}E$	The enthalpy of dissolution
A, B	Temperature parameters
T^{θ}	Reference temperature ($T = 298.15K$)
R	Gas constant
H	Henry's constant
r	A random number between 0 and 1
t	Iteration time
F	Flag that changes the direction of the search agent and provides diversity
γ	The ability of gas j in cluster i to interact with the gases in its cluster
α	Influence of other gases on gas i in cluster j and equal to 1
$P_{i,j}$	The partial pressure of gas i in cluster j
$H_j(t)$	Values of Henry's constant of type j
C_j	A constant value of type j
$S_{i,j}$	Solubility of gas i in cluster j
X_{best}	Best gas in the swarm
$X_{i,best}$	Best gas i in cluster j
$F_{(i,j)}$	Fitness of gas i in cluster j
F_{best}	Fitness of the best gas in the entire system
$W_{(i,j)}$	The position of gas i in cluster j
N_w	New worst agents
$X_{i,j}^{ta}$	Present positions of cheetah i in arrangement j
$X_{i,j}^{ta+1}$	Next positions of cheetah i in arrangement j
$\hat{r}_{i,j}^{-1}$	Random number used for each cheetah during different hunting periods
$\alpha_{i,j}^{ta}$	Step length of cheetah i in layout j
$\beta^{t}_{i,j}$	Random number used in the interaction factors of cheetah **i** in arrangement j
$\check{r}_{i,j}$	Random number used in the rotation factors of cheetah **i** in arrangement j
t_a	Actual hunting time
T_m	Maximum period of hunting time
X	Current position of the prey in arrangement j
V_i , V_j	Voltage magnitudes at node i and node j, respectively (p.u.)
B_{ij}	Susceptance of transmission line between buses i and j **(** imaginary part of admittance**)** (Ω^{-1})
G_{ij}	Conductance of transmission line between buses i and j (real part of admittance)(Ω^{-1})
Y_1	Admittance sub-matrix (vector of injected currents and load bus voltages)
Y_2	Admittance sub-matrix (vector of injected load bus currents and PV bus voltages)
$N_{T_{tap}}$	Number of tap settings of the transformer installed in the power system
N_{phase}	Number of phase shifters installed to the power system
n_l	Number of the transmission lines
N_L	Number of load buses (PQ buses)
N_T	Number of regulating transformers
N_C	Number of shunt compensator
N_{PV}	Number of PV buses
N_B	Number of buses

T_i	Regulating of transformer i
P_{Si}	Phase shifter of transformer i
P_{Di}	Active power of load demand at bus i (MW)
Q_{Di}	Reactive power of load demand at bus i (MVar)
P_i	Active power injection at bus i (MW)
Q_i	Reactive power injection at bus i (MVar)
δ_{ij}	Difference angle between voltage angles δ_i and δ_j of buses i and j, respectively (rad)
Q_W	Reactive power output of the wind farms
P_W	Active power output of the wind farms
N_W	Number of wind farms
N_{SVC}	Number of SVC devices
$d_{w,i}$	Direct cost coefficient for the i-th wind generator
β_i°	Optimal factor of the wind power penetration from the i th wind farm.
$f_w(P_w)$	Probability density function (PDF)
$K_{rw,i}$	Reserve cost coefficient for the overestimation of the i-th wind farm
$K_{pw,i}$	Penalty cost coefficient for the underestimation of the i-th wind farm
$C_{rw,i}$	Cost associated with wind power surplus (overestimation)
$C_{pw,i}$	Cost associated with wind power shortage (underestimation)
$P_{wr,i}$	Rated wind power from the i-th wind-powered generator
P_{Wi}	Active power generated by the wind generator at node i
$P_{ws,i}$	Scheduled wind power from the i-th wind-powered generator
$P_{wa,i}$	Available power output from the i-th wind-powered generator

CHAPTER : I

General Introduction

I.1.Thesis overview

The global energy system requires a fundamental transformation to meet the continuous increases in demand, from heavy reliance on fossil fuels (oil, natural gas and coal) to renewable energy sources (solar, wind, hydro and biomass). These sources play a crucial role in the transition to sustainable energy. By replacing fossil fuels, they help to reduce greenhouse gas emissions and limit the impact of human activity on the environment. Using natural resources, such as wind power, produces cleaner electricity and improves air quality.

This transition can potentially foster more inclusive and prosperous renewable energy societies in many countries. In response to the Fukushima accident, governments worldwide have restructured their electricity markets to integrate renewable resources into large-scale electricity grids for power generation. Such integration is essential for future sustainable electricity production. It reduces generation costs, active losses, improves grid stability, limits environmental impact, and increases countries' energy independence [1].

Electricity consumption in Algeria is projected to reach between 130 and 150 TWh by 2030. This growth in national energy consumption plans could disrupt the balance between supply and demand. Given these conditions, it has become essential to generate electricity from various renewable energy sources (RES) as an alternative solution to meet the fluctuating electricity demand at the lowest production cost[2].

Algeria has abundant and diverse energy resources, including conventional and renewable sources. It is among the top five natural gas and top ten oil producers globally. However, it is also one of the biggest emitters of carbon dioxide (CO2) in Africa. To reduce gas emissions by 193 million tons and meet energy demands, the government aims to install 22,000 MW of renewable energy capacity, which will account for 37% of total production by 2030. Wind energy is the second development axis, with a planned capacity of 5,010 MW, representing 23% of the total. This plan includes several wind farm projects currently under consideration[1].

The development and use of renewable energies have increased rapidly, and in 40 years, any sustainable energy system will be based on the rational use of conventional sources and the efficient use of renewable energies. However, the intermittent nature of renewable energy sources poses problems for the electricity grid. The variability of wind power generation can cause imbalances in the supply-demand system, leading to grid instability and voltage

fluctuations. To address these issues, flexible alternating current transmission systems (FACTS), such as static Var compensators (SVCs), have gained importance as devices capable of regulating voltage levels, improving power factor, providing reactive power support and enhancing the integration of renewable energy sources in the power grid[3].

Although the integration of renewable sources in electrical networks is beneficial from a technical, economic and environmental standpoint, this integration benefit remains restricted to the choice of the location for these renewable sources. The choice of location for wind farms in the Algerian DZ-114 bus electricity transmission network is subject to practical considerations depending on the target objective. Among these practical considerations is the structure of the meshed grid formed by 114 buses distributed across the Algerian national territory. This is why the techno-economic studies presented on the development of wind farms in Algeria remain technically not-concise without regard to the Algerian electrical network structure and the choice of wind farm locations among the 114 nodes. Determining the optimal state of the electric power system with the wind farms is achieved using Optimal Active Power Flow OPF.

The main objective of OPF is to find the optimal adjustment of each network regulating equipment that optimises a well-defined objective function. The voltage profile is an essential quality index for the management of electrical networks, which can be managed by reactive power compensators (SVC) to control and improve the voltage of a power system using optimal reactive power flow (ORPF). Optimal Active Power Flow (OAPF) can manage minimising active power transmission losses and the cost of producing active power. Optimisation encompasses a series of techniques for determining the optimum variables that maximise or minimise a given function, known as the 'objective function' [1].

The complexity of optimising power flows, particularly in a deregulated electricity market, is increased by adding new constraints, such as reducing polluting gas emissions (Kyoto Protocol, 2005) and integrating renewable energy sources. These challenges often limit the effectiveness of exact methods because they are not flexible enough to take into account a wide range of specific constraints. Thus, efficient methods, such as metaheuristics, are necessary to solve these problems.

Metaheuristics are often used as solution strategies due to their flexibility and adaptability. They can use it to find solutions in as many cases as possible. These stochastic global

optimisation algorithms can apply to any problem formulated as a criterion optimisation, progressing towards an optimum by sampling the objective function. Typically used as generic methods, metaheuristics can optimise a wide range of problems without requiring significant modifications in the algorithm. In addition, they are adaptable and can be extended to different problem extensions[4,5].

This thesis presents a technical and economic study aimed at identifying suitable locations for wind farms. As part of this study, the unit cost of wind energy was calculated and incorporated into the optimization of total electricity production costs. This problem was introduced in the context of OPF and solved using metaheuristic methods.

I.2. Problem statement

The remarkable growth in demand for electrical energy has created new challenges for electrical energy management, including the depletion of fossil energy resources, greenhouse gas emissions from conventional power plants, increased active transmission losses, and rising fuel consumption costs, all while a deregulated energy market and increased demands on modern electrical energy systems persist. Integrating renewable energy sources into power systems is an alternative solution to these challenges.

However, the integration of these renewable sources, especially wind power, remains limited to suitable locations based on their wind potential and economic criteria. For this reason, a technical and economic study is essential to determine the optimal cost and location of wind farms.

Although integrating renewable energy sources has positive economic and environmental impacts, it poses certain challenges for solving the Optimal Power Flow (OPF) problem. Due to uncertainties about the operational constraints associated with renewable energy sources, conventional methods for solving OPF problems cannot address certain practical considerations. In the context of this problem, our project topic proposes the development of a robust tool for solving the optimal power flow problem using a new meta-heuristic technique to overcome the complexity of the practical constraints associated with integrating renewable energy sources.

I.3.Motivation

Optimal Power Flow (OPF) is an essential tool for electricity network operators, widely used for network planning and operation. The main objective function for OPF is minimizing

the total generation cost, total active power losses, total emission of pollutant gases by the power plant, voltage deviation and voltage stability index. Traditional deterministic methods for solving OPFs often encounter non-linear, non-convex and non-differentiable problems, leading to non-optimal solutions. To address these challenges, meta-heuristic optimization algorithms have been developed to manage effectively complex problems involving mixed variables. They balance exploration (searching the full solution space) and exploitation (refining around optimal solutions) to find global optima. Although no method can universally solve all problems, as the no-free-lunch theorem indicates, researchers continue to search for an efficient technique to improve the problem-solving capabilities of OPF.

The optimisation of electricity networks in the presence of wind farms has become essential for solving the main power flow problems that have emerged in recent years. These challenges are mainly related to the consequences of renewable energy integration in conventional power grids, in particular on the performance of optimal energy management in a context where renewable sources play an increasing role. Determining the optimal operating state of the electricity network given the complexity of exploiting renewable sources is a major concern for researchers, governments and industry. The use of an efficient and robust metaheuristic algorithm to solve the optimal power flow problem (OPF) in power systems (integrating wind farms combined with SVC devices) can reduce electricity production costs and conserve fuel, minimise CO2 emissions, reduce power losses, improve voltage profiles and ensure optimal operation of power grids.

I.4.Research objective and contribution

The main objective of this thesis is to ensure the optimal management of electrical energy in the presence of renewable energy sources. For this purpose, meta-heuristic methods have been used to solve Optimal Power Flow (OPF) problems in electrical grids, including stochastic wind energy and SVC devices. The main contributions of this thesis are summarised below:

- Two innovative meta-heuristic techniques are proposed for solving the OPF problem: the Henry Gas Solubility Optimisation (HGSO) algorithm, inspired by the physical principle of Henry's law on gas solubility, and the Cheetah Optimizer (CO), which mimics the behavior of a cheetah hunting in the wild.

- The performance of the HGSO and CO algorithms has been studied through the analysis of the exploration and exploitation phases, maintaining the balance between these two mechanisms and avoiding local optima in the OPF solution, which is better than other meta-heuristics algorithms cited in the literature.

- The performance and efficiency of the proposed HGSO algorithm have been evaluated through experiments on standard electrical systems, including the IEEE-30 and IEEE-57 bus systems, and the 114-bus Algerian network. Additionally, the CO algorithm has been tested on the IEEE-30 bus system, demonstrating its robustness.

- The proposed algorithms have proved their effectiveness in minimising the six single-objective functions (total fuel cost, total gas emission, total active power losses, voltage stability index and voltage deviation) while respecting all the constraints (equality and inequality), resulting in the best optimal solution.

- A technical and economic study was conducted to determine the unit cost of energy (UCE) per kilowatt-hour (kWh) generated by four types of wind turbines installed in the Algerian highlands. This analysis considered the structure of the Algerian transmission network (DZ114-bus) to identify the optimal locations for wind farm installations.

- The UCE was implemented in the OPF problem to optimize the total cost of electricity production in the presence of wind energy within the Algerian power grid(114-bus).

- The total cost of electricity production in the 114-bus Algerian network, with 02 wind farms (Djelfa, Sétif), has been optimised using the HGSO method, demonstrating its effectiveness in generating financial and economic benefits.

I.5.Thesis organisation

Based on the presented objective, this thesis is divided into six chapters as follows:

Chapter I: A general introduction provides an overview of the thesis, followed by a problem statement regarding the integration of this energy directly into power grids. We then discuss the motivation for transition to optimal integration in the presence of renewable energy sources, highlighting our contribution and research objective.

Chapter II: This chapter describes the modelling of power system components and iterative methods for solving the power flow problem, which facilitates the management and control of the power system (generation, transmission and load). Next, we will provide an overview of the structure and operation of the electricity system.

Chapter III: This section provides an overview of global electricity production statistics, outlines the structure of the Algerian electricity market, and discusses Algeria's renewable energy development program, focusing on wind power systems. Additionally, it proposes a techno-economic study of wind energy integration into the power grid and addresses the selection of a key FACTS controller.

Chapter IV: This chapter examines the existing methods for solving the Optimal Power Flow (OPF) problem. This includes the OPF problem formulation, the objective function and the technical constraints involved in the optimisation. We classify the methods for solving the OPF problem into two main groups: conventional methods and intelligent methods. We also introduce two new meta-heuristic methods, outlining their concepts and algorithmic steps.

Chapter V: This chapter presents the simulation results and evaluation of proposed algorithms in solving OPF problems, based on experiments conducted on standard power systems, including IEEE-30, IEEE-57 bus systems, and the Algerian 114-bus network. Furthermore, the study assesses the cost of generating electricity from wind power at two sites in the Algerian highlands. It also compares the performance of four wind turbine models for electricity production at each site using a techno-economic study.

Chapter VI: The thesis concludes with a general summary and proposes research perspectives. Additional appendices and a bibliography are included at the end.

CHAPTER: II

Power Flow Analysis in Electrical Systems

II.1.Introduction

Power Flow (or Load flow) analysis, is a crucial method for understanding complex power systems (generation, transmission and load). This technique is widely covered in all textbooks on power system analysis, such as [6–9]. It use in power system operation, control, planning, and design. The objective is to solve the power flow problem by determining all variables of a balanced, steady-state power system using iterative techniques such as Newton-Raphson, Gauss-Seidel, and fast decoupling methods through computer programs. This makes it easier for operators in energy control centres to monitor and manage the status of the electrical system. Next, we will provide an overview of the structure and operation of the electricity system. Most of these features are in this chapter.

II.2.Electric network element modelling

Power systems are complex and require simplified diagrams to create equivalent models or schematics for the main components, such as generators, various types of transformers, lines, loads, and FACTS devices. These models are integrated into power flow programs to simulate their effects throughout the system[10,11].

II.2.1.Generator model

Generators convert various forms of energy (mechanical, kinetic, chemical, etc.) into electrical energy. They supply or consume active and reactive power to maintain the desired voltage level. The active power ($\mathbf{P_{Gi}}$) is regulated by turbine control, and the voltage (V_i) is determined by the injection of reactive power ($\mathbf{Q_{Gi}}$) into the generator bus (See Figure II.1). The following constraints define the production limits of the generator:

$$P_{Gi,min} \leq \mathbf{P_{Gi}} \leq P_{Gi,max} \quad \text{and} \quad Q_{Gi,min} \leq \mathbf{Q_{Gi}} \leq Q_{Gi,max}$$

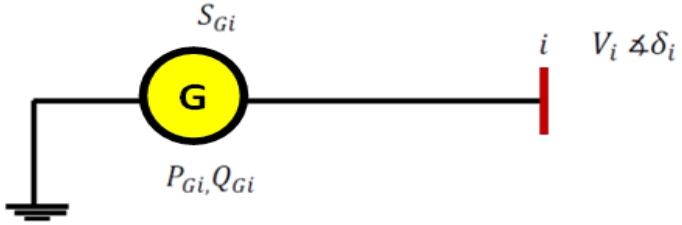

Figure II.1. Generator model

II.2.2.Transmission line model

Transmission lines can be represented as a π-model, consisting of series and shunt elements, as illustrated in Figure II. 2. This model depicts a line connecting buses (i, j), characterized by four parameters: the series resistance (rij) resulting from the resistivity of the conductor, the shunt conductance resulting from the leakage currents between the phases and the earth (in most cases due to their small size), the reactance (xij) consisting of the series inductance (L) due to the magnetic field surrounding the conductors, and the shunt capacitance (C) due to the electric field between the conductors [11,12].

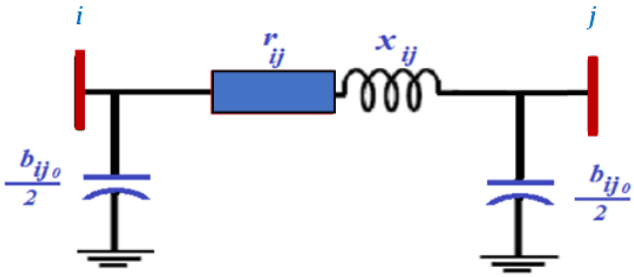

Figure II.2. Transmission line π model

The admittance matrix of a line (Y) connecting node i to node j, as below:

$$Y = \begin{bmatrix} y_{ij} + \frac{y_{ij0}}{2} & -y_{ij} \\ -y_{ij} & y_{ij} + \frac{y_{ij0}}{2} \end{bmatrix} \quad \text{(II.1)}$$

Where series admittance y_{ij} is:

$$y_{ij} = \frac{1}{z_{ij}} = \frac{1}{r_{ij} + jx_{ij}} = g_{ij} - jb_{ij} \quad \text{(II.2)}$$

The transverse admittance corresponding to capacitive effects is expressed as transversal susceptance (jb_{ij0}):

$$y_{ij0} = jb_{ij0} \quad \text{(II.3)}$$

II.2.3.Load model

The electric charge often modelled as a constant impedance. Most loads connecte to the electrical network via a variable tap transformer, which keeps the load voltage nearly constant so that constant values can represent the load's active and reactive power. The load bus voltage **V_L** and the apparent power **S_L** represented by static admittances **G_L** and **B_L**, as

shown in Figure II. 3. The equivalent admittance $\mathbf{Y_L}$ is calculated using data from the power flow study[10,12].

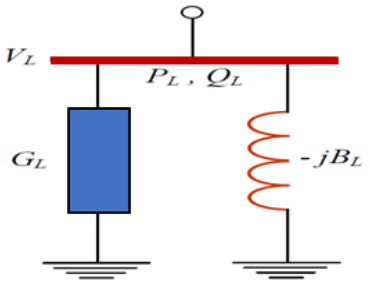

Figure II.3. Load model

$$Y_L = \frac{P_L}{V_L^2} - j\frac{Q_L}{V_L^2} \quad \text{(II.4)}$$

$$G_L = {P_L}/{V_L^2} \quad \text{(II.5)}$$

$$B_L = {Q_L}/{V_L^2} \quad \text{(II.6)}$$

II.2.4.Shunt elements models

Shunt elements compensate for reactive energy and control voltage using capacitors and reactors[11,13] . Shunt compensators are represented by their reactive power (Q_C), with a positive Qc indicating a capacitor that supplies reactive power and a negative Qc denoting an inductor that absorbs reactive power. Each element connected to a network is modelled as an equivalent admittance ($\mathbf{y_i}$) as shown in Figure II.4.

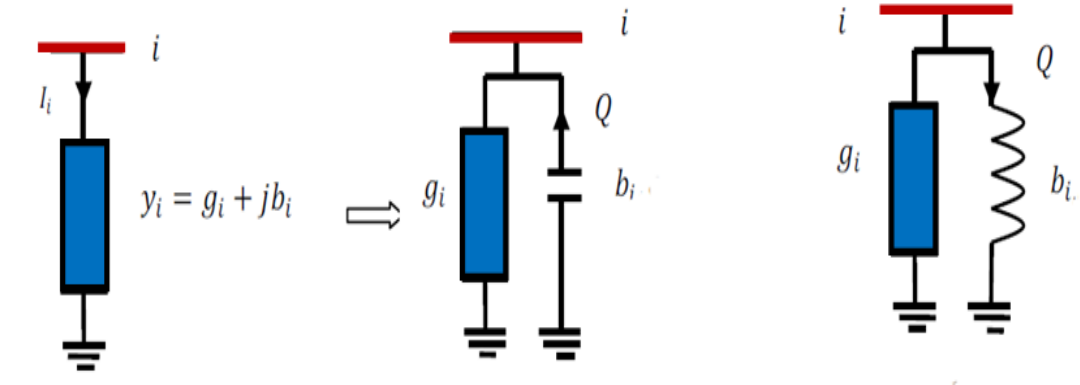

a)Symbol b)Capacitive element c)Inductive element

Figure II.4. Shunt element models

II.2.5.Transformer model

Power transformers are essential components in power systems, connecting different voltage levels in transmission and distribution networks. They can be modeled as an asymmetrical π quadrupole as shown in Figure II.5. Two important variables associated with transformers are the transformation ratio(aij) and the leakage impedance (z_{ij}) [10,11,14]. The admittance matrix of a transformer (Yt) is inserted between node i and node j as follows:

$$Y_t = \begin{bmatrix} \frac{y_{ij}}{a_{ij}^2} & -y_{ij}/a \\ -y_{ij}/a & y_{ij} \end{bmatrix} \quad \text{(II.7)}$$

Where Y_{ij} denotes the admittance of the transformer inserted between nodes i and j.

$$Y_{ij} = \frac{1}{z_{ij}} = \frac{1}{R_{ij} + X_{ij}} \quad \text{(II.8)}$$

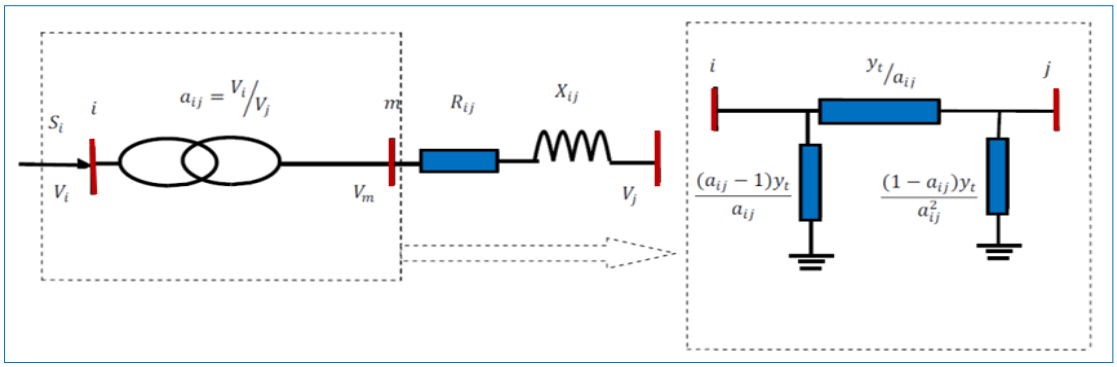

Figure II.5. Ideal transformer model

II.3. Power flow problem

The power flow problem involves calculating the voltage amplitude and phase angle at each bus in a balanced three-phase electrical system. It also includes determining the active and reactive power (absorbed or generated) and power losses across the lines during power transmission. Each bus has four variables, two specified and the other two determined by a program for solving energy flow problems. Multi-bus electrical networks, as illustrated in Figure II.6a, are classified into three distinct categories[6,7,15].

II.3.1.Bus types

II.3.1.1. Swing bus

The number 1 in the diagram shown in Figure II.6b represents the swing (slack) bus. This particular bus only has one generator, responsible for adjusting its scheduled power to

compensate for system losses (in MW and MVar), and connected to a constant voltage source. The flux program calculates the unknown quantities, P_1 and Q_1, based on the given magnitude values and the voltage's phase angle ($|V_1|=1.0$, $\angle\delta_1=0°$).

II.3.1.2. Control bus

In a control bus, also known as a PV bus (See Figure II.6c), the power flow program regulates the voltage amplitude $|V_i|$ and active power P_{gi} for each generator bus. However, the phase angle δ_i and reactive power Q_i are calculated as the two unknowns.

II.3.1.3. Load bus

The load (PQ) bus has no generators, as shown in Figure II.6d. The active and reactive power demand (P_{di}, Q_{di}) are obtained from historical data, load forecasts or measurements. The amplitude and phase angle of the bus voltage ($|V_i|$, δ_i), which are initially unknown, are then calculated. The active and reactive powers supplied to the bus (P_{gi}, Q_{gi}) are positive, while those consumed by the electrical system (P_{di}, Q_{di}) are negative.

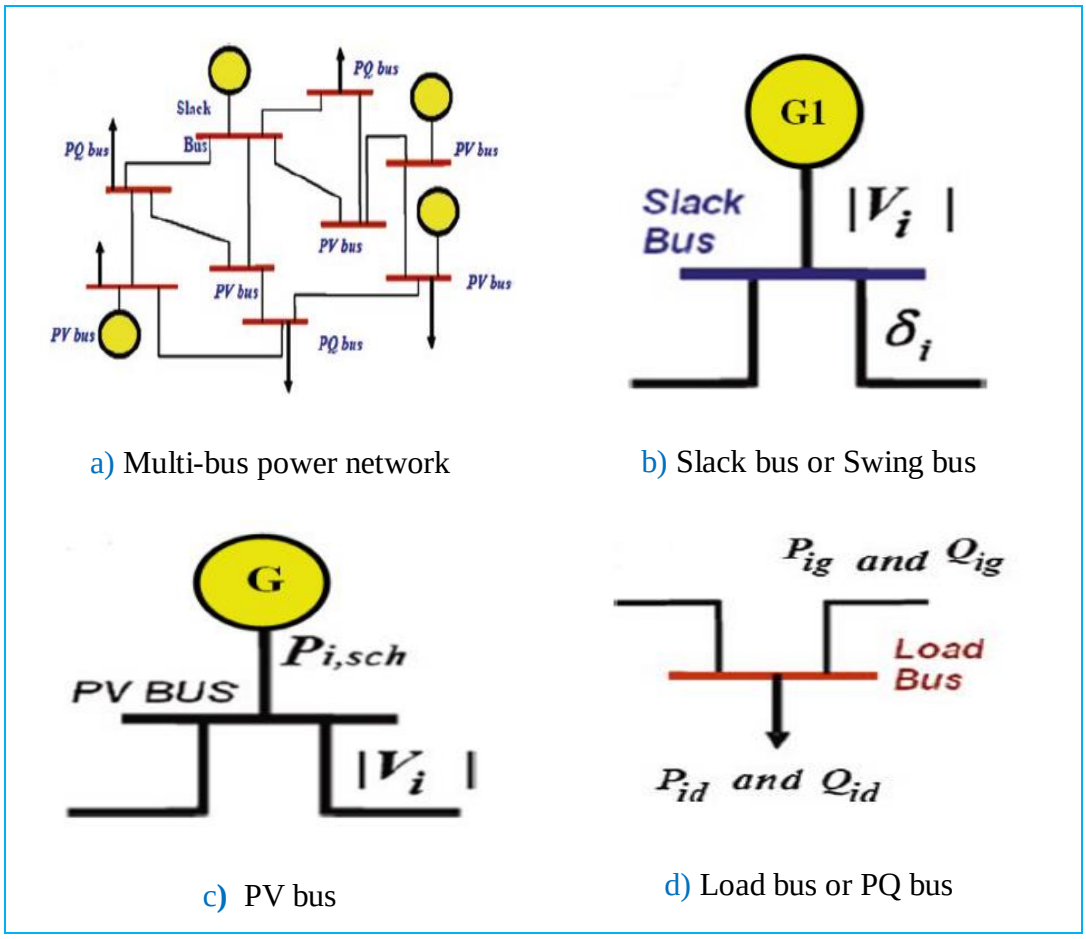

a) Multi-bus power network

b) Slack bus or Swing bus

c) PV bus

d) Load bus or PQ bus

Figure II.6. Types of buses

II.3.2. Admittance matrix

The bus admittance matrix [Y_{bus}] is a network model used to solve power flow problems. Ybus is easy to modify as the system changes, requires minimal computer memory, and reduces execution time[6]. Consider a simple 4-bus electrical system, as seen in Figure II.7, node 0; is considered as ground (reference node).The four-bus system, which corresponds to the single -line diagram in Figure II.7a can be represented by the network in Figure II.7b.

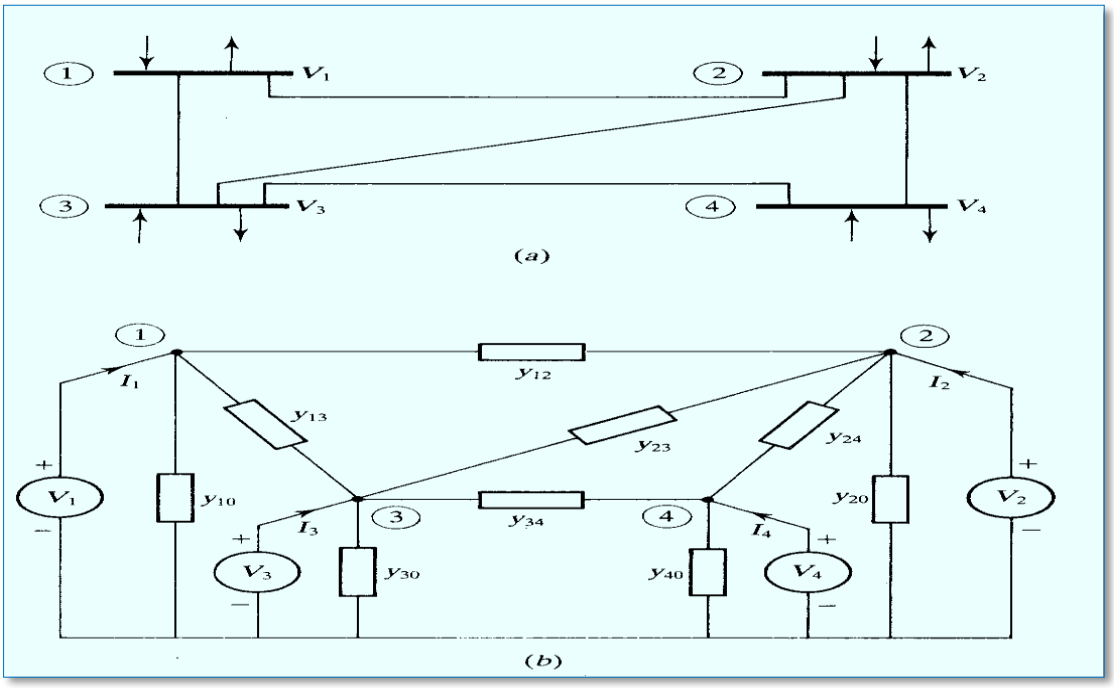

Figure II.7. Electrical network single-line diagram[9]

- Using Kirchhoff's current law(KCL) and the given admittances, we can derive equations for the node voltages (V_1, V_2, V_3, and V_4) by applying KCL to independent buses 1 to 4; we obtain the following equations [9]:

$$I_1 = V_1 * y_{10} + (V_1 - V_2) * y_{12} + (V_1 - V_3) * y_{13}$$
$$I_2 = V_2 * y_{20} + (V_2 - V_1) * y_{12} + (V_2 - V_3) * y_{23} + (V_2 - V_4) * y_{24}$$
$$I_3 = V_3 * y_{30} + (V_3 - V_1) * y_{13} + (V_3 - V_2) * y_{23} + (V_3 - V_4) * y_{34}$$
$$I_4 = V_4 * y_{40} + (V_4 - V_2) * y_{24} + (V_4 - V_3) * y_{34}$$

where,

$$Y_{11} = y_{10} + y_{12} + y_{13}$$
$$Y_{22} = y_{20} + y_{12} + y_{23} + y_{24}$$
$$Y_{33} = y_{30} + y_{13} + y_{23} + y_{34}$$
$$Y_{44} = y_{40} + y_{24} + y_{34}$$

$$Y_{12} = Y_{21} = -y_{12}$$
$$Y_{13} = Y_{31} = -y_{13}$$
$$Y_{14} = Y_{41} = -y_{14} = 0$$
$$Y_{23} = Y_{32} = -y_{23}$$
$$Y_{24} = Y_{42} = -y_{24}$$
$$Y_{34} = Y_{43} = -y_{34}$$

- The following equation is rewritten in matrix form:

$$\begin{bmatrix} I_1 \\ I_2 \\ I_3 \\ I_4 \end{bmatrix} = \begin{bmatrix} Y_{11} Y_{12} Y_{13} Y_{14} \\ Y_{21} Y_{22} Y_{23} Y_{24} \\ Y_{31} Y_{32} Y_{33} Y_{34} \\ Y_{41} Y_{42} Y_{43} Y_{44} \end{bmatrix} * \begin{bmatrix} V_1 \\ V_2 \\ V_3 \\ V_4 \end{bmatrix} \quad \text{(II.9)}$$

- The current is positive when flowing towards the bus and negative if flowing away from the bus. For a general network with N nodes, Kirchhoff's laws for current as a function of node voltages can be written as follows:

$$I_{bus} = [Y_{bus}] * V_{bus} \quad \text{(II.10)}$$

Where I_{bus} is the vector of the injected bus currents, V_{bus} is the vector of the bus voltage measured from the reference node, and Y_{bus} represents the bus admittance matrix(contains details of the lines, transformers and capacitors installed in the system).

- The diagonal element Y_{ii} is self-admittance (driving point admittance) of node i, it is the sum of all admittances connected to it and can be expressed by equation (II.11), while the off-diagonal element Y_{ij} is the mutual or transfer admittance, is equal to the negative of admittance between nodes i and j[8], presented in equation(II.12).

$$Y_{ii} = \sum_{\substack{j=0 \\ j \neq i}}^{n} y_{ij} \quad \text{(II.11)}$$

$$Y_{ij} = Y_{ji} = -y_{ij} \quad \text{(II.12)}$$

II.4. Power flow Formulation

The net injected power at any bus can be calculated using the bus voltage (V_i), the adjacent bus voltages (V_j), and admittances (y_{ij}) between the buses i and j, as shown in Figure II.8.

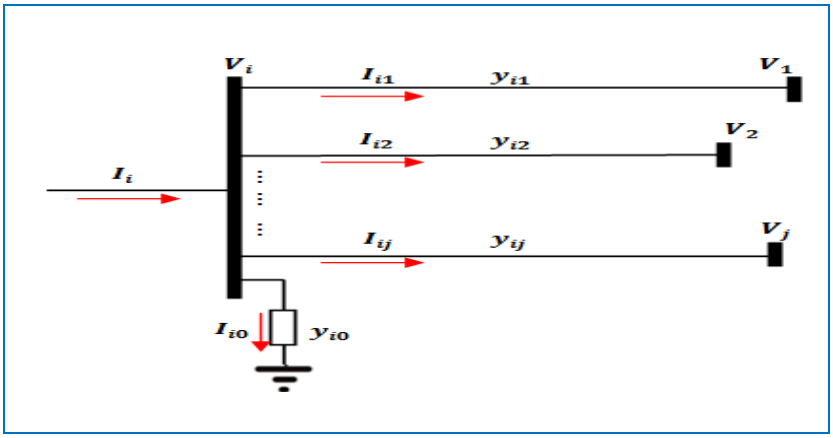

Figure II.8. Net injected power

- The net current (Ii) injected into bus i, is determined by the following summation:

$$I_i = V_i y_{i0} + (V_i - V_1)y_{i1} + (V_i - V_2)y_{i2} + \cdots + (V_i - V_j)y_{ij}$$

$$I_i = V_i(y_{i0} + y_{i1} + y_{i2} + \cdots + y_{ij}) - (V_1)y_{i1} - (V_2)y_{i2} - \cdots - (V_j)y_{ij}$$

$$I_i = V_i \sum_{\substack{j=0 \\ j\neq i}}^{N} y_{ij} - \sum_{\substack{j=1 \\ j\neq i}}^{N} y_{ij}V_j = V_i Y_{ii} + \sum_{\substack{j=1 \\ j\neq i}}^{N} Y_{ij}V_j \quad \text{(II.13)}$$

- And the current (Ii) can be written as a function of the power as follows:

$$I_i = V_i Y_{ii} + \sum_{\substack{j=1 \\ j\neq i}}^{N} Y_{ij}V_j = \frac{P_i - jQ_i}{V_i^*} \quad \text{(II.14)}$$

- The power flow equations are generally formulated in polar; the voltage in the bus **i** is expressed in the following form:

$$V_i = |V_i|\angle\delta_i = |V_i|(\cos\delta_i + j\sin\delta_i) \quad \text{(II.15)}$$

- The voltage at another bus j is similarly written by changing the subscript from i to j.

$$V_j = |V_j|\angle\delta_j = |V_j|(\cos\delta_j + j\sin\delta_j) \quad \text{(II.16)}$$

And

$$Y_{ij} = |Y_{ij}|\angle\theta_{ij} = |Y_{ij}|\cos\theta_{ij} + j|Y_{ij}|\sin\theta_{ij} = G_{ij} + jB_{ij} \quad \text{(II.17)}$$

II.4.1.Power flow equations

The power equation at any bus is written as follows:

$$S_i = P_i + jQ_i \quad \text{(II.18)}$$

- Rewriting the power flow equation (II.18) in complex form, we get :

$$S_i^* = V_i^* I_i = P_i - jQ_i = V_i^* \sum_{j=1}^{N} Y_{ij}V_j \quad \text{(II.19)}$$

- We substitute equations (II.15), (II.16), and (II.17), we obtain:

$$P_i - jQ_i = \sum_{j=1}^{N} |Y_{ij} V_i V_j| \angle \theta_{ij} + \delta_j - \delta_i \quad \text{(II.20)}$$

- Extending this expression and equating the active and reactive parts, we obtain:

$$P_i = \sum_{j=1}^{N} |Y_{ij} V_i V_j| \cos(\theta_{ij} + \delta_j - \delta_i) \quad \text{(II.21)}$$

$$Q_i = -\sum_{j=1}^{N} |Y_{ij} V_i V_j| \sin(\theta_{ij} + \delta_j - \delta_i) \quad \text{(II.22)}$$

- Let P_i and Q_i denote the net active and reactive power entering the network. Equations (II.21) and (II.22) represent the power flow equations used to calculate the net active power Pi and reactive power Qi entering bus i [7], as illustrated in Figure II.9.

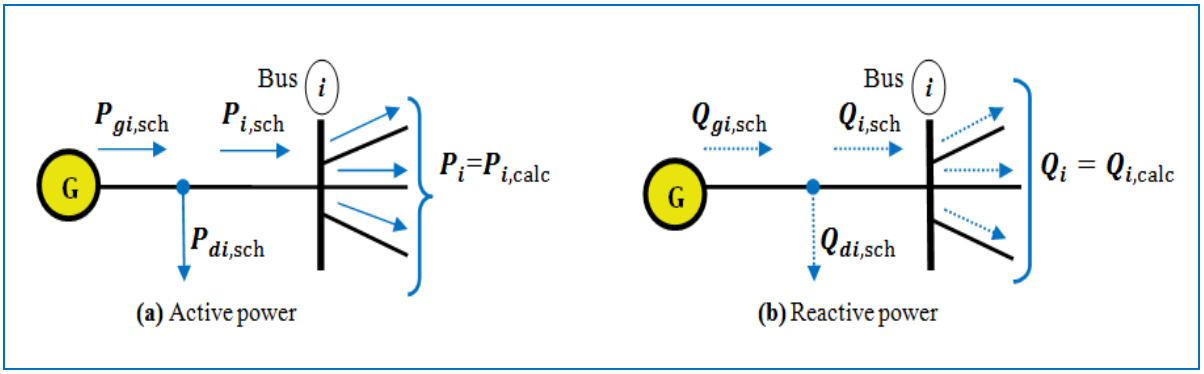

Figure II.9. Active and reactive power in a bus (i)

- Let $\mathbf{P_{gi,\,sch}}$ represent the scheduled power generated at bus i, and $\mathbf{P_{di,\,sch}}$ denote the load's scheduled power demand at this bus. So, $\mathbf{P_{i,\,sch} = P_i - P_{di}}$ is the net scheduled power injected into the network at bus i. (See Figure II.9).

$$P_{i,sch} = P_{gi,sch} - P_{di,sch} \quad \text{(II.23)}$$

$$Q_{i,sch} = Q_{gi,sch} - Q_{di,sch} \quad \text{(II.24)}$$

- Denoting the calculated value of $P_i = P_{i,\,calc}$ and $Q_i = Q_{i,\,calc}$, the active and reactive power imbalance at bus (i) given by the mismatch ΔP_i and ΔQ_i; are close to zero when the calculated values of Piand Qi coincide with the scheduled values.

$$\Delta P_i = P_{i,sch} - P_{i,calc} = (P_{gi,sch} - P_{di,sch}) - P_{i,calc} \quad \text{(II.25)}$$

$$\Delta Q_i = Q_{i,sch} - Q_{i,calc} = (Q_{gi,sch} - Q_{di,sch}) - Q_{i,sch} \quad \text{(II.26)}$$

- The iterative process is continued until the maximum power differences $(\Delta P_i^{(k)})$ $and (\Delta Q_i^{(k)})$ are less than the specified accuracy $(\epsilon \cong 0)$

$$\text{Max}\begin{cases}\left|\Delta P_i^{(k)}\right| \leq \epsilon \\ \left|\Delta Q_i^{(k)}\right| \leq \epsilon\end{cases} \quad \text{(II.27)}$$

II.4.2.Line power losses

Consider the transmission line connecting the two buses i and j in Figure II.10. The system losses in active and reactive power can be calculated as follows[6,15]:

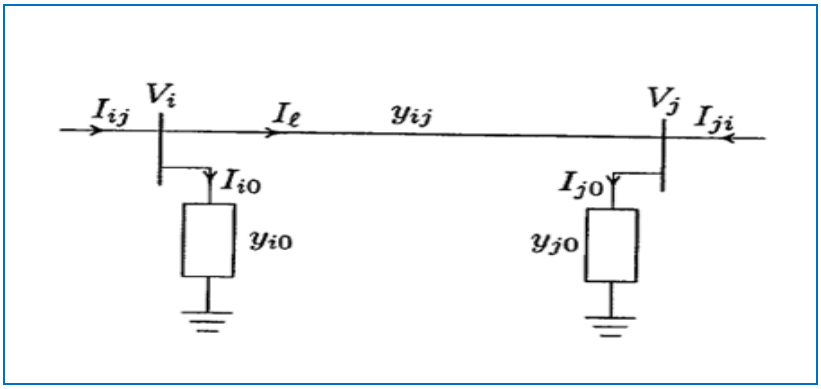

Figure II.10. Transmission line model (loss calculation)

- The complex powers $\mathbf{S_{ij}}$ from bus i to j and $\mathbf{S_{ji}}$ from bus j to i are given by :

$$S_{ij} = V_i I_{ij}^* = P_{ij} + Q_{ij} \quad \text{(II.28)}$$

$$S_{ji} = V_j I_{ji}^* = P_{ji} + Q_{ji} \quad \text{(II.29)}$$

$$S_{L\,ij} = S_{ij} + S_{ji} \quad \text{(II.30)}$$

- The power losses in the line (S_{Lij}), given by Eq. (II.30), correspond to the algebraic summation of the power flows in Eqs. (II.28) and (II.29). The active and reactive losses(P_L, Q_L) can be calculated in the following form:

$$P_L = \sum_{i=1}^{N}\sum_{j=1}^{N}(P_{ij} + P_{ji}) = \sum_{i=1}^{N} P_{gi} - \sum_{i=1}^{N} P_{di} \quad \text{(II.31)}$$

$$Q_L = \sum_{i=1}^{N}\sum_{j=1}^{N}(Q_{ij} + Q_{ji}) = \sum_{i=1}^{N} Q_{gi} - \sum_{i=1}^{N} Q_{di} \quad \text{(II.32)}$$

II.5. Power flow resolution

Power flow analysis is performed using iterative methods such as Newton-Raphson, Gauss-Seidel and fast-decoupled methods, which solve linear algebraic equations and all power flow problems using the admittance matrix[9]. Details of each method are given below.

II.5.1. Gauss-Seidel method

Gauss-Seidel is a simple iterative method for solving power flow equations. It is suitable for small power systems and continues to solve the equations until the voltage differences between the buses become negligible. It also provides an initial solution to the Newton-Raphson method for large systems, saving the computation time required for each iteration.

a) As an example, consider a four-bus system as shown in Figure II.7, bus (1) is designated the swing bus. Initial estimates of the unknown voltages at all load buses (2, 3 and 4) have been set at $\mathbf{1.0}^{\angle \mathbf{0}^{\circ}}$ per unit[7]. The calculations start at bus (2)

$$\frac{P_{2,sch} - jQ_{2,sch}}{V_2^*} = Y_{21}V_1 + Y_{22}V_2 + Y_{23}V_3 + Y_{24}V_4 \qquad (II.33)$$

- The solution proceeds by iteration based on the scheduled active and reactive power at buses (2, 3, and 4). The scheduled slack bus voltage ($V_1 = |V_1|^{\angle \delta_1}$), and initial voltage estimates $(V_2^{(0)}, V_3^{(0)}, V_4^{(0)})$ at the other buses. The corrected voltage $V_2^{(1)}$ is calculated from the following equation:

$$V_2^{(1)} = \frac{1}{Y_{22}}\left[\frac{P_{2,sch} - jQ_{2,sch}}{V_2^{(0)*}} - \left(Y_{21}V_1 + Y_{23}V_3^{(0)} + Y_{24}V_4^{(0)}\right)\right] \qquad (II.34)$$

- The first corrected voltage $V_3^{(1)}$ on bus 3 is calculated using equation (II.35).

$$V_3^{(1)} = \frac{1}{Y_{33}}\left[\frac{P_{3,sch} - jQ_{3,sch}}{V_3^{(0)*}} - \left(Y_{31}V_1 + Y_{32}V_2^{(1)} + Y_{34}V_4^{(0)}\right)\right] \qquad (II.35)$$

- Similar solution for equation (II.36) gives the corrected voltage $(V_4^{(1)})$ determined from:

$$V_4^{(1)} = \frac{1}{Y_{44}}\left[\frac{P_{4,sch} - jQ_{4,sch}}{V_4^{(0)*}} - \left(Y_{41}V_1 + Y_{42}V_2^{(1)} + Y_{43}V_3^{(1)}\right)\right] \qquad (II.36)$$

- The iteration procedure repeats until $\left|V_i^{(k+1)} - V_i^{(k)}\right| \leq \varepsilon$.

- For a system of N buses, the general iterative equation for calculating voltage at bus i is as follows[6]:

$$V_i^{(k+1)} = \frac{1}{Y_{ii}}\left[\frac{P_{i,sch} - jQ_{i,sch}}{V_i^{(k)*}} - \sum_{j=1}^{i-1} Y_{ij}V_j^{(k+1)} - \sum_{j=i+1}^{N} Y_{ij}V_j^{(k)}\right] \quad \text{(II.37)}$$

Where (k) is the number of the iteration in which the voltage is calculated, and (k + 1) is the previous iteration, $V_i^{(k)*}$ is the conjugate of value$V_i^{(k)}$.

b) If the system has a control bus with known values (δi and V_i), then Q_{Gi} must be calculated by satisfying the condition $Q_{min} \leq Q_{Gi} \leq Q_{max}$. The net reactive power injected is calculated based on iterative voltages $V_i^{(k+1)}$ using the given equation[7,8]:

$$Q_{Gi}^{(k+1)} = -Im\left[V_i^{(k)*}\sum_{j=1}^{i-1} Y_{ij}V_j^{(k+1)} + \sum_{j=i+1}^{N} Y_{ij}V_j^{(k)}\right] \quad \text{(II.38)}$$

c) The procedure for the Gauss-Seidel solution of the power flow is as follows:

- Choose an initial value $V_i^{(0)} = 1.0^{\angle 0^\circ}$ P.u, for all buses except the slack bus.
- Use $V_i^{(0)}$ to calculate $V_i^{(1)}$ using equation (II.37).
- Use $V_i^{(1)}$ to calculate $V_i^{(2)}$ using equation (II.37).
- Repeat the process until$\left|V_i^{(k+1)} - V_i^{(k)}\right| \leq \varepsilon$; ε is the tolerance (calculation accuracy).

II.5.2. Newton-Raphson method

The Newton-Raphson method is an iterative technique for solving the power flow problem by converting nonlinear equations into linear ones using Taylor series expansion. It is the most efficient and practical method, especially for large power systems. A key advantage of this method is that the number of iterations required to reach a solution does not depend on the system size[6,15].

- Let us return to equations (II.21) and (II.22), which represent simultaneous nonlinear equations in polar form for each bus in the electrical network. The study of power flow consists of solving these equations to determine the voltage amplitudes, |V|, and phase angles, δ. For small variations in δ and |V|, a linear relationship can be established by solving the

following partial differential equations. The linear resolution is obtained by establishing the following partial differential equations:

$$\Delta P_i = \sum_{j=1}^{N} \frac{\partial P_i}{\partial \delta_j} \Delta\delta_j + \sum_{j=1}^{N} \frac{\partial P_i}{\partial |V_j|} \Delta|V_j| \tag{II.39}$$

$$\Delta Q_i = \sum_{j=1}^{N} \frac{\partial Q_i}{\partial \delta_j} \Delta\delta_j + \sum_{j=1}^{N} \frac{\partial Q_i}{\partial |V_j|} \Delta|V_j| \tag{II.40}$$

- Again, Eqs. (II.39) and (II.40) can be written as :

$$\Delta P_i = \sum_{j=1}^{N} J_1 \Delta\delta_j + \sum_{j=1}^{N} J_2 \Delta|V_j| \tag{II.41}$$

$$\Delta Q_i = \sum_{j=1}^{N} J_3 \Delta\delta_j + \sum_{j=1}^{N} J_4 \Delta|V_j| \tag{II.42}$$

- In matrix form, these equations can be represented as follows:

$$\begin{bmatrix} \Delta P \\ \Delta Q \end{bmatrix} = \begin{bmatrix} J_1 & J_2 \\ J_3 & J_4 \end{bmatrix} \begin{bmatrix} \Delta\delta \\ \Delta|V| \end{bmatrix} \tag{II.43}$$

- The equation below applies to a system with N buses (excluding the control buses)[6].

$$\begin{bmatrix} \Delta P_2^{(k)} \\ \vdots \\ \Delta P_N^{(k)} \\ \hline \Delta Q_2^{(K)} \\ \vdots \\ \Delta Q_N^{(k)} \end{bmatrix} = \left[\begin{array}{ccc|ccc} \frac{\partial P_2^{(k)}}{\partial \delta_2} & \cdots & \frac{\partial P_2^{(k)}}{\partial \delta_N} & \frac{\partial P_2^{(K)}}{\partial |V_2|} & \cdots & \frac{\partial P_2^{(K)}}{\partial |V_N|} \\ \vdots & \ddots\ (J_1) & \vdots & \vdots & \ddots\ (J_2) & \vdots \\ \frac{\partial P_N^{(k)}}{\partial \delta_2} & \cdots & \frac{\partial P_N^{(k)}}{\partial \delta_N} & \frac{\partial P_N^{(K)}}{\partial |V_2|} & \cdots & \frac{\partial P_N^{(K)}}{\partial |V_N|} \\ \hline \frac{\partial Q_2^{(k)}}{\partial \delta_2} & \cdots & \frac{\partial Q_2^{(k)}}{\partial \delta_N} & \frac{\partial Q_2^{(K)}}{\partial |V_2|} & \cdots & \frac{\partial Q_2^{(K)}}{\partial |V_N|} \\ \vdots & \ddots\ (J_3) & \vdots & \vdots & \ddots\ (J_4) & \vdots \\ \frac{\partial Q_N^{(k)}}{\partial \delta_2} & \cdots & \frac{\partial Q_N^{(k)}}{\partial \delta_N} & \frac{\partial Q_N^{(K)}}{\partial |V_2|} & \cdots & \frac{\partial Q_N^{(K)}}{\partial |V_N|} \end{array}\right] \begin{bmatrix} \Delta\delta_2^{(k)} \\ \vdots \\ \Delta\delta_N^{(k)} \\ \hline \Delta|V_2^{(k)}| \\ \vdots \\ \Delta|V_N^{(k)}| \end{bmatrix} \tag{II.44}$$

- Equation (II.44) has four blocks. The elements of the Jacobian matrix are obtained by the partial derivatives of (II.21) and (II.22), for $\Delta\delta_i$ and $\Delta|V_j|$as follows [6,15]:

- The diagonal and the off-diagonal elements **[J1]** are:

$$\frac{\partial P_i}{\partial \delta_i} = \sum_{\substack{j=1 \\ j\neq i}}^{N} |V_i||V_j||Y_{ij}| \sin(\theta_{ij} + \delta_j - \delta_i) \tag{II.45}$$

$$\frac{\partial P_i}{\partial \delta_j} = -|V_i||V_j||Y_{ij}|\sin(\theta_{ij} + \delta_j - \delta_i); \quad i \neq j \tag{II.46}$$

- The diagonal and the off-diagonal elements **[J2]** are:

$$\frac{\partial P_i}{\partial |V_i|} = 2|V_i||Y_{ii}|\cos(\theta_{ii}) + \sum_{\substack{j=1 \\ j\neq i}}^{N} |V_j||Y_{ij}|\cos(\theta_{ij} + \delta_j - \delta_i) \tag{II.47}$$

$$\frac{\partial P_i}{\partial |V_j|} = |V_i||Y_{ij}|\cos(\theta_{ij} + \delta_j - \delta_i); \quad i \neq j \tag{II.48}$$

- The diagonal and the off-diagonal elements **[J3]** are:

$$\frac{\partial Q_i}{\partial \delta_i} = \sum_{\substack{j=1 \\ j\neq i}}^{N} |V_i||V_j||Y_{ij}|\cos(\theta_{ij} + \delta_j - \delta_i) \tag{II.49}$$

$$\frac{\partial Q_i}{\partial \delta_j} = -|V_i||V_j||Y_{ij}|\cos(\theta_{ij} + \delta_j - \delta_i); \quad i \neq j \tag{II.50}$$

- The diagonal and the off-diagonal elements **[J4]** are:

$$\frac{\partial Q_i}{\partial |V_i|} = -2|V_i||Y_{ii}|\sin(\theta_{ii}) + \sum_{\substack{j=1 \\ j\neq i}}^{N} |V_j||Y_{ij}|\sin(\theta_{ij} + \delta_j - \delta_i) \tag{II.51}$$

$$\frac{\partial Q_i}{\partial |V_j|} = -|V_i||Y_{ij}|\sin(\theta_{ij} + \delta_j - \delta_i); \quad i \neq j \tag{II.52}$$

- The equation below determines the voltage magnitudes and phase corrections:

$$\begin{bmatrix} \Delta\delta \\ \Delta|V| \end{bmatrix} = \begin{bmatrix} J_1 & J_2 \\ J_3 & J_4 \end{bmatrix}^{-1} \times \begin{bmatrix} \Delta P \\ \Delta Q \end{bmatrix} \tag{II.53}$$

- The new estimated values (voltage magnitude and phase angle) for the bus voltage are :

$$|V_i|^{(k+1)} = |V_i|^{(k)} + \Delta|V_i|^{(k)} \tag{II.54}$$

$$\delta_i^{(k+1)} = \delta_i^{(k)} + \Delta\delta_i^{(k)} \tag{II.55}$$

- The Newton-Rapson algorithm is shown in Figure II.11:

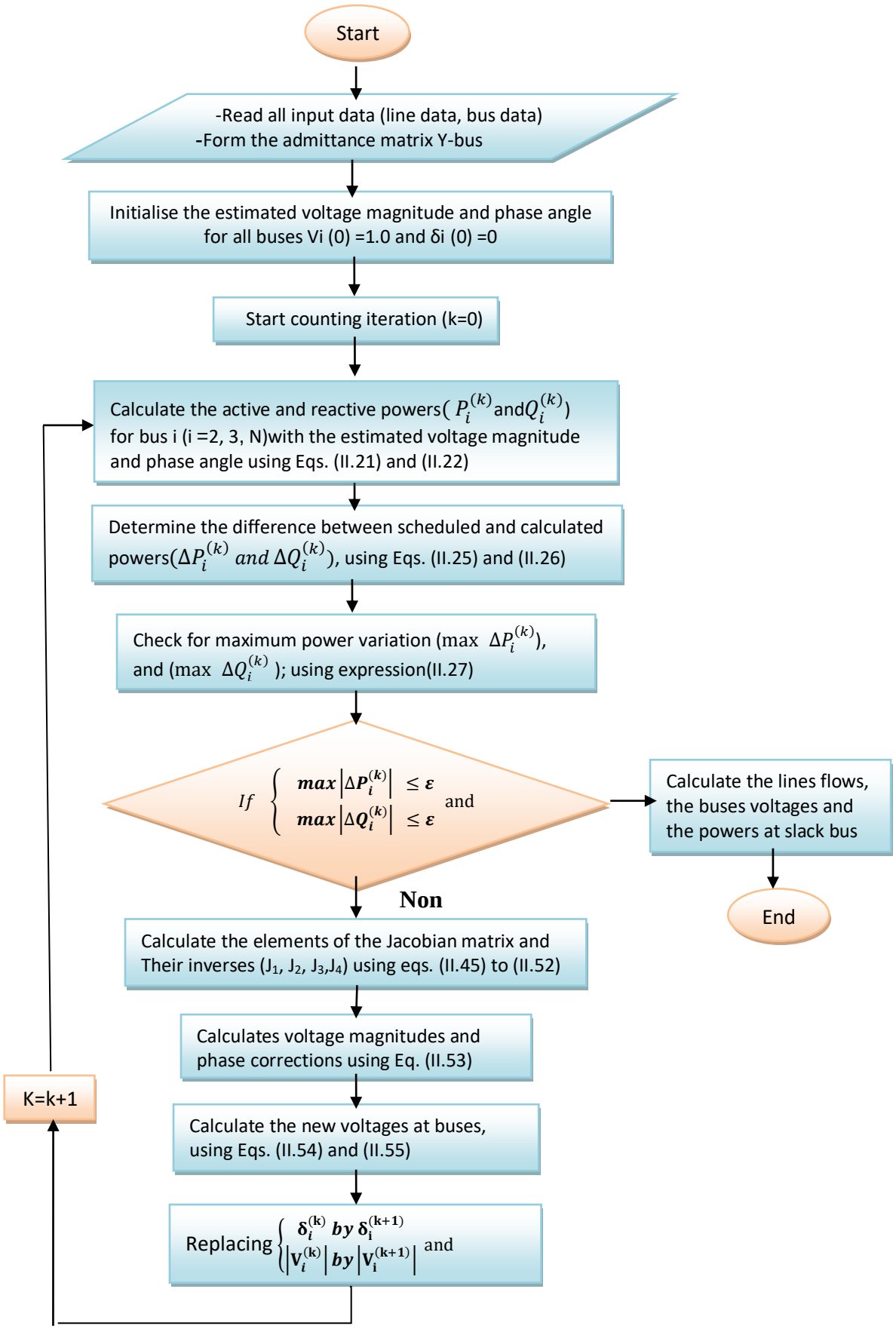

Figure II.11. Newton -Raphson algorithm

II.5.3. Fast Decoupled method

In high-voltage transmission systems, adjacent buses have small voltage angles and high X/R ratios. This leads to a significant correlation between active power and voltage angle, and between reactive power and voltage amplitude. The correlation between active power and bus voltage, and between reactive power and bus voltage angle, is usually weak, the fast decoupled load flow is derived from the N-R method[6,8].

- By setting elements J2 and J3 in Eq. (II.43) of the N-R method to zero, we obtain:

$$J = \begin{bmatrix} J_1 & J_2 \\ J_3 & J_4 \end{bmatrix} \approx \begin{bmatrix} J_1 & 0 \\ 0 & J_4 \end{bmatrix};\ J_2 = \frac{\partial P}{\partial |V|} \approx 0;\ J_3 = \frac{\partial Q}{\partial \delta} \approx 0$$

- These low values (J_2 and J_3) can be explained because the active power P depends necessarily on the δ and not on the |V|, while Q depends on the |V| and not on the δ.
- For transmission lines X/Rratio is high, so the line susceptances B_{ij} become much larger than the line conductances G_{ij}, and the differences between voltage angles(δj – δi) are minimal:

$$G_{ij} \sin(\delta_j - \delta_i) \ll B_{ij} \cos(\delta_j - \delta_i)$$

$$\cos(\delta_j - \delta_i) \approx 1; \quad \sin(\delta_j - \delta_i) \approx (\delta_j - \delta_i)$$

- Under steady-state operation, the reactive power injected into any bus (Qi) is significantly less than the reactive power that would flow if all the lines connected to that bus were short-circuited to the reference. This gives

$$Q_i \ll |V_i|^2 B_{ii}\ ; \quad \text{and} |V_i|^2 \approx |V_i|$$

- Again, Eq.(II.43)can be reduced to

$$\begin{bmatrix} \Delta P \\ \Delta Q \end{bmatrix} = \begin{bmatrix} J_1 & 0 \\ 0 & J_4 \end{bmatrix} \begin{bmatrix} \Delta \delta \\ \Delta |V| \end{bmatrix} \qquad \text{(II.56)}$$

- The Eq. (II.56) can be expanded as:

$$\Delta P = J_1 * \Delta \delta \qquad \text{(II.57)}$$

$$\Delta Q = J_4 * \Delta |V| \qquad \text{(II.58)}$$

- Thus, Eqs. (2.57) and (2.58) take the following form :

$$\frac{\Delta P}{|V_i|} = -B'\Delta\delta \tag{II.59}$$

$$\frac{\Delta Q}{|V_i|} = -B"\Delta|V| \tag{II.60}$$

Where $[B']$and $[B"]$ are relevant imaginary parts of the Y-bus matrix elements. $[B']$ is related to the buses at which active power is scheduled (δ is unknown), and $[B"]$ is related to the buses at which reactive power is scheduled ($|V|$ is unknown).

- The diagonal elements of **J1** reconsidered by Eq. (II.45)may be written as :

$$\frac{\partial P_i}{\partial \delta_i} = \sum_{\substack{j=1 \\ j\neq i}}^{N} |V_i||V_j||Y_{ij}| \sin(\theta_{ij} + \delta_j - \delta_i) - |V_i|^2|Y_{ii}|\sin\theta_{ii} \tag{II.61}$$

- From Eq. (II.61), it can be written as:

$$\frac{\partial P_i}{\partial \delta_i} = -|V_i|B_{ii} \tag{II.62}$$

- The off-diagonal elements of **J1** as given by Eq. (II.62)may be written as :

$$\frac{\partial P_i}{\partial \delta_i} = -|V_i|B_{ij} \tag{II.63}$$

- The diagonal elements of **J4** reconsidered by Eq. (II.51) may be written as :

$$\frac{\partial Q_i}{\partial |V_i|} = -|V_i||Y_{ii}| \sin(\theta_{ii}) + \sum_{\substack{j=1 \\ j\neq i}}^{N} |V_i||V_j||Y_{ij}| \sin(\theta_{ij} + \delta_j - \delta_i) \tag{II.64}$$

$$= -|V_i||Y_{ii}| \sin(\theta_{ii}) + Q_i$$

- Eq. (II.64) is written as:

$$\frac{\partial Q_i}{\partial |V_i|} = -|V_i|B_{ii} \tag{II.65}$$

- Where the off-diagonal elements of **J4** are described by Eq. (II.52) may be written as :

$$\frac{\partial Q_i}{\partial |V_j|} = -|V_i|B_{ij} \tag{II.66}$$

- In the first decoupled power flow solutions, Eqs. (II.54) and (II.55) give the new bus voltage magnitudes, and estimated phase angles.

II.6. Electrical system structure and operation

The electrical system is a complex network, shown in Figure II.12, divided into four main parts: Generation, Transmission and sub-transmission, Distribution (Primary and secondary), and Customer (Loads) [16].

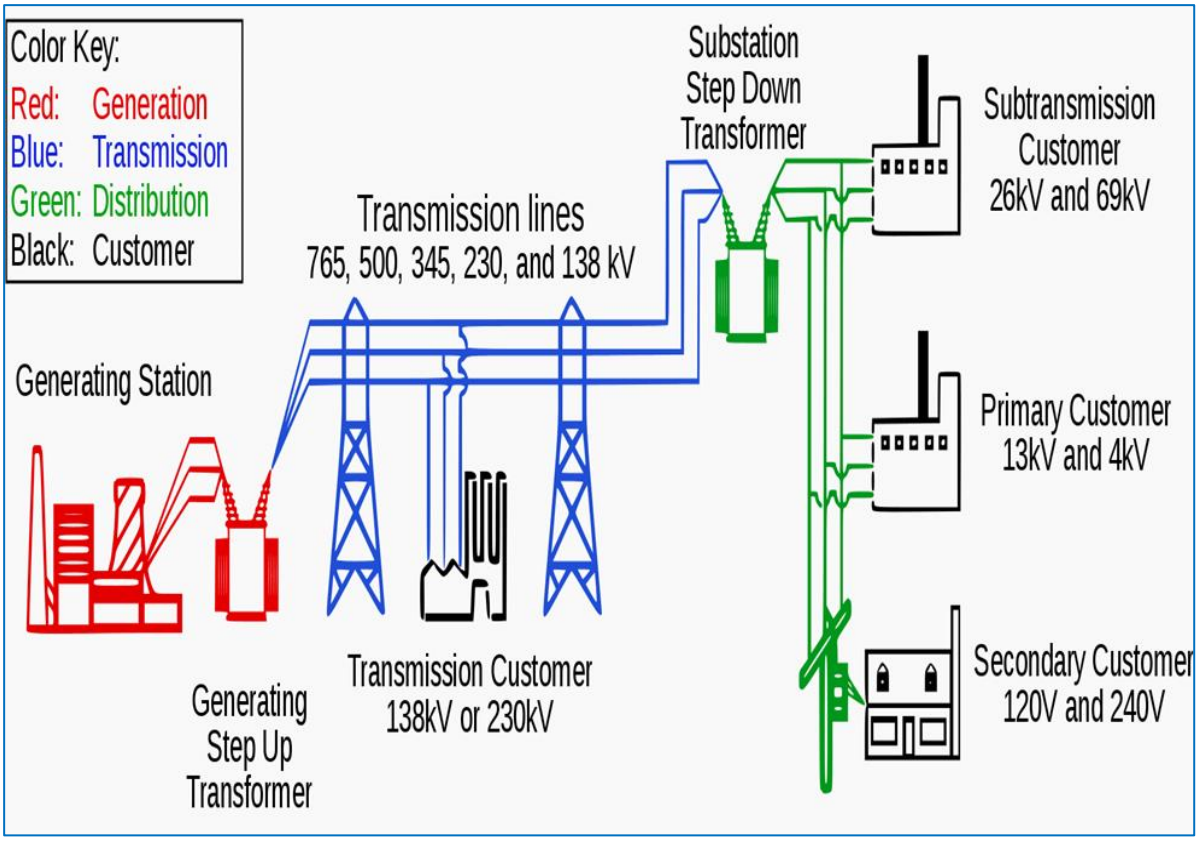

Figure II.12. Basic electrical system diagram [16]

II.6.1.Generation

Power plants convert the energy stored in fuel (mainly coal, oil, natural gas, or uranium) or renewable energy sources (such as water, wind, or solar) into electrical energy [17]. Large synchronous generators produce electricity in conventional power plants. Wind turbines use asynchronous generators, where the voltage waveform generated is not necessarily synchronised with the rotation of the generator. The integration of these power plants into an electricity system (Figure II.13) affects the electricity quality, which manifests itself in voltage fluctuations and network overloads. To overcome this problem, we use FACTS systems on the electricity network in the presence of renewable energies to improve its performance.

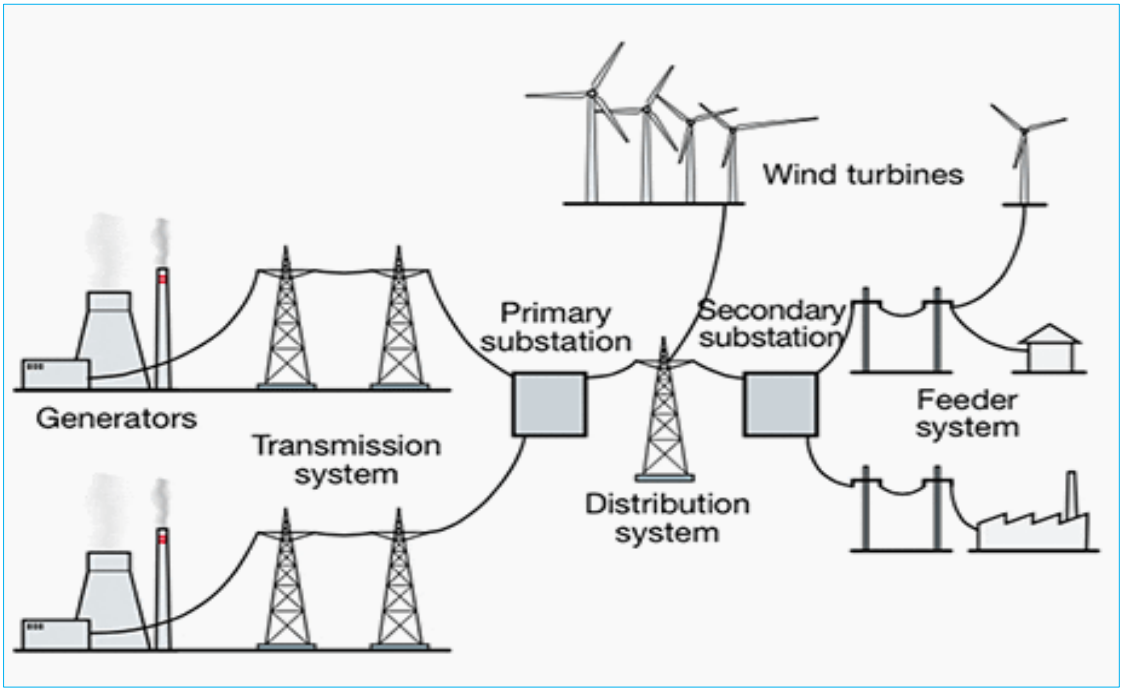

Figure II.13. Integration of wind turbines into the grid

II.6.1.1. Power plant types

A power plant, known as a power station, generation plant or production plant, is an industrial sector that produces and supplies electrical energy to consumers according to their needs. Production must always match demand (consumption + losses). Electricity is produced by converting a primary energy source (see Table II.1), whether chemical (fossil or non-fossil fuels), mechanical (hydraulic or wind), nuclear or solar, into electrical energy using a turbine and an alternator[17].

Tableau II. 1. Types of power plants

Power plant types	Subfamily	Primary source of energy	Primary energy
Thermal power plant	Flame thermal power plant -Conventional thermal	Coal, fuel oil, gas or biomass	Fossil or renewable
	- Combined cycle	Gas or fuel oil	Fossil
	Nuclear plant	Uranium or plutonium	Nuclear
	Geothermal power plant	Soilheat	Renewable
Solar power plant	Thermodynamic solar power plant	Sun	
	Solar thermal power plant		
	Photovoltaic solar power plant		
Hydroelectric power plant		Water (river)	
Tidal power plant		Water (tide, sea or river currents)	
Wind turbine plant		Wind	

II.6.1.2. production unit function

In a power plant as shown in Figure II.14, the electrical energy is generated by a synchronous generator (alternator), driven by a turbine. The generator is equipped with a governor to control the fluid flow (steam, gas or water) to the turbine by opening and closing control valves, and adjusting the speed or power output. An exciter supplies the DC excitation current needed to create the magnetic field inside the generator. The automatic voltage regulator (AVR) controls the excitation current and the generator output voltage. The step-up transformer increases the voltage for transmission to the grid, while the secondary transformer supplies auxiliary services within the power plant[12,18].

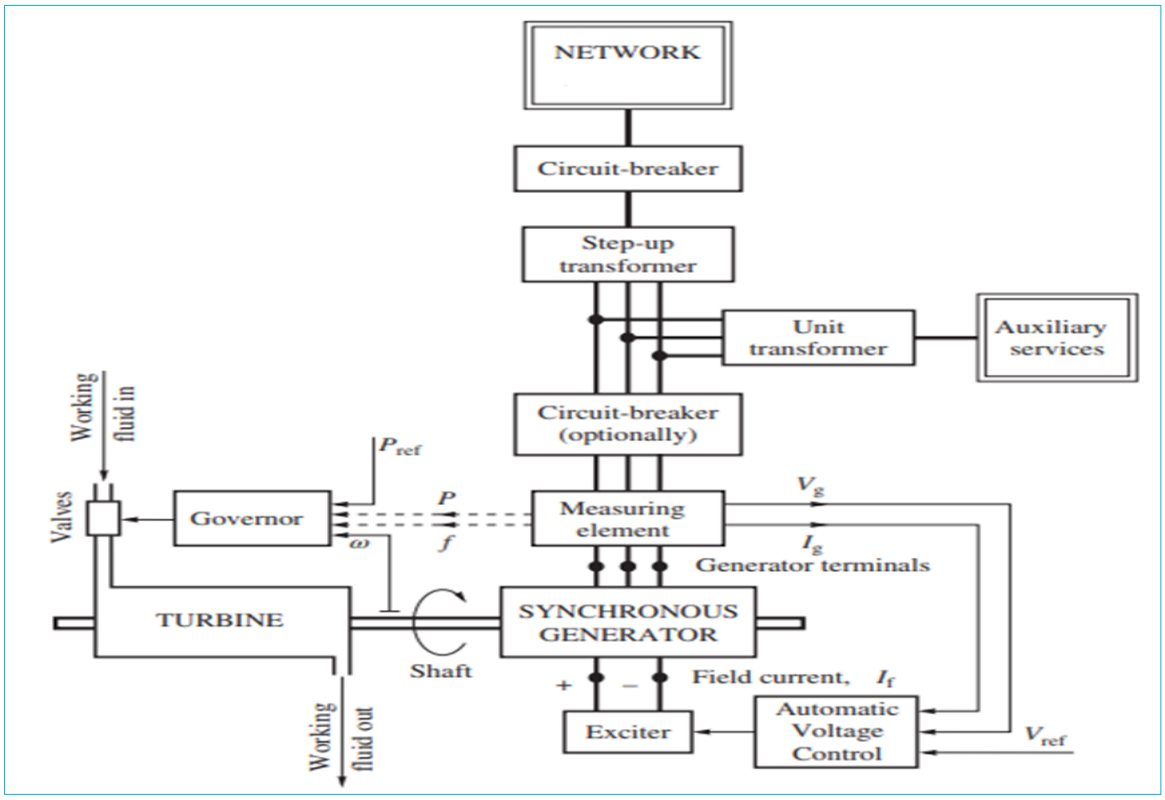

Figure II.14. Diagram of a power generation unit.

II.6.2. Transmission and interconnection

The electricity transmission network transports energy from major production centres to regions with high electricity consumption. Its structure is meshed or interconnected (Figure II. 15a), ensuring very high voltage and a high level of supply security. The transmission lines link neighbouring utilities, facilitating both the economic distribution of electricity within regions under normal conditions and the transfer of electricity between regions during emergencies. The high-voltage transmission lines end at receiving substations, which serve large industrial customers and distribution networks[19,20].

II.6.3.Distribution

The purpose of distribution networks is to supply all consumers. They function at two voltage levels[20]:

- Medium voltage (MV) networks consist of overhead networks, which are commonly found in rural areas with a tree structure (Figure II. 15b). These networks supply power to low-voltage (LV) networks where small consumers are connected. On the other hand, in urban areas, underground networks with double-branched or radial structures (Figure II. 15c), are used to ensure greater supply security.
- The low-voltage networks (120-240 V) provide electricity to domestic consumers.

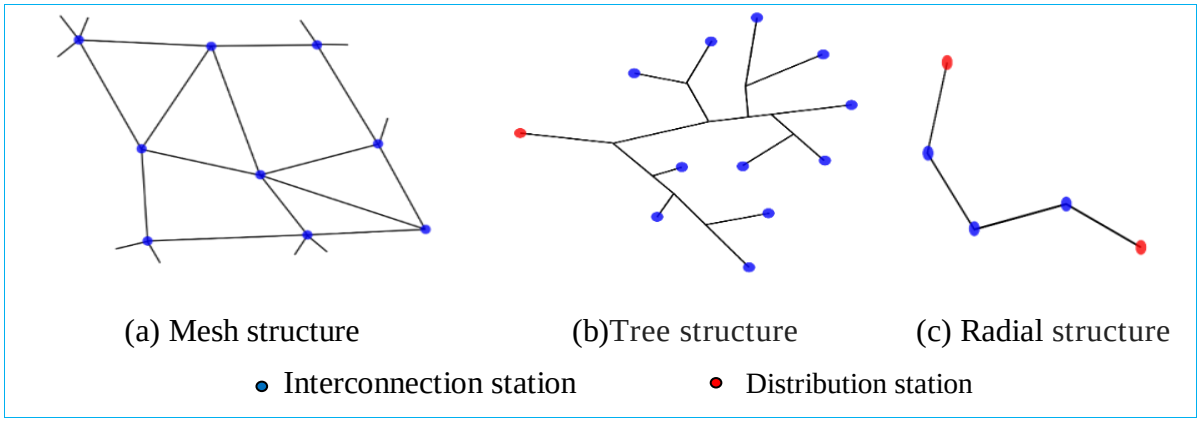

Figure II.15: Electrical network topologies

II.6. 4. Consumers (load)

The load on the electricity network is divided into industrial, commercial and residential sectors (see Figure II.12). The main substation provides power to large industrial consumers at 138 kV to 230 kV. The secondary substation (69 KV to 240 V) supplies large industrial, small commercial and residential consumers.

II.7.Conclusion

This chapter has introduced an overview of power system component modelling and iterative methods for solving the power flow problem, which is essential for efficiently managing and controlling power generation, transmission and load distribution. An overview of the structure and operation of an electrical network, covering the different subsystems from generation (power plants) has been defined. The next chapter will focus on integrating renewable energy sources with FACTS devices in the power system.

CHAPTER: III

Integration of Renewable Energy and SVC in Electrical Network

III.1.Introduction

The electricity grid is a network of interconnected infrastructures in which power lines connect different substations. This allows the electrical energy produced in power stations, such as wind or thermal power stations, to be transmitted to consumers through intermediate stages. Electricity production must always meet demand, which includes consumption and losses. In this chapter, we will examine global statistics on electricity generation and the structure of the electricity market in Algeria. We will also discuss the Algerian electricity grid and the country's renewable energy development program, focusing particularly on wind energy systems, including wind turbine components and their functions. We will delve into a double-fed induction generator model and various mathematical models related to wind energy, and investigate the technical and economic feasibility of incorporating wind power into the grid. Furthermore, we will provide an overview of the Flexible AC Transmission System (FACTS) devices, focusing on the configuration and modelling of the Static Var Compensator (SVC) to enhance the performance of the power system. These points are discussed below:

III.2. World electricity production statistics

The massive integration of renewable energy (RE) into the energy mix is a major challenge to conserve fossil resources, diversify the power generation sector, contribute to sustainable development, and limit carbon dioxide emissions. Ten countries, shown in Figure III.1, account for almost 80% of total renewable capacity growth in 2021-2026, with China leading at 43%, followed by the United States, India, and Germany[21].

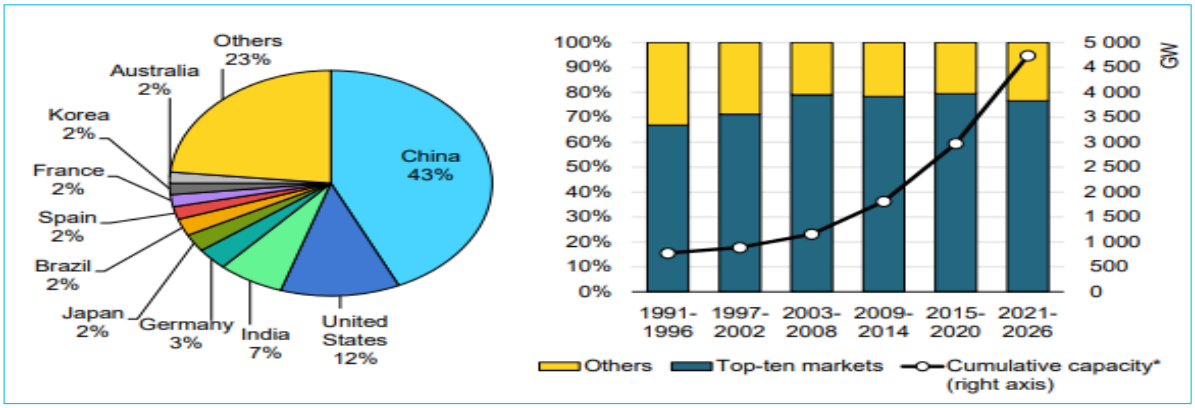

Figure III. 1. Installed renewable capacity by country

In other countries(23% in Figure III.1), such as Africa, many governments, including Morocco, Tunisia and Saudi Arabia, have also turned to renewable energy to reduce their consumption of fossil fuels. Figure III.2 illustrates the planned renewable energy capacity

installed in each country by 2020 and 2030.An analysis of each country's share reveals that Algeria is the least developed country, and has the smallest investments in this sector, despite having the greatest potential in renewable energy, especially solar energy. In 2011, Algeria aimed to generate 40% of its electricity from renewable sources by 2030 according to the government program. However, this target lowered to 27% in 2015[22].

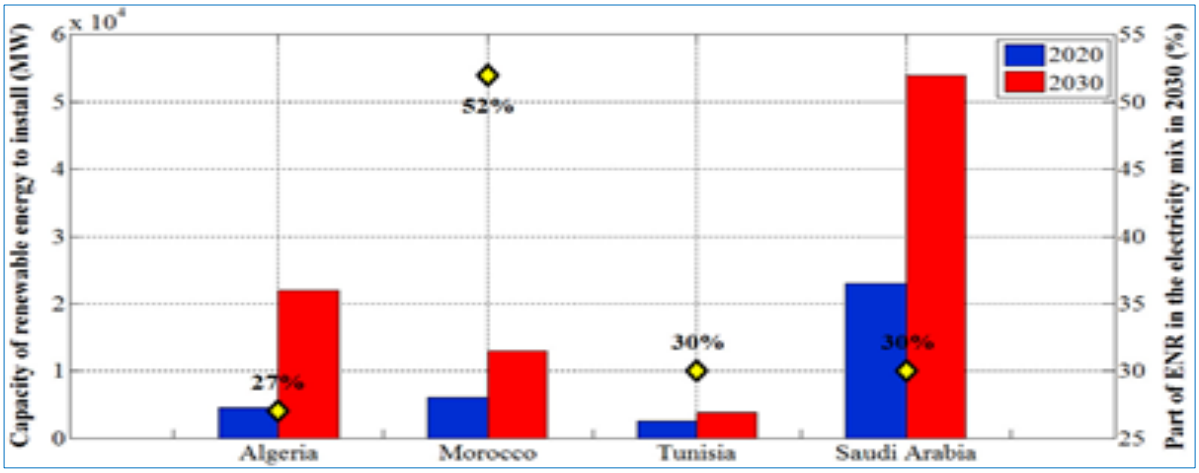

Figure III. 2. Planned electricity generation capacity by country

III.3. Algerian electricity market structure

The Algerian government has granted Sonelgaz a monopoly for the production, transmission and distribution of electricity and the marketing of natural gas[23]. The Algerian electricity market is divided into four segments (see Figure III. 3).

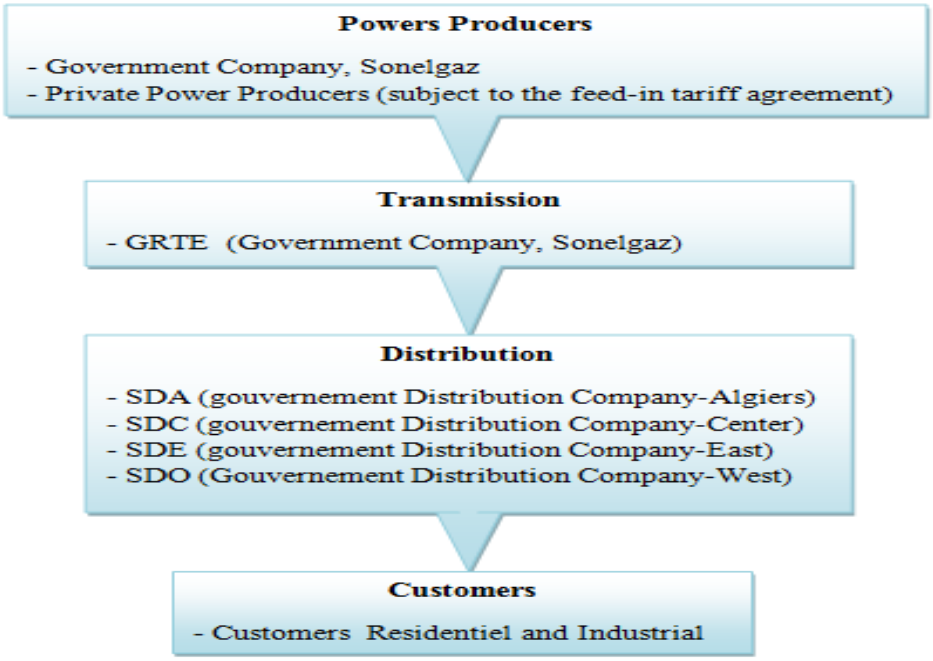

Figure III. 3. Structure of the Algerian electricity market.

III.3. 1. Powers producers

The main players in Algeria's electricity generation market are private and state-owned companies. However, private producers are subject to the Feed-in Tariff (FiT) agreement for solar PV and wind[23,24] in 2014, which is valid for 20 years (see Table III.1).

Table III.1. Feed-in tariffs for RE in Algeria

Source	Contribution	FiT(DZD/kWh)		FiT(USD/kWh)	
		First 5 Years	5 to15 Years	First 5 Years	5 to 15 Years
Wind	<5MW	13.10	9.55 – 16.66	0.098	0.072 – 0.13
	>5MW	10.48	7.64 – 13.33	0.079	0.057 – 0.10

The national electricity Park comprises power plants operated by the Algerian Electricity Production Company (SPE) and its partners, including Kahrama Arzew, Shariket Kahraba Skikda "SKS"; Shariket Kahraba Berrouaghia"SKB", Shariket Kahraba Hadjret Ennouss "SKH"; Shariket Kahraba Terga SKT"; Shariket Kahraba Koudiet Edraouch "SKD" [25,26].

III.3.2. Transmission system operator

The Transmission Network Operator (GRTE) operates, maintains, and develops Algeria's electricity transmission network to ensure adequate electricity capacity for transit, reserve requirements, and interconnection with neighbouring countries[27], as shown in Figure III. 4.

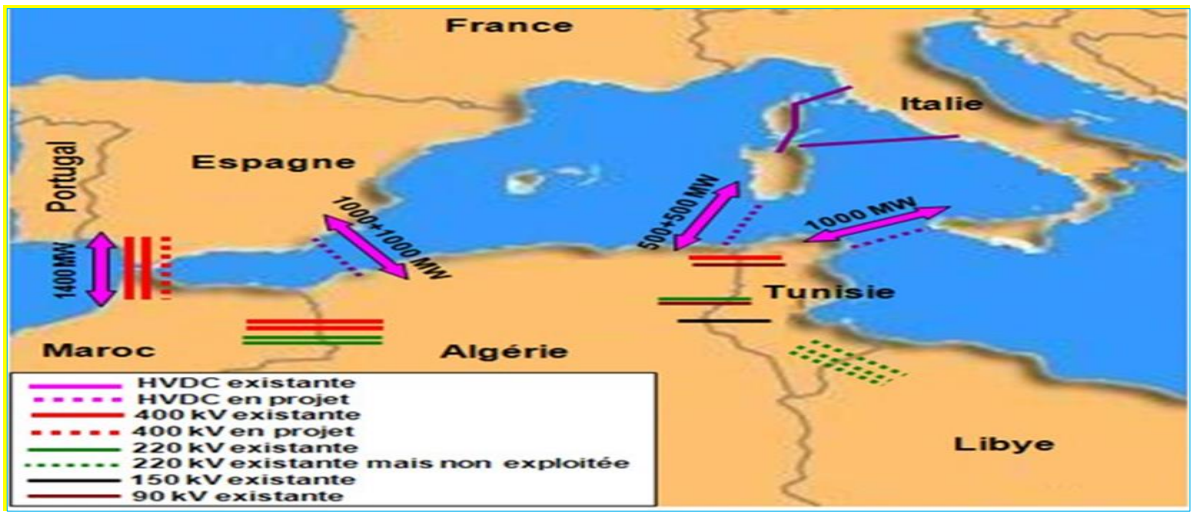

Figure III. 4. Electricity interconnections between Algeria and its border countries

III.3. 3.Distribution companies:

There are four (04) Regional Distribution Companies (SDA, SDC, SDE, and SDO), each responsible for two tasks: managing the distribution network and selling electricity to different types of customers (residential and industrial).

III.4. Algeria electrical network description

Algeria's electricity network comprises three main grids, as seen in Figure III.5[2,28]:

- The National Interconnection Network (**RIN**) comprises 40 power plants connected by 400 kV and 220 kV transmission lines. This network supplies electricity to northern Algeria and regions including Béchar, Hassi Messaoud, Hassi R'Mel, and Ghardaïa, as well as to the In Salah-Addar-Timimimoun Pole (**PIAT)** and the Isolated Southern Networks (**RIS)**.
- The **PIAT** is an interconnected network of 28 power plants, mostly gas turbines, with a 220 kV capacity covering large areas in the country's southwest.
- The **RIS** is a group of isolated power plants spread over 26 locations in central and southern Sahara. This electricity network covers remote areas far from the main networks.

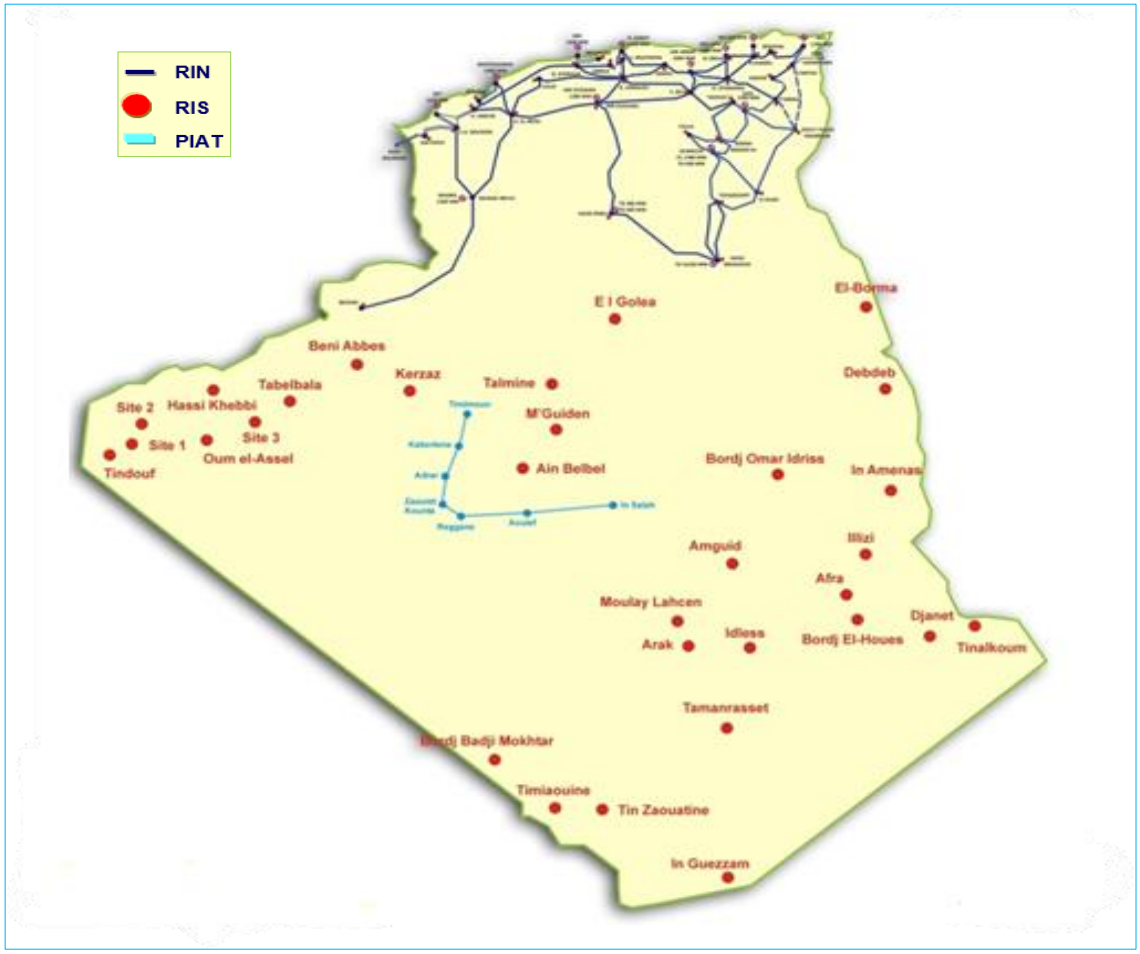

Figure III. 5. Algerian electricity networks

III.4. 1. Algerian electricity production

Electricity production in Algeria is managed by SONELGAZ, which supervises the maintenance and operation of its power plants (see Figure III. 6). It has an installed capacity of over 18GW and plans to reach around 23GW by 2030[29].

Algeria's power plants are subdivided into four sectors based on power levels: steam turbines (ST), mobile or fixed gas turbines (GT), hydraulic turbines (HT), and combined cycle (CC). The following table summarises the power stations in the national power generation park[2,26,30].

Table III.2. Algerian electric power stations

Region	Location	Type	Power (MW)	Region	Location	Type	Power (MW)
Alger	Algier port	GT	72	El oued	Guemar	GT	184
	Hamma2	GT	418	Laghouat	Tilghemt 1.3	GT	791
	Bab Ezzouar	GT	108	HassiR'mel	H.R.North	GT	88
	Hamma	GT	48		Tilghemt 2	GT	368
	Baraki	GT	72	Ghardaia	Ghardaia	GT	17
	Sablette	GT	100	Bechar	Bechar	GT	24
Mostaganem	Sonaghter	CC	1450	Adrar	Adrar 1.2	GT	231
	Larbaa	GT	560		Timimoun	GT	192
	Boufarik 1.2.3	GT	849		Kabertene	GT	46
	Beni Mered	GT	48		Z.Kounta	GT	192
Tipaza	Ahmer El Ain	GT	72	Tamanrasset	In Salah 1.2	GT	99
	HadjretEnous	CC	1227	Chlef	Oued Fodda	HT	15.6
Boumerdes	Ras Djinet	ST	672	Khenchela	Labreg	GT	420
	Ras Djinet	CC	1131		Kais	CC	1266
Bejaia	Amizour	GT	184	Médéa	Berrouaghia	ST	500
	Darguina	HT	71.5	Timimoun	Timimoun	GT	102
	Toudja	HT	08	Djelfa	Ain ouessara	CC	1262
Oran	Marsat	ST	840	El Meniaa	El-Goléa 1.2	GT	205
	Ravin Blanc	ST	73	Setif	Ain Arent	CC	1015
	Oran East	GT	80	Naama	Naama	GT	184
	Marsat	GT	184		Méchria	CC	1163
	Boutlelis	GT	446	Jijel	Bellara	CC	1398
	Messerghine	GT	400		Jijel	ST	588
Relizane	Relizane	GT	465		Manouriah	HT	100
Tiaret	Tiaret 1 .2	GT	420	Mila	Tessala	HT	4.2
Skikda	Skikda	ST	262	Annaba	Annaba	GT	72
Mascara	Bou Hanifia	HT	15.5	AïnDefla	Oued Cherfa	HT	07
Taref	Koudiet Edderaouch	CC	1200	Oum El Bouagui	F'kirina 1.2	GT	392
Ain Temouchent	Terga	CC	1200	Ouargla	H. Massoud south	GT	72
Tizi Ouzou	Gouriet	HT	6.5		H.M.West	GT	492
	Tizi Meden	HT	4.40		H.M.North 1.2.3	GT	980
	Ighzernchebel	HT	03		Ouargla	GT	96
M'sila	M'sila 1.2.3.4	GT	1064	Biskra	Oumach 1	CC	1338
Batna	Ain Djasser 1.2.3	GT	793.5		Oumach 2	GT	457

Figure III. 6. Electrical energy production sites in Algeria

III.4. 2. Algerian electric transmission network

Algeria's electricity generation and transmission network structure comprises various generation plants, high-voltage substations and transmission lines (see Appendix C). The transmission and interconnection networks connect the generating units to the consumers (industrial and domestic) via the distribution network (MV and LV). The most commonly used voltage levels are 400 kV/220 kV for transmission, 60 KV for dispatch and 30 kV/380 V for distribution, at 50 Hz frequency[2,31].

III.4. 3. Transmission lines

Transmission line design; is based on factors such as transmission power, distance, cost and ease of installation. To enhance network stability and increase the power transmitted, compensation devices are added to each type of transmission line as follows:

- Overhead lines are made of conductors, insulators, and supports to transmit power in high-voltage systems via pylons (see Figure III. 7)

- Underground cables commonly used in low and medium-voltage urban distribution networks. They are limited to specific circumstances, such as densely populated urban areas, major river crossings or areas with major environmental problems[2,20].

- High Voltage Direct Current (HVDC) overhead lines, as well as underground and submarine cables, are essential technologies for the long-distance transmission of renewable electrical power, offering high efficiency and low losses[27].

(a) Overhead lines

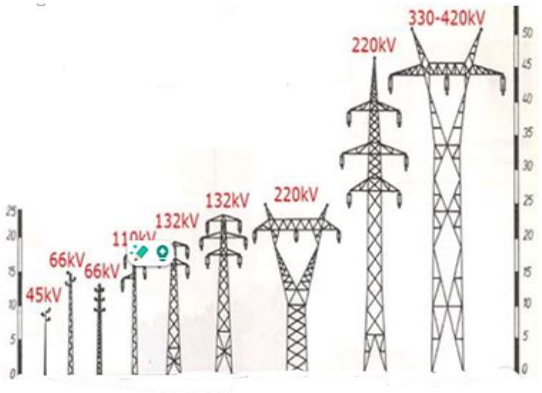

(b)Pylone types

Figure III. 7. Transmission systems

III.5. Algeria renewable energy development

Algeria, a leading producer of natural gas and oil, is also one of Africa's largest CO2 emitters, with total emissions projected to reach more than 193 Mt by 2030[32] (Figure III. 8). To tackle this and meet its energy needs, Algeria launched an ambitious renewable energy development program in February 2011(see Figure III. 9)[22]. The program aims to install around 22,000 MW of renewable energy (RE) for domestic use by 2030 (see Figure III. 10), while also exploring export opportunities, depending on market conditions, to offer sustainable solutions to environmental challenges and preserve fossil energy resources[33].

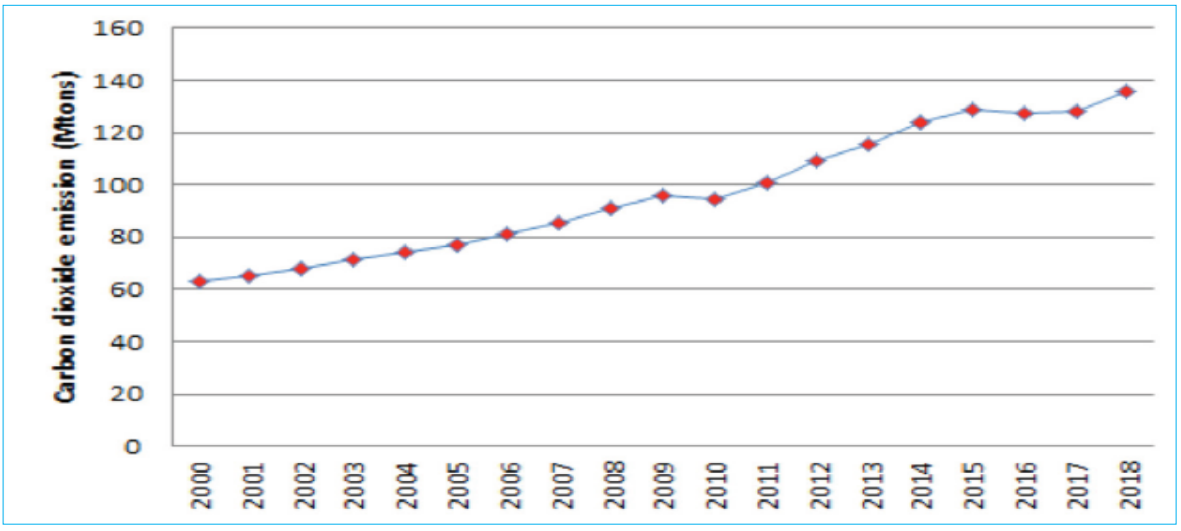

Figure III. 8. Evolution of CO2 emission in Algeria

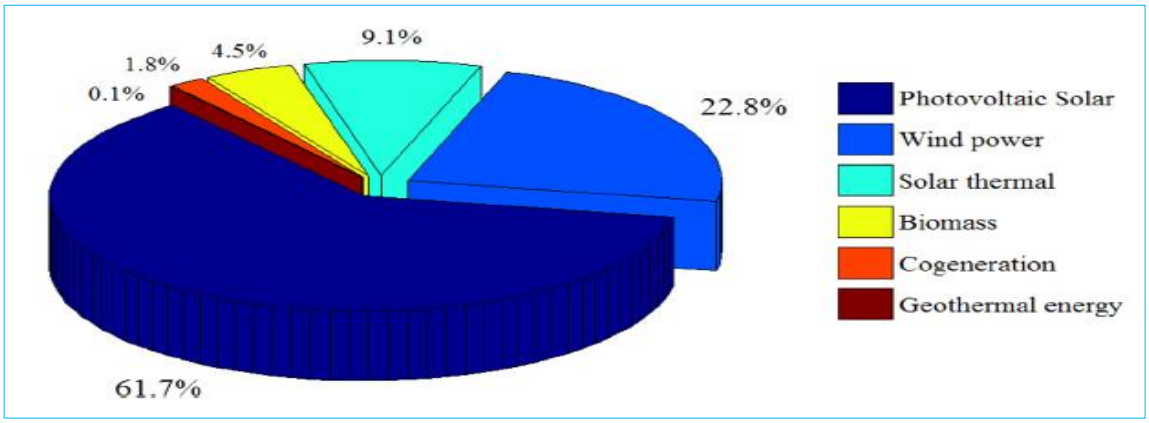

Figure III. 9. Distribution of renewable energy development program

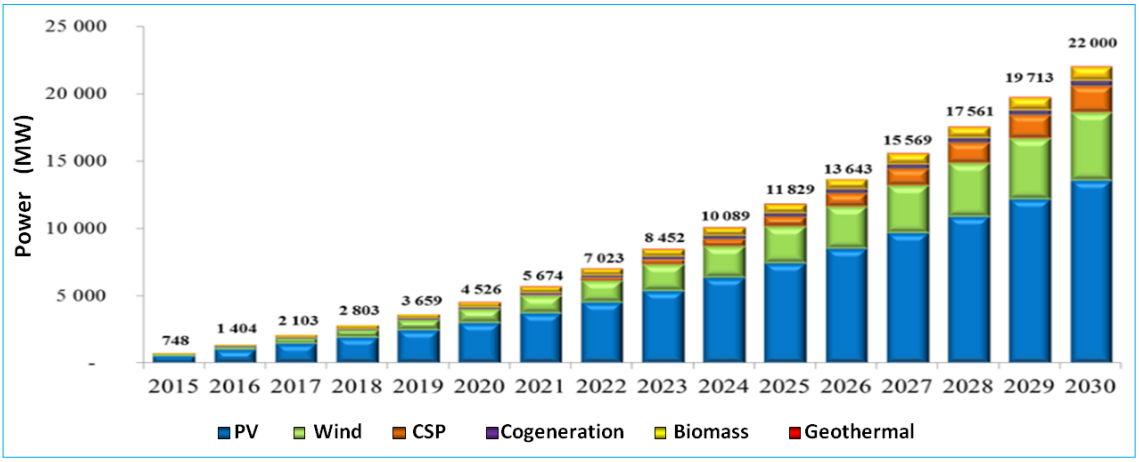

Figure III. 10. Installed renewable energy capacity by 2030

III.5. 1. Renewable energies program

Renewable energy in Algeria, particularly solar power, is vital for economic and social development. Additionally, Algeria has launched various wind power projects and experimental projects in biomass, geothermal, and cogeneration. Renewable electricity production projects for the national market were implemented in two stages[22,33], detailed in Table III.3.

TableIII.3. Electricity production program

Renewable energies (MW)	First phase 2015-2020	Second phase 2021-2030	Total (MW)
Photovoltaic (PV)	3 000	10 575	13 575
Wind	1 010	4 000	5 010
Concentrating solar power (CSP)	-	2000	2 000
Cogeneration	150	250	400
Biomass	360	640	1 000
Geothermal	05	10	15
Total (MW)	4 525	17 475	22 000

III.5. 2.Renewable energy potential in Algeria

Algeria has abundant sources of renewable energy (RE), including hydroelectricity, solar energy, wind energy, geothermal energy and biomass, described below[28]:

III.5.2.1. Solar potential

Solar resources in Algeria are among the largest in the world (Figure III. 11a). It enjoys more than 2,000 hours of sunshine a year, with some regions, such as the high plateaux and the Sahara, reaching up to 3,900 hours. Annually, the energy received on a horizontal surface of 1m² is around 3 kWh/m² in the north and more than 5.6 kWh/m² in the far south.

III.5. 2.2. Hydraulic potential

Algeria has great potential for hydroelectric power generation, with 103 dam sites identified and over 50 dams currently operational due to the high rainfall of 65 billion cubic metres per year. Most of them are in northern Algeria[24,28,33] (see Figure III. 11b).

III.5. 2.3. Geothermal potential

More than 240 hot springs are in northern Algeria, identified by geological, geochemical, and geophysical data (see Figure III. 11c). Around 33% of these sources have temperatures above 45°C, with the highest temperature being 118°C in Biskra. Thermal gradient studies have identified areas greater than 5°C/100m, such as Relizane, Mascara, Aïne Boucif, SidiAïssa, Guelma and Jebel El Onk.

III.5. 2.4. Bio-power potential

Algeria possesses a wealth of diverse bioenergy resources, making it essential to assess these resources, particularly biomass, to foster the growth of this sector. The country's potential for generating electricity from bioenergy includes both domestic biomass and solid waste, as summarized in Table III.4.

TableIII.4. Potential bio-power in Algeria.

Bio-power resources		Potential energy(GWh)
Agribusiness and industry waste	Amurca available from the olive oil industry	17.74
	Pomace available from the olive oil industry	215.5
	Whey available from the dairy industry	3.97
Urban waste	The organic fraction of household waste	1646
	Sewage from waste water treatment plants	38.72
Total		1706.43

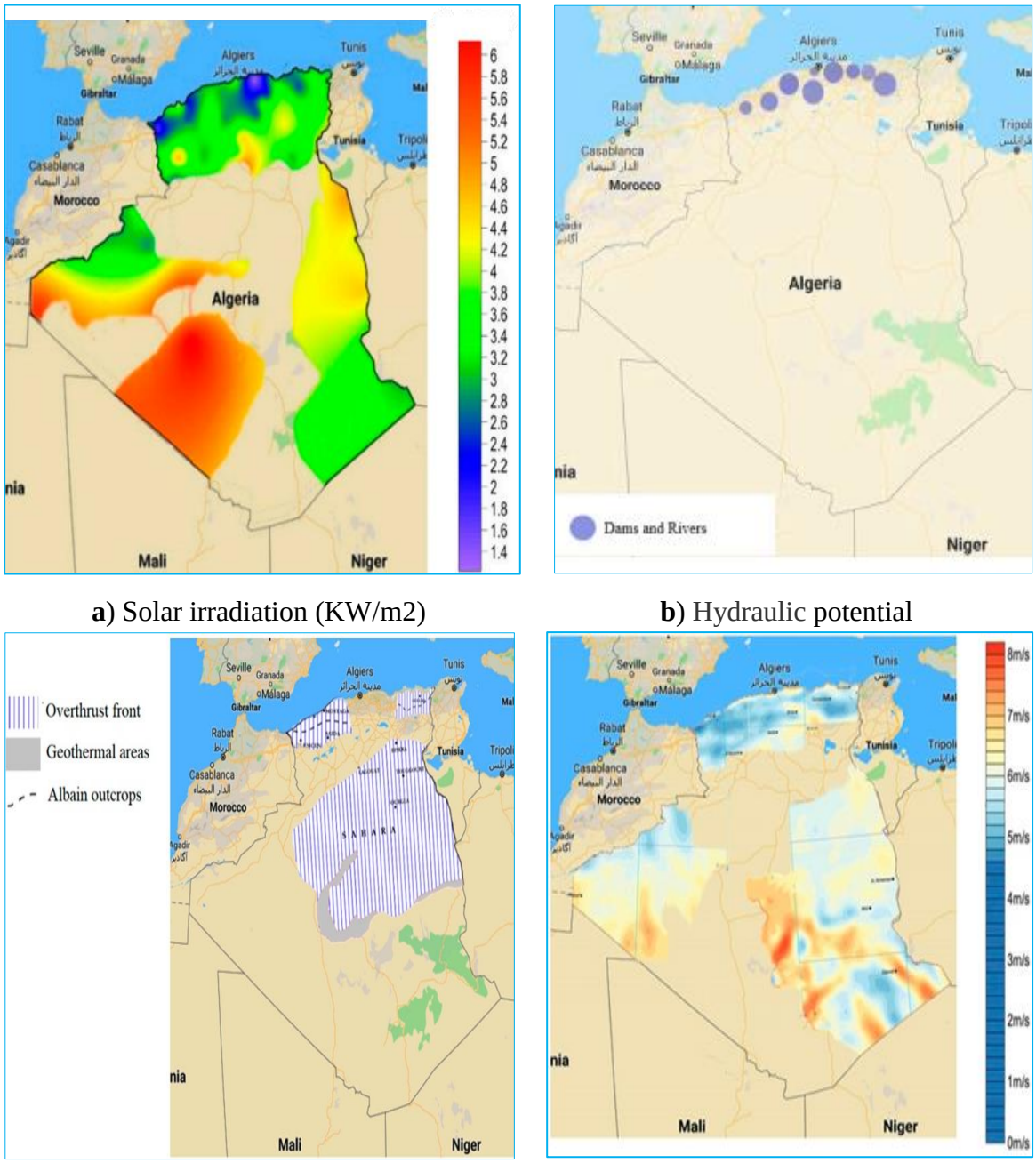

a) Solar irradiation (KW/m2) **b**) Hydraulic potential

c) Geothermal potential **d**) Average annual wind speed potential

Figure III. 11. Algeria RE potentials

III.5. 2.5. Wind potential

Algeria has diverse wind resources due to its varied topography and climate, divided into the Mediterranean north and the Saharan south (Figure III. 11 d). Wind speeds are higher in the south, particularly in Tamanrasset (Amguel), where they can exceed 7-8 m/s. In the north, average wind speeds are generally low, but microclimates in coastal areas like Oran, Bejaïa, and Annaba, as well as on the highlands plateaus of Tébessa, Biskra, M'sila, and El Bayadh, experience speeds of 6 to 7 m/s, with the far south exceeding 8 m/s.

III.6. Wind power systems

Wind power systems play a crucial role in exploiting wind resources, producing clean, sustainable electricity with minimal greenhouse gas emissions.Wind turbines are essential for reducing dependence on fossil fuels and addressing climate change. This section presents the components, functions and technologies associated with wind turbines.

III.6.1. Wind power plants history

In the last two decades, wind power has emerged as one of the cleanest and most affordable forms of energy. The first working wind turbine was installed by James Blyth in Scotland in 1887, and in 1888, Charles Brush set up the first large-scale wind turbine for electricity production in Cleveland, Ohio. European countries continued to advance wind turbine technology from the early 20th century onwards[34]. In Algeria, the first attempt to connect wind turbines to the power grid occurred in 1957 (Figure III. 12a) by installing a 100 KW wind turbine at the Grand Vent site (Algiers), designed by the French engineer ANDREAU. It was later purchased by SONELGAZ and reinstalled in Algeria[35]. In 2014, Algeria's first wind farm was installed, with 12 wind turbines (10 MW) connected to the local grid[28], serving the regions of Adrar, In Salah, and Timimoun (Figure III. 12 b).

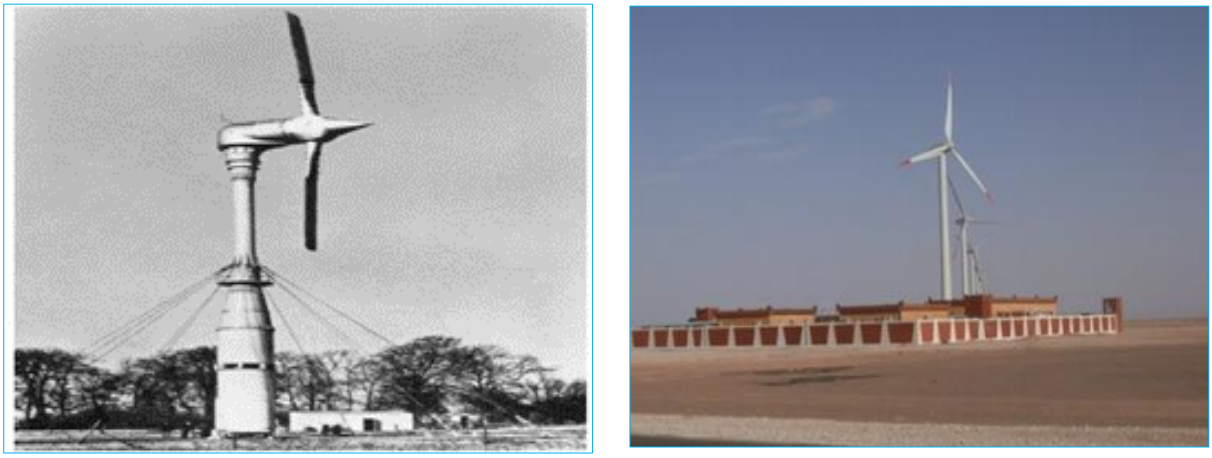

a) Wind turbine in 1957 **b)** Wind turbines farm (Kaberten)in 2014

Figure III. 12. Wind turbines installed in Algeria

III.7.2. Wind turbine components and functions

A wind turbine converts the wind's kinetic energy into mechanical energy to produce electricity (see Figure III. 13). It consists of five main components: the tower, rotor, nacelle, generator, and foundations or base, along with several auxiliary parts[3,36].

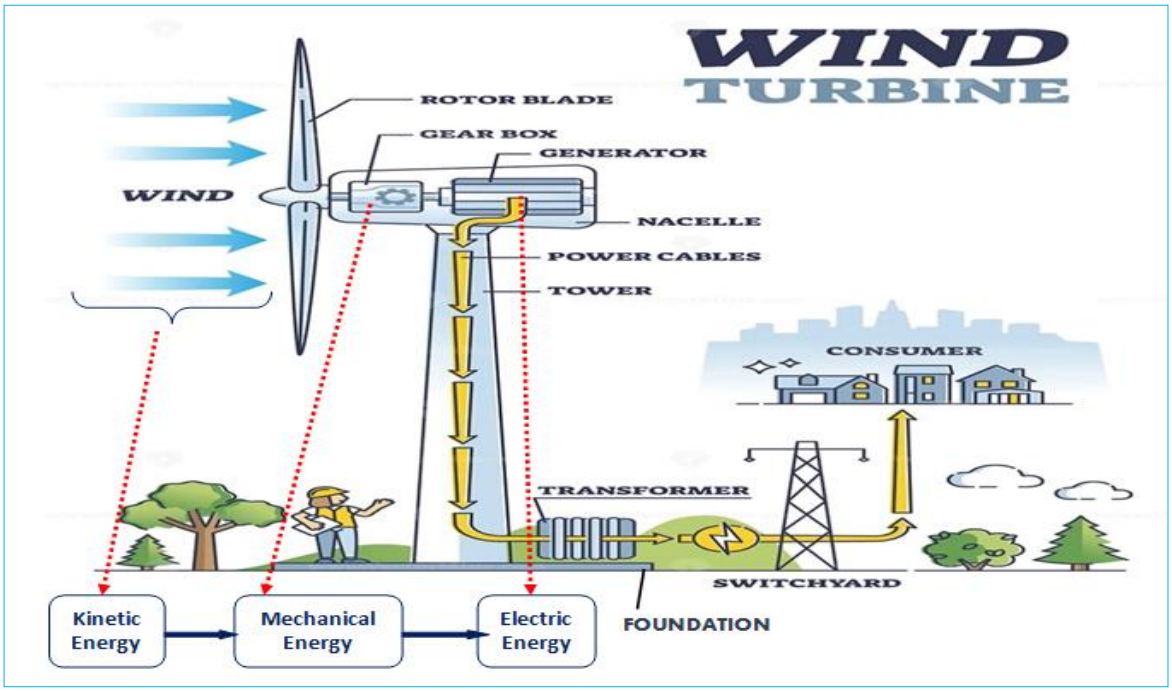

Figure III. 13. Wind energy conversion principle

- **Foundation:** Wind turbine foundations support the turbine and its forces. Onshore wind turbines have a large textured concrete block under the ground, while offshore wind turbines have an underwater or floating foundation.
- **Tower:** This structure supports the turbine and raises it to a greater height where wind speeds are more consistent and higher. Taller towers provide turbines with more powerful and steady winds, increasing overall energy production.
- **Nacelle**: a casing at the top of the wind turbine tower that houses important components, including the generator and the turbine shaft, which transfers the energy from the wind to the generator via a gearbox.
- **Generator**: synchronous or asynchronous (induction), convert the wind's mechanical energy into electrical energy via the rotor and are structured as electric motors.
- **Rotor**: the rotating part of the wind turbine comprises three blades attached to a hub, connected to the main wind turbine shaft, which is driven by a generator.
- **Gearbox**: increases the speed of the shaft to produce electricity from the mechanical energy of the turbine. The electric current generated flows through the cable inside the turbine tower.
- **Step-up transformer**: converts electricity into a higher voltage for transmission to the electrical grid.

III.6.3.Wind turbine technologies

There are two main configurations of wind turbines, as shown in Figure III. 14, the horizontal axis turbine (Danish wind turbine), and the vertical axis turbine (Darrieus

rotor)[37].Most large modern wind turbines have a horizontal axis and are used primarily to generate electricity.There are three main types of wind turbines [18,34]:

- Fixed-speed wind turbines, typically using an asynchronous cage generator, directly connected to the grid and always consume reactive power. Capacitor banks or other reactive power compensators can offset some or all of this undesirable reactive power.
- Variable-speed wind turbines controlled by the stator using static converters. These wind turbines can have asynchronous generators with induction cages and synchronous machines with wound rotors or permanent magnet machines.
- Variable speed wind turbine with a doubly fed induction generator (DFIG) rotates at varying speeds.

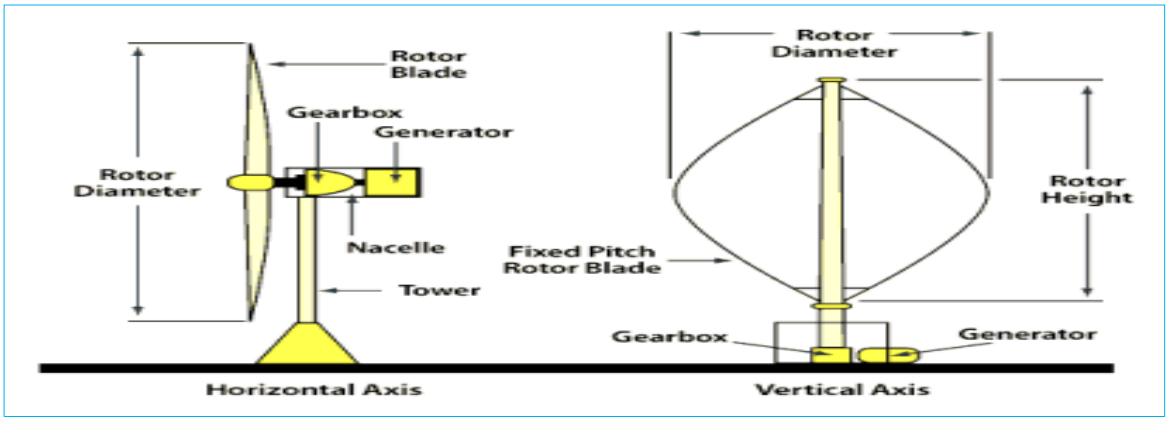

Figure III. 14. Horizontal and vertical axis wind turbines

III.6.3.1. Modelling a double-fed induction generator

The double-fed induction generator (see Figure III. 15) is the most widely used technology in the wind turbine industry due to its superior performance, high-energy transfer efficiency, and flexible control, including decoupled control of active and reactive power[18].

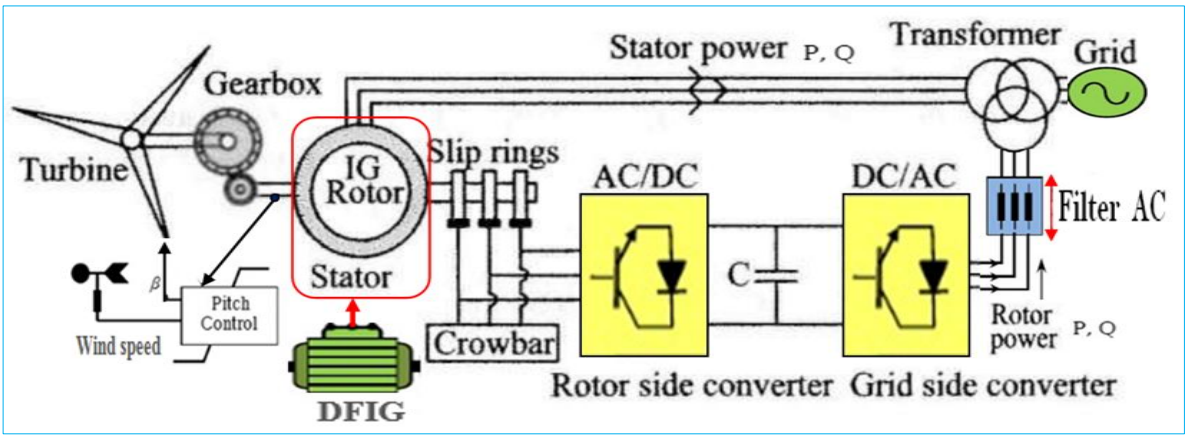

Figure III. 15. An overview of the wind turbine with DFIG.

The generator connects to the wind turbine via a **gearbox** to match the low speed of the wind turbine to that of the generator. The generator stator directly linked to the grid through a **transformer**, while the rotor windings are **via slip rings**, back-to-back voltage source converters, and a transformer. This setup delivers energy to the grid from the stator and the rotor. Power electronic converters enable the DFIG to operate at optimal rotor speed and maximise power generation by controlling the active and reactive power injected into the grid at a constant voltage frequency. During external grid faults, voltage drops can cause excessive currents in the stator and rotor. The rotor is short-circuited using a **crowbar**, allowing the wind farms to continue operating during these voltage drops. New turbines feature **pitch control** to adjust blade angles and maximise power output without overloading the generator and mechanical structures.[34,36].

III.7. Mathematical modelling of wind power

III.7. 1. Wind power generation

Wind energy is generated via wind turbines or windmills. The kinetic energy in the moving air is transformed into mechanical energy by the turbine blades, which is then converted into electrical energy by the generator. The kinetic energy (K_{Ew})of air particles with mass ($m = A\rho v^2$), speed (**v**), and time (**t**) can be written as[18,34,38]:

$$K_{Ew} = \frac{1}{2}mv^2 \qquad \Longrightarrow \qquad K_{Ew} = \frac{1}{2}A\rho v^3 t \tag{III.1}$$

Since power is energy per unit of time, the blade of the turbine captures only part of the available wind energy; then the theoretical wind power(P_{aw}) is given as follows:

$$P_{aw} = \frac{K_{Ew}}{t} = \frac{1}{2}A\rho v^3 \tag{III.2}$$

The power in the wind varies as the cube of wind speed, but unfortunately, the blade of the turbine can only extract a fraction of the available wind energy, and the actual power extracted by a wind turbine (P_{wr}) is given below:

$$P_{wr} = \frac{1}{2}\rho A v^3 C_P \qquad \Longrightarrow \qquad P_{wr} = P_{aw} * \mathbf{C_P} \tag{III.3}$$

Where **ρ** is air mass density, '**A**' = π $r^2$is the blade swept area, '**r**' is the radius of the area swept, and '$\mathbf{C_P}$' is the coefficient of performance or power coefficient known as Betz, Limit. The German engineer Betz showed that the maximum mechanical energy that can extracted from the kinetic energy is not more than 59.3%. Figure III. 16 shows wind energy production in four different zones as follows:

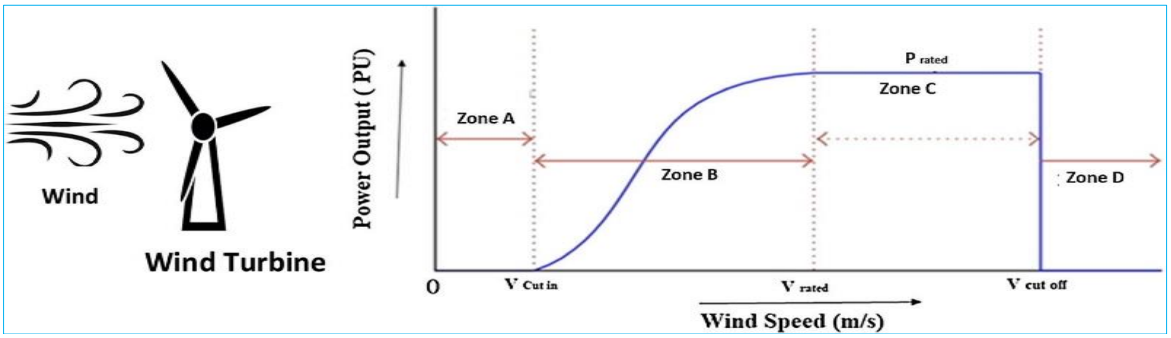

Figure III. 16. Wind turbine curve

- In zone A, wind power generation is zero because the wind speed is lower than the cut-in speed, which is the speed at which the turbine starts to generate power.
- Zone B is the range between the cut-in and the rated speed, where the generated power increases rapidly, reaching the rated output power capacity at Vrated.
- Zone C refers to the range between Vrated and cut-off speed, at which constant output power is achieved. Vcut-off is the maximum allowable speed for power generation.
- Zone D is where the turbine stops above the Vcut-off speed to prevent damage caused by high winds.

III.7. 2. Wind speed modelling:

III.7.2.1. Weibull distribution function

Weibull and Rayleigh functions are two common ways to describe wind speed data. The Weibull function is part of a more complex distribution, while the Rayleigh function is simpler. We will often use the Weibull probability distribution function (PDF) in wind power engineering to model the variation in wind speed[1]. Its probability density function fv (v) is given in Eq. (III.4), while the cumulative distribution function (CDF) is defined in Eq. (III.5).

$$f_v(v) = \frac{k}{c}\left(\frac{v}{c}\right)^{k-1} * e^{-(v/c)^k}, \quad v > 0 \tag{III.4}$$

$$F(v) = 1 - e^{-(v/c)^k}, \quad v > 0 \tag{III.5}$$

Where **v** is a random wind speed variable, **k** is the dimensionless shape factor of the Weibull distribution, and **c** is the scale factor with the unit m/s.

III.7.2.2. Weibull parameters calculation method

Various numerical models exist to calculate Weibull parameters.Our study uses the Justus method to determine (k_0-c_0) values based on wind speed at 10 m height. These values can be used for sites with different variability.The shape and scale parameters based on the mean wind speed are determined using the following equations:

$$k_0 = \begin{cases} 1.05 * (v_m)^{0.5} \rightarrow (\text{low}) \\ 0.94 * (v_m)^{0.5} \rightarrow (\text{average}) \\ 0.83 * (v_m)^{0.5} \rightarrow (\text{high}) \end{cases} \quad \text{(III.6)}$$

$$c_0 = \frac{v_m}{\Gamma\left(1 + 1/k_0\right)} \quad \text{(III.7)}$$

- Equation(III.8) adjusts the parameters ki and ci of the Weibull equation for each hub of the wind turbine hi relative to the standard hub height h0 using the method of Justus and Mikhail:

$$\begin{cases} k_i = k_0 * \dfrac{1 - 0.088 \ln(h_0/10)}{1 - 0.088 \ln(h_i/10)} \\ c_i = c_0 * \left(\dfrac{h_i}{h_0}\right)^z \\ z = \dfrac{[0.37 - 0.088 \ln(c_0)]}{[1 - 0.088 \ln(h_0/10)]} \end{cases} \quad \text{(III.8)}$$

- The extrapolated average wind speed for different turbine hub heights h_i ; using the following equation:

$$\frac{v_i}{v_0} = \left(\frac{h_i}{h_0}\right)^{\alpha} \quad \text{(III.9)}$$

Where $\boldsymbol{\alpha}$ varies from 0.05 to 0.5. The most commonly assumed value is 0.143 or 1/7, applicable to low-roughness surfaces. It can be determined using the following expression:

$$\alpha = \frac{[0.37 - 0.088 \ln(v_0)]}{[1 - 0.088 \ln(h_0/10)]} \quad \text{(III.10)}$$

III.7.2.3.Wind power output based on wind speed

The power output of a wind turbine depends primarily on two factors: the wind speed at the site and the parameters of the power curve. Once the Weibull probability density function has been generated, the wind power output can be calculated using a specific equation[3]:

$$P_w(v) = \begin{cases} 0\,, & \text{for } v \leq v_{in}\,, \text{ and } v \geq v_{out} \\ P_{wr} \times \left(\dfrac{v - v_{in}}{v_r - v_{in}}\right) & \text{for } v_{in} \leq v \leq v_r \\ P_{wr}\,, & \text{for } v_r \leq v \leq v_{out} \end{cases} \quad \text{(III.11)}$$

Where $\mathbf{P_{wr}}$ is the Power rating of the wind turbine and can be determined using Eq. (III.3).

III.8.2.4.Wind power probability for variable wind speeds

a) Discrete portions of the wind power

For the distinct portions of the wind power output defined by Eq. (III.11), the probability of generating power is zero ($P_r\ \{P_w = 0\}$) when **v** is less than v_{in} and greater than v_{out} ($v \le v_{in}$, and $v \ge v_{out}$). Similarly, the probability of $P_r\ \{P_w = P_{wr}\}$ if the condition $v_r \le v \le v_{out}$ is met, the wind turbine generates P_{wr}[3,39]. We can calculate the probability for this zone from Eqs. (III.12) and (III.13).

$$f_w(P_w)\{P_w = 0\} = 1 - \exp\left(-\left({}^{v_{in}}/_{c}\right)^{k}\right) + \exp\left(-\left({}^{v_{out}}/_{c}\right)^{k}\right) \quad \text{(III.12)}$$

$$f_w(P_w)\{P_w = P_{wr}\} = \exp\left(-\left({}^{v_r}/_{c}\right)^{k}\right) + \exp\left(-\left({}^{v_{out}}/_{c}\right)^{k}\right) \quad \text{(III.13)}$$

b) Continuous portion of the wind power

In contrast to discrete regions, wind power generation is continuous when $v_{in} \le v \le v_r$. Therefore, we can describe the probability density function (PDF)for this condition as follows:

$$f_w(P_w) = \frac{k(v_r - v_{in})}{c^k * P_{wr}}\left[v_{in} + \frac{P_w}{P_{wr}}(v_r - v_{in})\right]^{k-1} \exp\left[-\left(\frac{v_{in} + \frac{P_w}{P_{wr}}(v_r - v_{in})}{c}\right)^{k}\right] \quad \text{(III.14)}$$

III.8. Integration of wind power into the grid

Wind energy is an important and growing renewable energy source, increasingly integrated into global electricity markets. Algeria is among the 15 African countries with good wind energy potential[40]. Therefore, the government is advancing wind power integration into the grid (Algerian DZ114 bus transmission network) to achieve a high penetration level.

III.8. 1. Technical and economic feasibility study

This study analyzes the techno-economic assessment of electrical energy production from four selected wind turbines: Vestas V-80, Suzlon S-82, Enercon E-58, and Gamesa G-114, installed at three locations in the Algerian highlands: El Beidh, Setif, and Djelfa, chosen for their favourable wind potential. Additionally, the Algerian transmission electrical network, specifically the DZ-114 bus, encounters technical issues in the highlands, particularly related to low voltage levels. Therefore, integrating wind farms at these three sites can provide valuable voltage support. Furthermore, this integration can significantly reduce reliance on fossil fuels and decrease emissions from conventional power plants. [1].

III.8. 1.1.Wind and geolocation data

The study used annual average wind speeds at 10m above ground level. Geolocation data for the regions (Sétif, Djelfa, and El-Beidh for ten years), obtained from the Algerian National Meteorological Office, shown in Figure III. 17 and Table III. 5. The Weibull parameters adjusted using Eqs. (III.6) and (III.7). Figure III. 18 shows the flowchart of the work program.

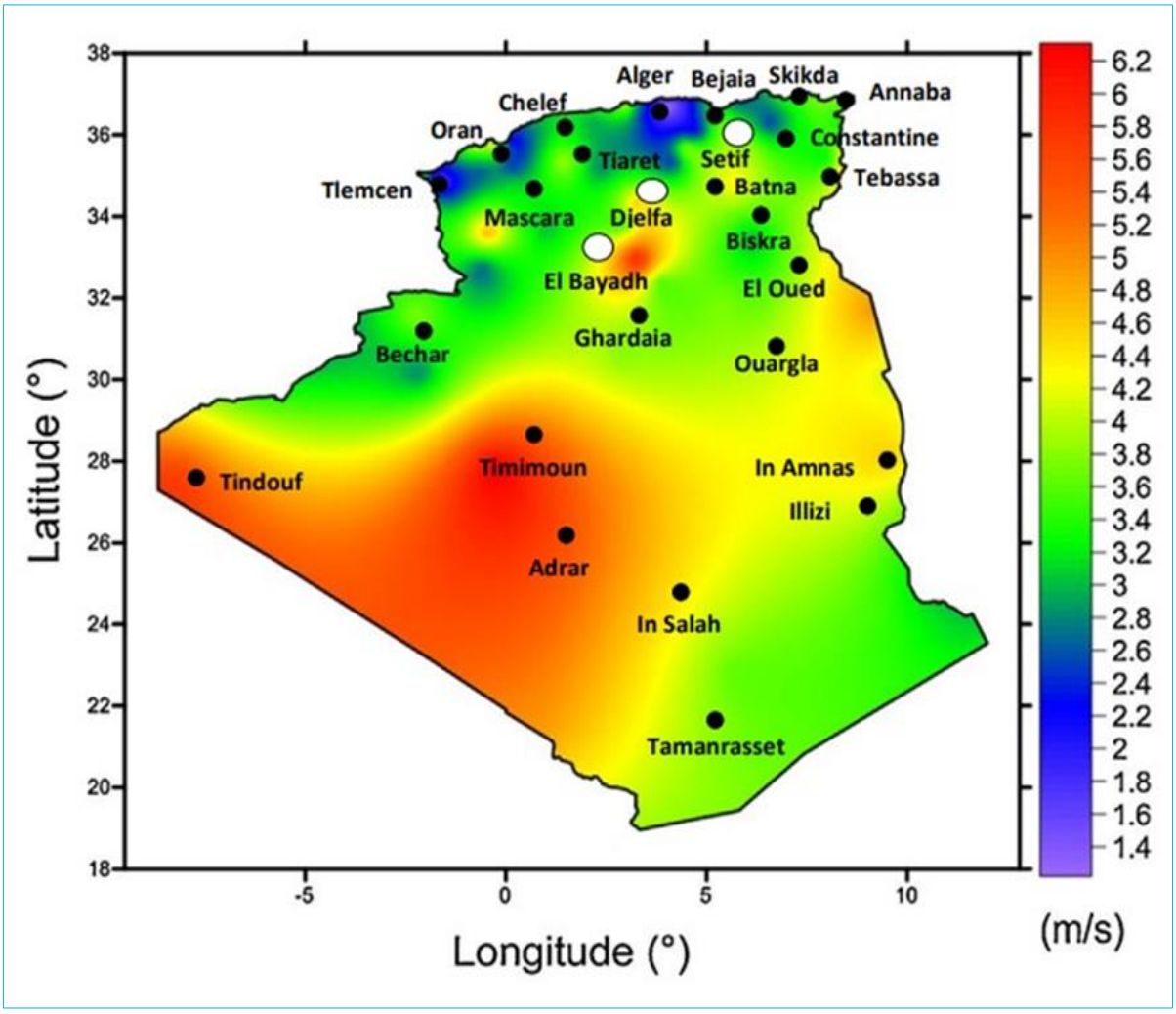

Figure III. 17. Annual wind map of Algeria at 10 m height

Table III.5. Wind speed and Weibull parameters for chosen sites at 10m height

Sites	Latitude Nord(°)	Longitude Est(°)	Altitude (m)	Measurement duration	v_0 (m/s)	c_0 (m/s)	k_0
Setif	36°18'	05°41'	1038	2001/2010	3.46	3.90	1.40
Djelfa	34°33'	03°25'	1144	2001/2010	3.92	4.40	1.71
El Bayadh	33°66'	01° 00'	1347	2001/2010	4.75	5.30	1.62

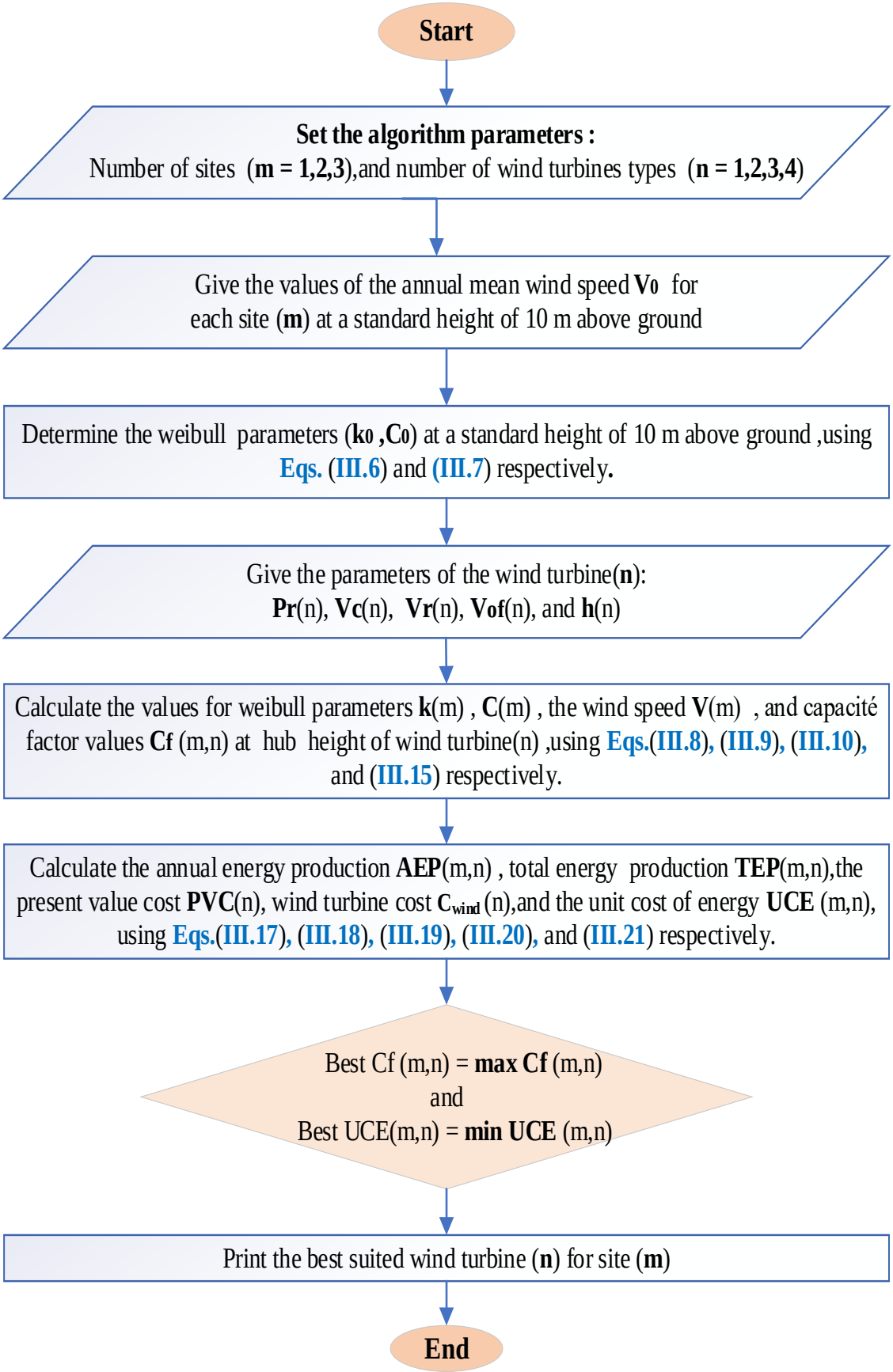

Figure III. 18. Flowchart of the work program

III.8. 1.2. Wind turbine capacity factor

The capacity factor (C_f) is a crucial indicator of a wind turbine's efficiency, determined by the location, turbine characteristics, and wind speeds. The formula used to calculate the capacity factor based on the Weibull parameter and the turbine's wind speeds:

$$C_f = \frac{e^{-(v_{in}/c)^k} - e^{-(v_r/c)^k}}{(v_r/c)^k - (v_{in}/c)^k} - e^{-(v_{out}/c)^k} \quad \text{(III.15)}$$

Where v_{in}, v_{out}, and v_r are the wind speeds of wind turbines considered (See Table III. 7).

III.8. 1.3.Total energy production.

Efficient wind conversion systems require site-specific design, necessitating wind characteristic assessment, including wind speeds and rated power. Wind turbine performance is evaluated using the capacity factor and the average power output (Pout) over a given period, as defined in Eq. (III.16). For a single wind turbine, the annual energy production (AEP) estimated by Eq. (III.17). The calculation of energy production (kWh) over the 20-year turbine lifetime based on Eq. (III.18).

$$P_{out} = P_r * C_f \quad \text{(III.16)}$$

$$AEP = 8760 * P_{out} \quad \text{(III.17)}$$

$$TEP_{20y} = AEP * t \quad \text{(III.18)}$$

Where 8760 is the number of hours in a year, and **t** is 20 years

III.8. 1.4. Performance and effectiveness of wind turbines

To conduct an economic analysis of wind energy in a specific region, it is essential to examine different types of wind turbines[1]. Table III. 6 shows the technical characteristics of four wind turbines selected for this study, with rated outputs between 1 and 2 MW.

Table III. 6. Technical characteristics of wind turbines.

Wind turbines Caracteristiques	Suzlon S-82	Vestas V-80	Enercon E-58	Gamesa G-114
Hub height h (m)	78.5	67	89	93
Rated power P_r (kW)	1500	2000	1000	2000
Rotor diameter (m)	82	80	58.6	114
Design life (years)	20	20	20	20
Cut-in wind speed $\mathbf{v_{in}}$(m/s)	4	4	2.5	2.5
Rated wind speed $\mathbf{v_r}$(m/s)	14	16	12	10
Cut-off wind speed $\mathbf{v_{out}}$(m/s)	20	25	34	25

III.8. 1.5.Present value cost

Wind farm planning involves evaluating technical and economic criteria to achieve low operational costs per unit of energy. The present value cost (PVC) method estimates the total cost of a wind farm project, including all costs associated with a wind energy conversion system. The PVC of the electrical energy produced per year will be determined using a specific expression:

$$PVC = \left[I + C_{omr} * \left[\frac{1+i}{r-i}\right] * \left[1 - \left(\frac{1+i}{1+r}\right)^{t}\right] - S * \left(\frac{1+i}{1+r}\right)^{t}\right] \quad \text{(III.19)}$$

Previous studies have shown that the cost of electricity (kWh) generated by wind turbines installed on site depends on several factors, such as:

- The machine is designed for 20 years (t), according to the manufacturer.
- The cost of operation, maintenance, and repair (C_{OMR}) is estimated at 25% of the annual turbine price (TP) (TP/ design life).
- The value of the S-scrap; is evaluated at 10% of the investment (I).
- The investment (I) represents the total price of the wind turbine plus an additional 20% for other initial costs (including civil works provisions, land, equipment transport, installations, and grid integration).
- The inflation rate (i), and interest rate (r) are assumed to 12% and 15%, respectively.
- The Wind turbine cost (C_{wind}) depends on its specific cost (C_{spc}), which is determined by nominal power. Three ranges (Table III. 7) show cost decreases as size increases. Machines over 200 kW have an average price of 1300 $/kW. Specific cost is calculated by the formula:

$$C_{wind} = P_r * C_{spc} \quad \text{(III.20)}$$

Table III. 7. Wind turbine- specific costs

Wind turbine size (kW)	Specific cost ($/kW)	Average specific cost ($/kW)
<20	2200–3000	2600
20 - 200	1500–2300	1900
>200	1000–1600	1300

III.8.1.6.Cost of energy

The unit cost of energy (UCE) per kWh of electricity produced from wind turbines is determined for each site by dividing the present value cost by the total energy produced over the lifetime of the turbine according to the equation:

$$UCE = \frac{PVC}{TEP_{20\,y}} (Cost/KWh) \quad (III.21)$$

III.9.Facts controllers

Flexible Alternating Current Transmission Systems (FACTS) are defined by the IEEE as"Alternating current transmission systems that incorporate power electronics-based controllers and other static controllers to improve the controllability of the power system and the transmission capability of the line[10]. The FACTS concept was defined by Hingorani in 1988; they were introduced in 1986 by the Electric Power Research Institute, and it helps to address the problems encountered in the operation of power grids. The FACTS technology is based on power electronics for the control of different parameters of power grids (voltage, phase shift, active and reactive power, current), which allows the improvement of the operation of power grids[25]. Several basic devices, divided into two categories: conventional devices and FACTS devices[41], are shown in Figure III. 19. This section will focus on configuring and modelling the static var compensator (SVC) for integration into the power grid connected to wind farms. The goal is to improve the power grid's performance by minimising total transmission losses, reducing voltage deviation, and enhancing voltage stability.

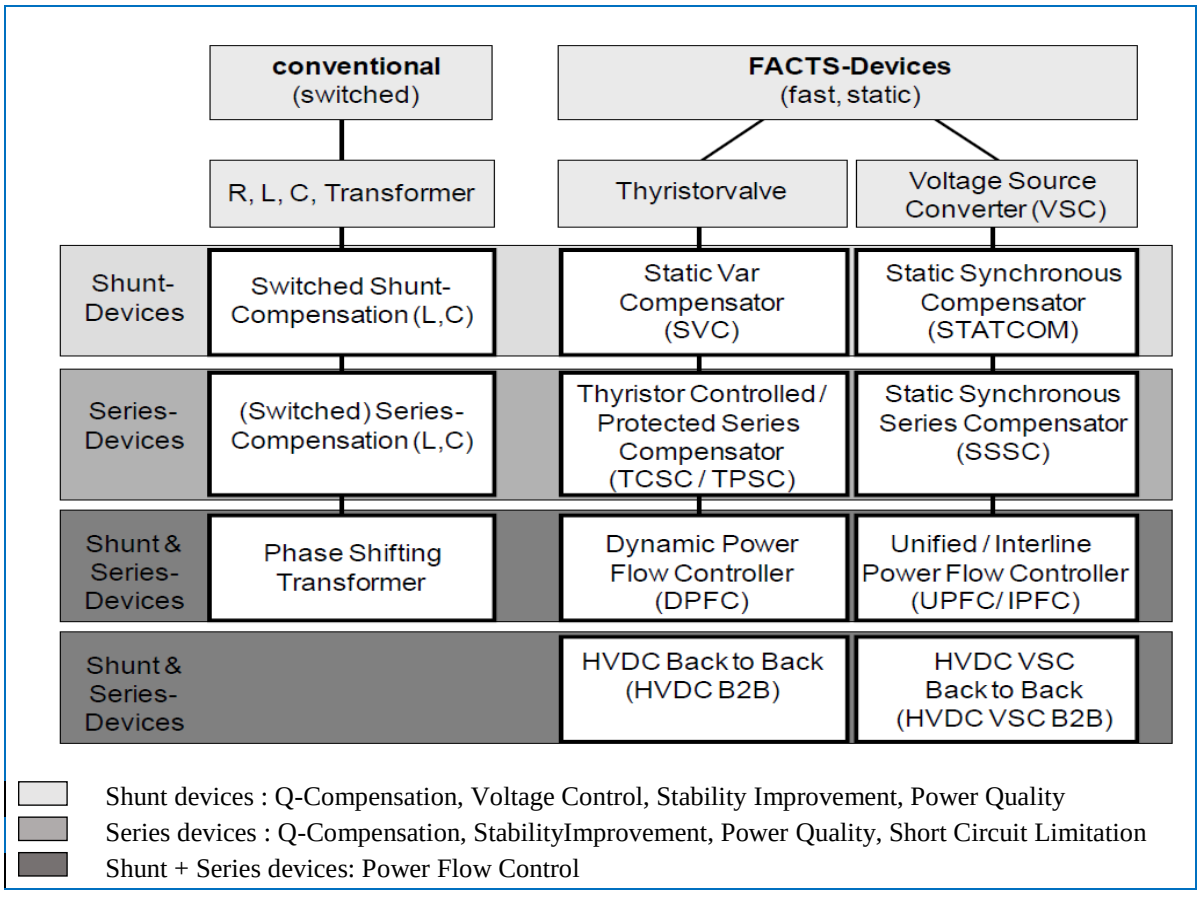

Figure III. 19. Overview of major FACTS-Devices

III.9.1. SVC Configuration

This controller combines a Thyristor Controlled Reactor (TCR) with a Thyristor Switched Capacitor (TSC), Thyristor-Switched Reactor (TSR), or Fixed Capacitors (FC) as illustrated in Figure III. 20, to control voltage amplitude and improve grid stability and adapts to new situations. It connects in parallel to the grid via a coupling transformer[3,25,41].

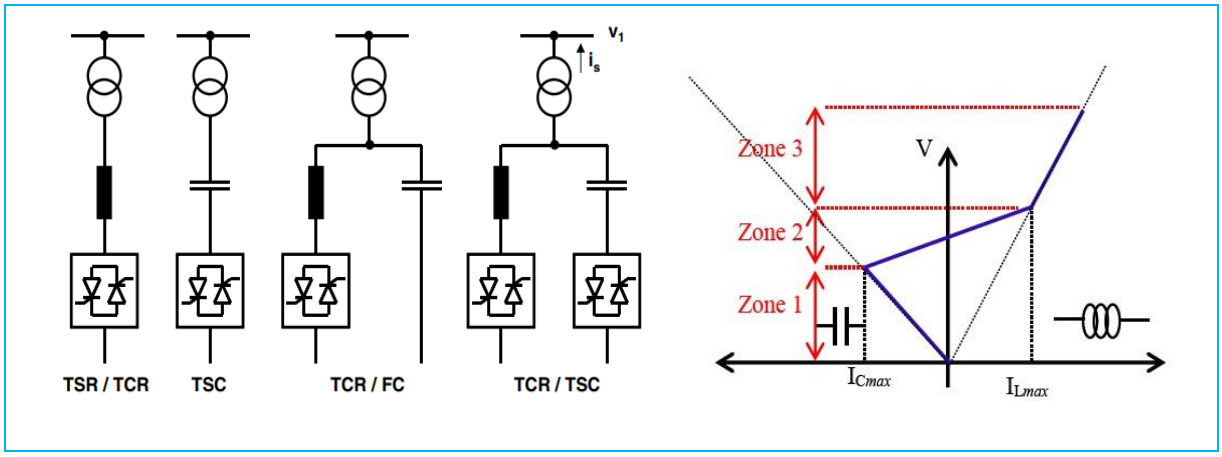

Figure III. 20. SVC building blocks and voltage / current characteristics

This device functions in three distinct zones as follows[2,13] :

- Zone 1 (Capacitive), where the TSC provides maximum energy; only the capacities are connected to the network .
- Zone 2 (Mixed) or regulation, where the reactive energy combines TCR and TSC.
- Zone 3 (Inductive), where the TCR gives its maximum energy (regulation limit), the capacitors are disconnected.

III.9.2. SVC modeling

In the electrical system, the SVC's function is to maintain the magnitude of the bus voltage at the desired level by supplying or absorbing reactive power. The SVC; is modeled by a variable shunt admittance, which is used to regulate the reactive power compensation of a system. This admittance ($\mathbf{Y_{SVC}}$) has only its imaginary part since the power loss of the SVC device is assumed negligible and defined by Eq. (III.22). The equivalent circuit for the SVC controller in a power system shown in Figure III.21[3,42].

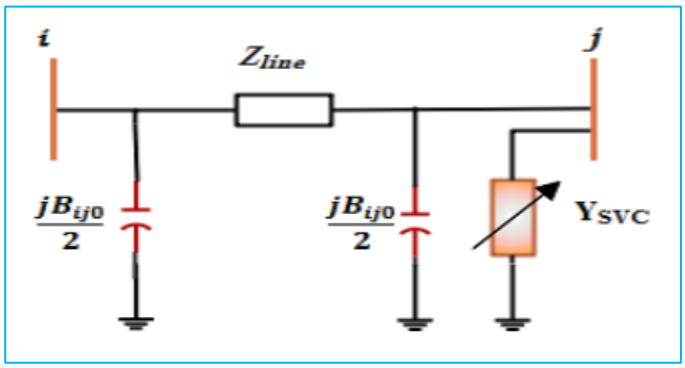

Figure III. 21. Basic model of the SVC device in power system

$$Y_{SVC} = jB_{SVC} \tag{III.22}$$

Where the susceptance (B_{SVC}), which can be capacitive or inductive to supply or absorb reactive power, is limited by its minimum and maximum values as below:

$$B_{SVC}^{min} \leq B_{SVC} \leq B_{SVC}^{max} \tag{III.23}$$

In this study, the SVC is installed in the electrical system as a PV bus to regulate the magnitude of the voltage V_k (k= i or j bus) by injecting reactive power into a bus to which it is connected. Reactive power absorbed or injected (**Qsvc)** by the SVC device is given by Eq. (III.25). The negative sign (-) indicates that the SVC supplies reactive power to the system when it is capacitive, and consumes it when it is inductive.

$$Q_{SVC} = -V_k^2 * B_{SVC} \tag{III.24}$$

- Current **I**svc, and susceptance **B**svc, are determined using the following equations:

$$I_{SVC} = jB_{SVC} * V_k \tag{III.25}$$

$$B_{SVC} = B_C - B_{TCR} = \frac{1}{X_C * X_L}\left(X_L - \frac{X_C}{\pi}[2(\pi - \alpha) + \sin(\alpha)]\right) \tag{III.26}$$

Where,

$$X_L = \omega L \quad \text{and} \quad X_C = \frac{1}{\omega L}$$

- If an SVC is installed in node j, only the $\mathbf{Y}_{jj}$ element of the nodal admittance matrix is modified, and the SVC admittance is added[13].

$$Y'_{jj} = Y_{jj} * Y_{SVC} \tag{III.27}$$

In this case, the modified admittance matrix is as follows:

$$= \begin{bmatrix} Y'_{ii} & Y'_{ij} \\ Y'_{ji} & Y'_{jj} \end{bmatrix} = \begin{bmatrix} y_{ij} + {y_{ij0}}/{2} & -y_{ij} \\ -y_{ij} & y_{ij} + y_{svc} + {y_{ij0}}/{2} \end{bmatrix} \quad \text{(III.28)}$$

III.11. Conclusion

This chapter offers an overview of global electricity generation statistics and the structure of the Algerian electricity market. It covers the various subsystems of the Algerian network, including generation (power plants), transmission (RIN, PIAT, RIS), and distribution. Furthermore, it gives an outlook on Algeria's renewable energy program, focusing on the wind energy system using a double-fed asynchronous machine and the Weibull model to calculate the wind energy probability at different wind speeds. In addition, the section includes a techno-economic assessment of electricity generation from wind turbines installed at three sites in the Algerian highlands. This analysis aims to identify the most appropriate wind turbine for each site and its integration into the main grid. We formulate the optimisation problem in the presence of renewable energy by choosing objective functions and constraints. To improve the electrical system's performance, we have chosen the SVC device as an important element in the FACTS family of controllers. The following chapter presents metaheuristic methods for solving the optimal power flow problem.

CHAPTER : IV

Power Flow Optimisation Methods

IV .1.Introduction

Optimization involves making the best possible decisions under specific conditions to minimize effort or maximize benefits in engineering processes[43]. Optimisation in power systems aims to minimize undesirable factors such as costs, gas emissions, and energy losses, while maximizing desirable outcomes like profit, quality, and network efficiency, all within the constraints of available limits[2]. This chapter examines the existing methods for solving the Optimal Power Flow (OPF) problem, including the problem formulation, the objective function, and the technical constraints involved in the optimisation process. The methods for solving the OPF problem can be classified into two main groups: conventional and intelligent. This paper introduces two new meta-heuristic methods, detailing their concepts and algorithmic steps.

IV .2.Optimization problem description

An optimization problem aims to find the best combination of parameters (independent variables) to maximise or minimise a specific quantity, known as the objective function, while adhering to certain constraints. The adjustable parameters represent the control or decision variables, and the constraints define their permissible values[44]. An optimisation problem typically consists of several steps, as illustrated in Figure IV.1.

- Setting the limits of the variables
- Formulating the constraints.
- Formulating the objective functions
- Choosing an algorithm to solve the problem
- Solving the problem to obtain the optimum solution

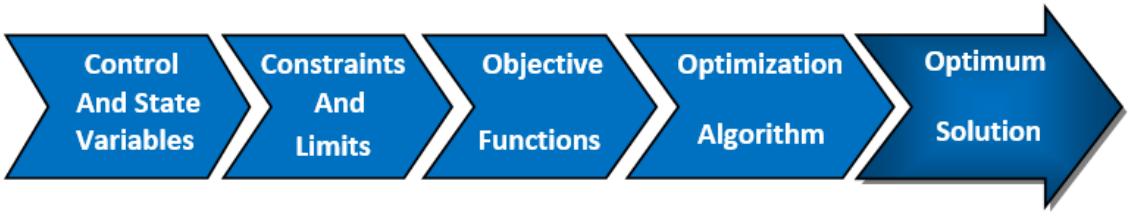

Figure IV.1. Steps for solving an optimization problem

IV .3.History of power system optimisation

Since 1919, engineers and researchers have focused on optimizing power supply systems. In 1943, Steinberg and Smith authored "Economy Loading of Power Plants and Electric Systems," introducing the incremental method. George incorporated the loss model into the problem's formulation. In 1951, Kirchmayer and Stagg developed the classical economic equations that form the basis of economic dispatching methodology. Their book in 1958, 'Economic Operation of Power Systems', introduced the conventional formulation of the economic dispatching problem. These studies led to the first power flow resolution algorithms and laid the foundation for researchers Squires (1961) and Carpentier (1962) to embark on optimization power flow[2,45].

IV .4.Optimal power flow problem classification

The Optimal Power Flow (OPF) problem involves determining an operational plan based on predicted electricity consumption and production. This plan must comply with constraints related to energy transportation while minimizing economic factors, such as losses due to the joule effect in the transmission lines or deviations from the initially forecasted production. Managing energy production and enhancing the quality of electrical energy within network constraints are significant challenges in optimal power flow[13]. The OPF problem can be classified, based on a predefined objective function, into the following two sub-problems (see Figure IV.2.), which are the subject of this study[13,46,47].

- Optimal active power dispatch OAPD (Economic and Environmental Dispatch), aims to achieve two key objectives in conventional power plants. The first objective is to minimise the total cost of electricity generation, while the second is to reduce greenhouse gas emissions. These objectives are subject to specific operational and system constraints.

- Optimal reactive power dispatch ORPD (Control Dispatch) has three main objective functions. The first consists of minimising the total active losses in the transmission lines. The second objective function aims to minimise the voltage deviation. The third objective function is concerned with minimising the voltage stability index L_index.

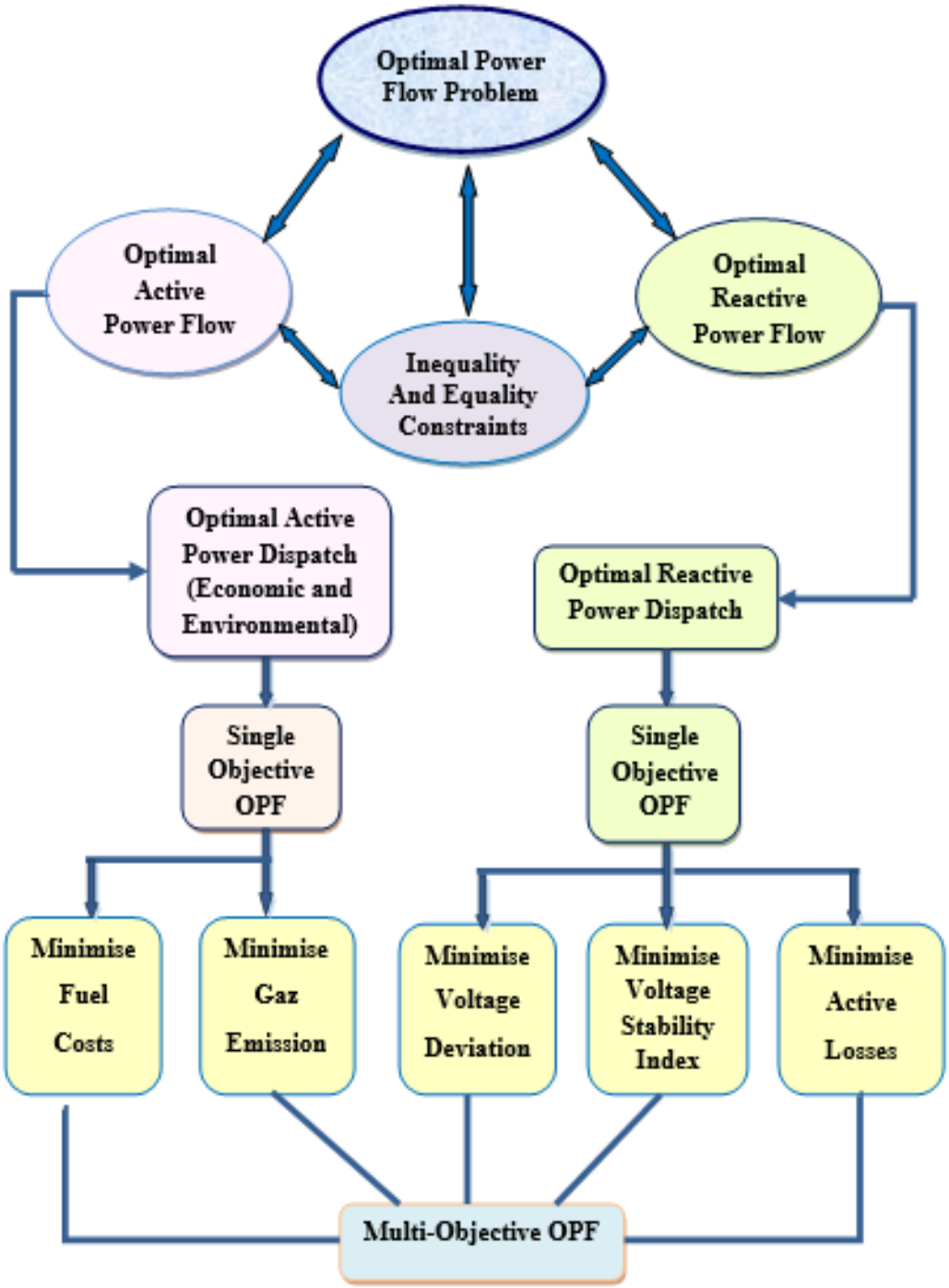

Figure IV.2. Types of optimal power flow problems

IV .5. Methods for solving optimal power flow problems

Optimisation has grown rapidly in recent decades, with new advancements in solving power flow issues. Progress in methods can be categorized into deterministic and heuristic approaches [48], resulting in a pseudo-class of hybrid methods as shown in Figure IV.3.

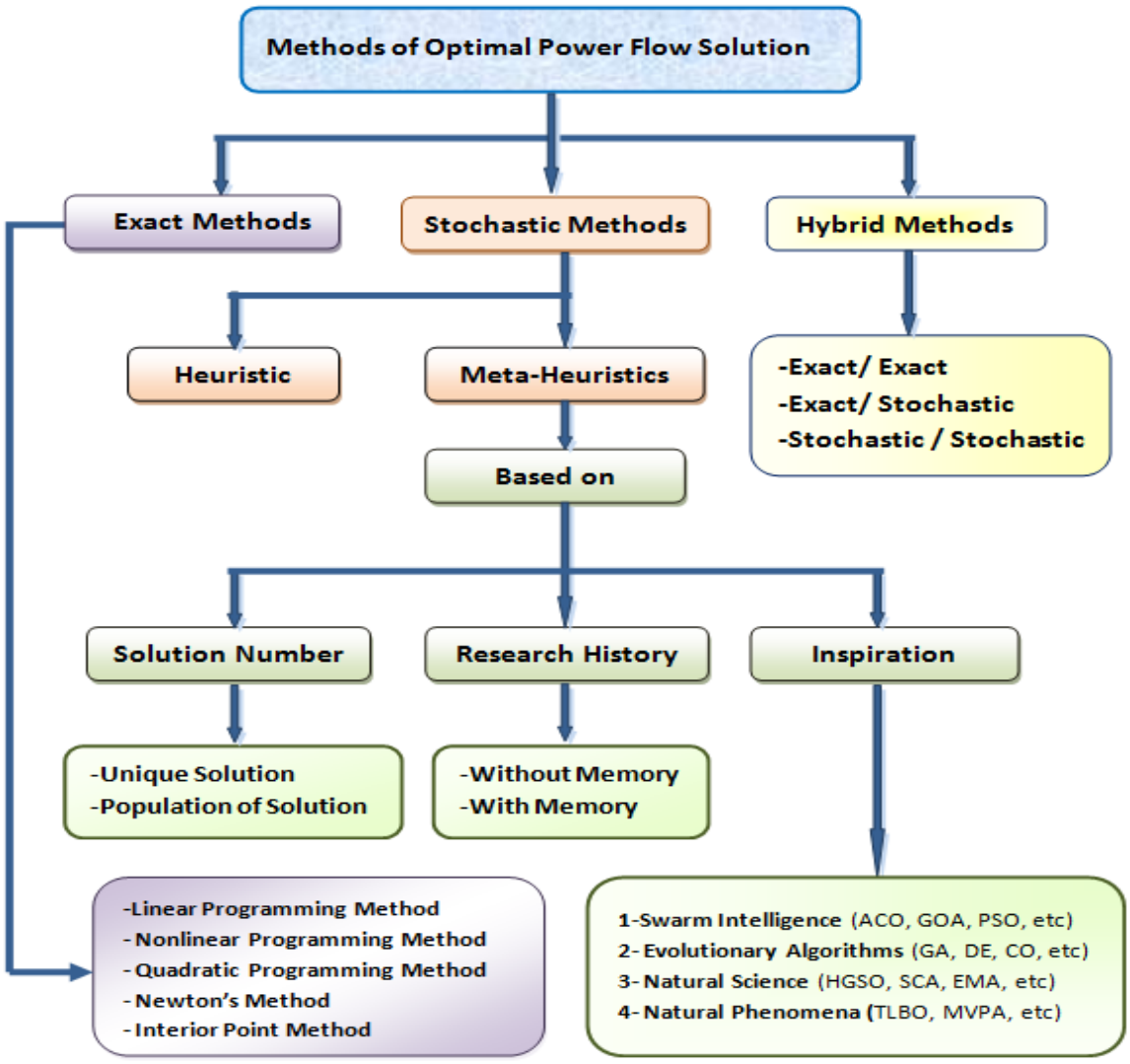

Figure IV.3. Methods used to solve the OPF problem.

IV .5.1.Exact methods (Deterministic Methods)

Deterministic optimization is a classical branch of mathematical programming that searches for stationary points in response variables, resulting in the optimal solution. However, the obtained solution may be a local optimum rather than a global optimum[49]. It can solve a variety of problems, including continuous, linear, discrete, and mixed-exact problems, subject to linear constraints, such as non-linear and quadratic programming (NLP, QP)[50], Newton, linear programming and interior point methods (NM, LP, IPM)[51].

There are two deterministic methods: local methods explore nearby solutions to find the nearest optimal function, while global methods search for the global optimum function without a starting point[52,53]. However, these methods can get stuck in a local minimum for multimodal objective functions(see FigureIV.4.) and are often unsuitable for high-

dimensional problems[54]. Stochastic techniques become essential when exact methods are inadequate or when the time required to solve optimisation problems is excessive.

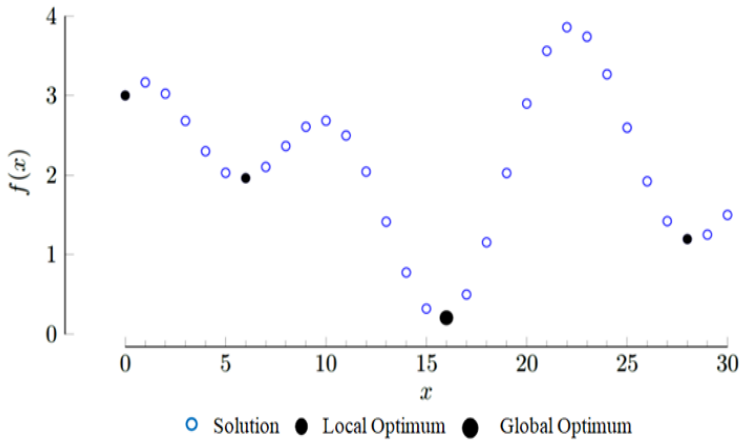

Figure IV.4. Local and global optimum multimodal function

IV .5.2.Stochastic methods (Non-deterministic methods)

There are two categories of problem-solving methods: heuristic and meta-heuristic. Unlike exact methods, these techniques do not require a starting point or knowledge of the objective function's gradient to find optimal solutions. They are more effective for solving difficult and complex problems, or problems with multiple objectives[12].

IV .5.2.1.Heuristic methods

Heuristic techniques are adaptable and efficient. They are designed for specific problems and finding an approximate solution. They rely on domain knowledge based on empirical rules derived from experience and involve iterations to improve a single solution. The objective is to progress towards an optimal solution by testing solutions closest to the current one. Figure IV.5 illustrates this path optimization or heuristic method[12].

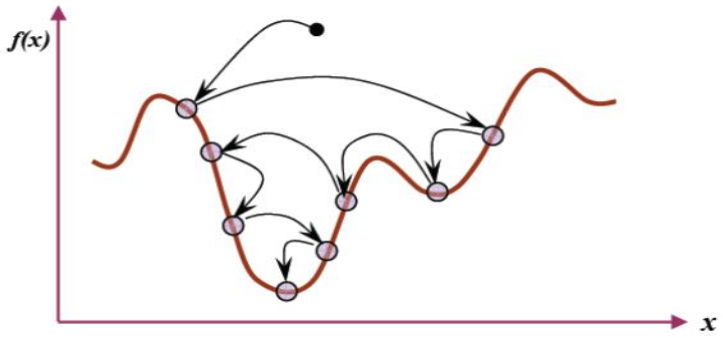

Figure IV.5. Simplified representation of a heuristic approach

IV .5.2.2.Metaheuristic methods

The term "metaheuristics" is derived from two Greek words: "heuristics," from the verb "heuristic" (euriskein), which means "to find," and "meta-," a prefix meaning "superior." [46,53]. Metaheuristics are stochastic algorithms designed to solve complex optimization problems. They start with a random set of candidate solutions and refine them iteratively to converge rapidly on the optimal solution. These methods aim to identify the global optimum of an objective function while avoiding local optima [55]. Figure IV.6 shows a schematic illustration of metaheuristics, which shows that metaheuristics (M) try to find the global optimum (G) for a difficult optimisation problem f(x) (for example, a problem with discontinuities (D)), without getting trapped by local optima (L) [12].

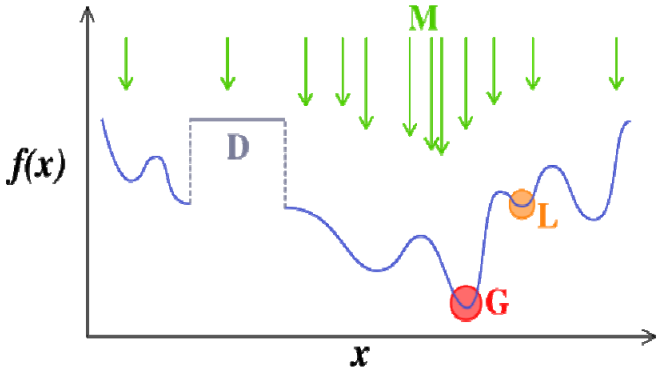

Figure IV.6 . Simplified representation of a metaheuristic approach

IV .5.2.2.1.Exploration and exploitation phases

The effectiveness of a metaheuristic technique in solving an optimization problem relies on its ability to maintain a good balance between exploration and exploitation[53,55]:

- **Exploration**, also known as diversification, involves the algorithm's capacity to navigate through various areas of the search space. This helps prevent premature convergence and avoids local optimal solutions.

- **Exploitation**, also known as intensification, refers to the algorithm's capacity to concentrate its efforts on the most promising areas of the solution space, to discover the global optimal solution near the best candidates.

IV .5.2.2.2.Inspiration sources for meta-heuristics

Metaheuristic optimization algorithms can be classified into four main categories (see Figure IV.2.) based on their inspiration sources[56], as below:

a) Swarm intelligence algorithms (SIA) are a class of algorithms that mimic the collective social behaviour of swarms, birds, insects, and animal groups.

b) Bio-inspired algorithms (BIAs), also known as evolutionary algorithms (EAs); are inspired by natural or biological evolutionary principles, excluding SIA.

c) Natural science-based algorithms (NSA) simulate specific physical phenomena or chemical laws, such as gravity, ion movement, electrical charges, and water systems.

d) Natural phenomena-based algorithms (NPA); are derived from different sources, such as social phenomena, human behaviours, natural occurrences, and emotional traits.

IV .5.3.Hybrid methods

Hybrid optimization methods combine exact and stochastic techniques to achieve more effective and efficient solutions. There are three types of hybridization[53]:

a) Hybridizing exact methods

b) Hybridizing exact and stochastic methods

c) Hybridizing stochastic methods

IV.6.Comparison of methods for solving OPF problems

To select the most suitable method for a specific optimization problem, we take into account the following factors[47]:

a) The ability to avoid local minima: The choice of optimization method depends on the complexity of the problem. For instance, a convex objective function suggests using a local method for quick optimization, while a multimodal function indicates the need for a global method.

b) The robustness of an optimal solution to uncertainties: Designers need to consider the robustness of an optimal solution when choosing an optimization algorithm. The shape determined by optimisation is generally linked to the manufacturing processes, which is often overlooked. To mitigate performance risks in real applications, it is essential to look for robust optimal solutions that are less sensitive to uncertainties.

c) The speed of convergence: In other words, how many variables need to be evaluated to achieve an overall optimum? The answer lies in the balance between exploration and exploitation.

IV. 7. OPF in electrical networks using metaheuristic methods

Several meta-heuristic optimization algorithms have been successfully applied to solve the OPF problem and the practical engineering design in power systems. These algorithms inspired by various natural phenomena, animal behaviour, physical effects, or mathematical laws[57], such as Teaching-Learning-Based Optimization (TLBO)[58], Shuffled Frog Leaping Algorithm (SFLA)[59], Differential Evolution Algorithm (DEA)[60], Cuckoo Search Algorithm (CSA)[61], Moth Flame Optimisation (MFO)[62], Ant-Lion Optimisation[63] (ALO), Grasshopper Optimisation Algorithm (GOA)[64], Slime Mould Algorithm (SMA)[65], Harris Hawks Optimisation (HHO)[66], Slap Swarm Algorithm (SSA)[67], Novel Bat Algorithm (NBA)[68], Particle Swarm Optimization (PSO)[69], Moth Swarm Algorithm (MSA)[70], and Jellyfish Search Optimization (JSO)[71]. Unfortunately, no method can effectively resolve all optimisation problems better than the others[72], attested by the statement of the no-free-lunch theorem. As a result, the experts in this area are always searching for new and better approaches to solve OPF problems. In this work, we have introduced two new optimisation techniques based on metaheuristics: Henry's Gas Solubility Optimization (HGSO)[56] and the Cheetah Optimizer (CO) algorithm[73], to solve OPF problems.

IV.7.1.HGSO optimisation method

Henry's Gas Solubility Optimisation (HGSO) is a natural science-based algorithm, proposed in 2019 by F. Hashem et al. [56], inspired by the principle of the physical phenomenon of Henry's Law. This method has been tested and implemented through optimisation experiments on 47 standard reference mathematical functions, the CEC'17 test suite, and three real engineering design problems. The HGSO algorithm parameters have been selected for their best values to reach the best OPF problem solution. In this optimisation problem, the number of "gases" represents the size of the population of solutions, with the positions of the "gases" being considered as potential solutions[56].

IV.7.1.1.HGSO inspiration

William Henry proposed Henry's Law in 1800 and formulated the gas law in 1803. According to Henry's Law, the solubility Sg of a specific quantity of gas dissolved in a specified volume and type of liquid under a predefined temperature T is proportional to the partial pressure Pg of that gas. Two main factors affecting solubility are temperature and

pressure. Solids become more soluble at higher temperatures, while gases become less soluble. Additionally, the solubility of gases increases with increasing pressure. The HGSO algorithm was inspired by Henry's Law, and simulates the solubility mechanism of a specific gas in a liquid, which varies with temperature (refer to Figure IV. 7). The solubility of poorly soluble gases in liquids is in Eqs (IV.1-IV.5). The updated solutions of these equations are[56]:

$$S_g = H * P_g \tag{IV.1}$$

- In addition, Henry's Law constants will be modified by the change in temperature of a system, described in Van't Hoff's equation as follows:

$$\frac{d \ln H}{d(1/T)} = \frac{-\nabla_{sol} E}{R} \tag{IV.2}$$

- Therefore, Eq.(IV.2) can be integrated as follows:

$$H(T) = \exp(B/T) * A \tag{IV.3}$$

$$H(T) = H^{\theta} * \exp\left(\frac{-\nabla_{sol} E}{R}\left(1/T - 1/T^{\theta}\right)\right); \quad \text{Where, } \nabla_{sol} E/R = C \tag{IV.4}$$

- Therefore, Eq. (IV.4) can be reformulated as follows:

$$H(T) = \exp\left(-C \times \left(1/T - 1/T^{\theta}\right)\right) * H^{\theta} \tag{IV.5}$$

- In addition, solubility is affected by two variables: pressure and temperature. For pressure, the solubility of gases increases with pressure; however, for high temperatures, gases are less soluble, but solids become more soluble. The present study focuses on gas solvability, shown in Figure IV.7.

IV.7.1.2.HGSO evolution steps

The present section provides the mathematical steps for the proposed HGSO algorithm, sourced from [56].

- **Step 1: initialization mechanism.** Initial positions of gases are created based on N population size using the following equation:

$$X_i(t+1) = X_{min} + r * (X_{max} - X_{min}) \tag{IV.6}$$

$$H_j(t) = l_1 * \text{rand}(0,1) \quad \text{(IV.7)}$$

$$P_{i,j} = l_2 * \text{rand}(0,1) \quad \text{(IV.8)}$$

$$C_j = l_3 * \text{rand}(0,1) \quad \text{(IV.9)}$$

- **Step 2: clustering process.** The clustering is accomplished by dividing the whole population into identical groups equivalent to the number of gas types. Each group ***j*** has similar gases and has the same value of Henry's constant ($\mathbf{H_j}$).

- **Step 3: evaluation of fitness.** A fitness function evaluation is carried out to discover the gas with a better equilibrium state than others in each group **j**. Then, these gases are classified to determine the optimal gas in the entire population of gases.

- **Step 4: update Henry's coefficient**. Updating Henry's coefficient is performed by using the following equation:

$$H_j(t+1) = H_j(t) * \exp\left(-C_j * \left({}^{1}/_{T(t)} - {}^{1}/_{T^{\theta}}\right)\right) \quad \text{(IV.10)}$$

$$\text{Where,} \quad T(t) = \exp((-t) \,/\, \text{iter})$$

- **Step 5: update solubility**. Updating the solubility is accomplished based on the following:

$$S_{i,j}(t) = K * H_j(t+1) * P_{i,j}(t) \quad \text{(IV.11)}$$

- **Step 6: update position**. The novel position of gas ***i*** in cluster ***j*** is determined under the following formula:

$$X_{i,j}(t+1) = X_{i,j}(t) + F * r * \gamma * \left(X_{i,best}(t) - X_{i,j}(t)\right) + F * r * \alpha * \left(S_{i,j}(t) * X_{best}(t) - X_{i,j}(t)\right) \quad \text{(IV.12)}$$

$$\text{where, } \gamma = \beta * \exp\left(-\frac{F_{best}(t) + \varepsilon}{F_{i,j}(t) + \varepsilon}\right); \varepsilon = 0.05$$

$\mathbf{X_{(i,best)}}$ and $\mathbf{X_{best}}$ are two variables that have the main responsibility for balancing between exploitation and exploration capabilities.

- **Step 7: escaping from the local optimal solution**. In the aim of escaping from a local optimal solution, the worst gases are classified into new worst agents according to the following:

$$; \ N_w = N * (\text{rand}(C_2 - C_1) + C_1) \qquad \text{Where, } C_1=0.1; \ C_2=0.2 \qquad \text{(IV.13)}$$

- **Step 8: updating the worst agent position**. The positions of the ranked worst agents are updated based on the following formula:

$$W_{i,j} = W_{\min(i,j)} + r * \left(W_{\max(i,j)} - W_{\min(i,j)}\right) \qquad \text{(IV.14)}$$

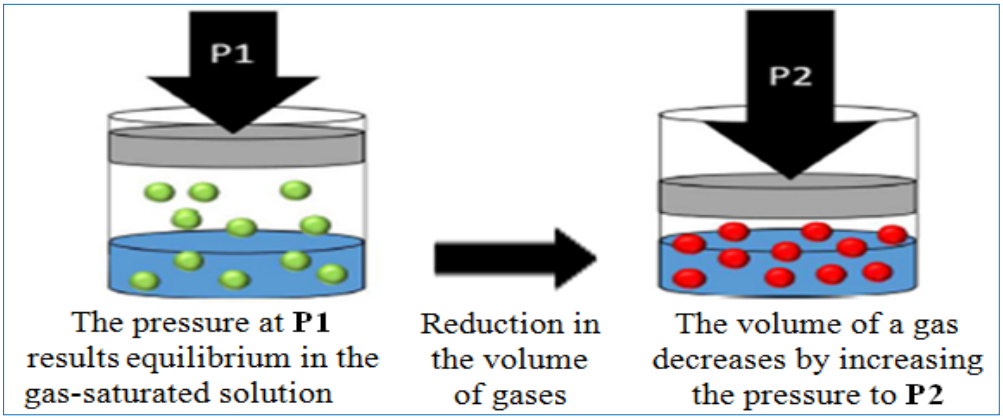

Figure IV. 7. General principle of solubility for Henry's gases

IV. 7.1.3. HGSO exploration and exploitation phases

The balance between the exploration and exploitation phases is controlled by fine-tuning the right amount of randomness, enabling the algorithm to escape from local optima and perform an effective global search. The HGSO has three primary control parameters:

1) $\mathbf{S_{i,j}}$ represents the solubility of gas i in cluster j and is based on the time of iteration. Hence, the search agents are transferring from the global exploration phase to the local exploitation phase as well as moving toward the best position; Consequently, it ensures an effective balance between the exploration and exploitation processes.

2) $\boldsymbol{\gamma}$ denotes the ability of gas j in cluster i to interact with the gases in its cluster and aims to transfer the search agents from global to local phase and vice versa according to the state of the given individual.

3) **F** serves as a directional flag parameter, taking values of ±1, which determines the movement orientation of each search agent. This parameter introduces population diversity and improves the algorithm's ability to escape local optima, ensuring a more comprehensive exploration of the solution space.

The flowchart and pseudo-code of the HGSO algorithm for solving the OPF problem are shown in Figure IV. 8 and Figure IV. 9 respectively.

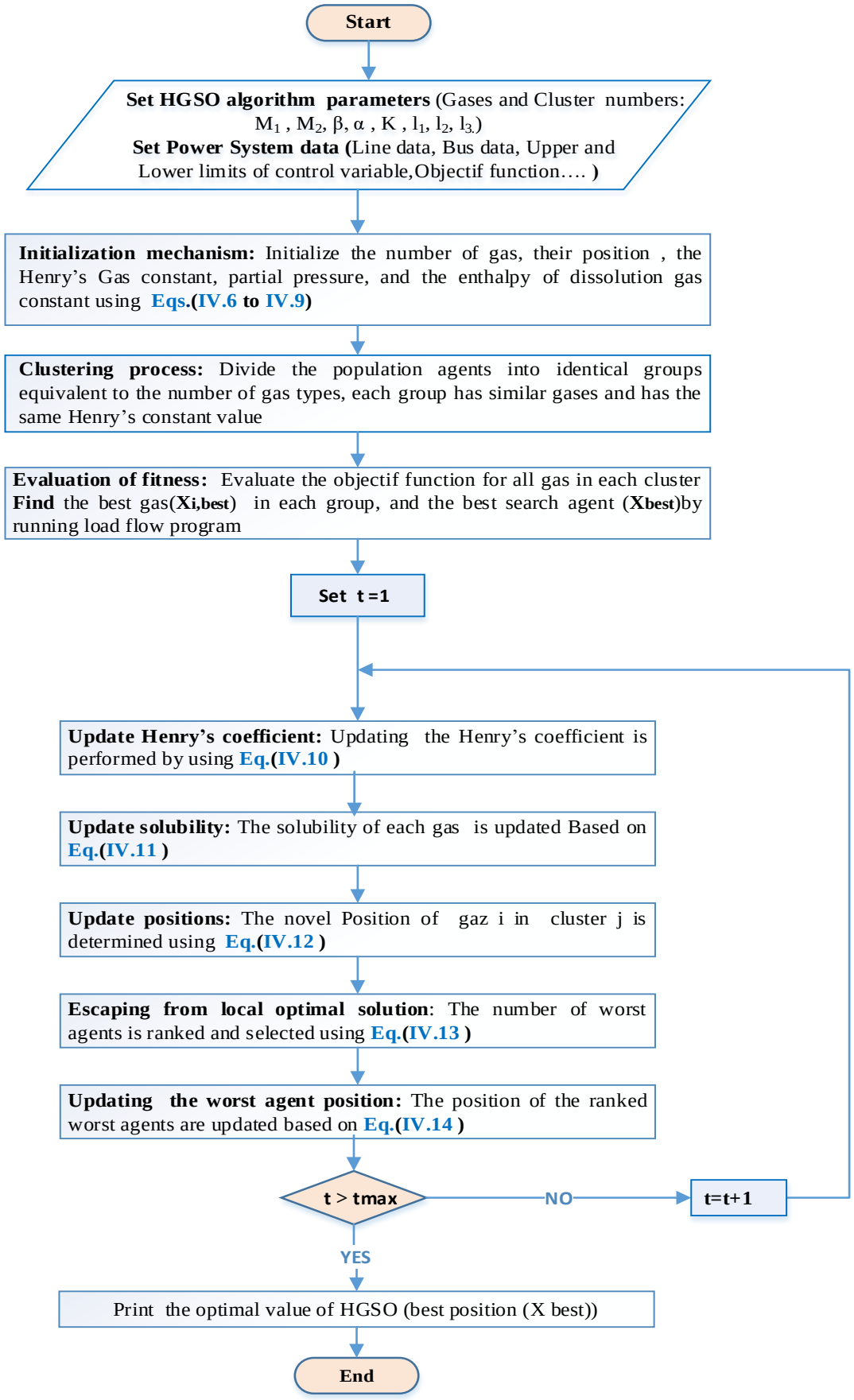

Figure IV. 8. Flow chart of the HGSO algorithm.

1. **Initialization**: $X_i(1 = 1,2, \ldots . N)$, number of gas types i,H_j,$P_{i,j}$,C_j ,l_1,l_2 and l_3
2. Divide the population agents into many gas types(clusters) with the same Henry's constant value ($\boldsymbol{H_j}$)
3. Evaluate each cluster $\boldsymbol{j}$
4. Get the best gas $\boldsymbol{X_{i,best}}$ in each cluster, and the best search agent $\boldsymbol{X_{best}}$.
5. **While** $\boldsymbol{t}$≺maximum number of iterations **do**
6. **for** each search agent **do**
7. Update the positions of all search agents using Eq. (IV.12)
8. **end for**
9. Update Henry's coefficient of each gas type using Eq.(IV.10)
10. Update the solubility of each gas using Eq.(IV.11)
11. Rank and select the number of worst agents using Eq. (IV.13)
12. Update the position of the worst agents using Eq. (IV.14)
13. Update the best gas $\boldsymbol{X_{i,best}}$, and the best search agent $\boldsymbol{X_{best}}$.
14. **end while**
15. $\boldsymbol{t = t + 1}$
16. **return** $\boldsymbol{X_{best}}$

Figure IV. 9. Pseudo-code of the HGSO algorithm.

IV.7. 2. CO optimisation method

The Cheetah Optimizer (CO) algorithm, based on natural or biological evolutionary principles, is a meta-heuristic algorithm for solving OPF problems. It was proposed in 2022 by Mohammad Amin Akbari et al.[73], inspired by the hunting behaviour of cheetahs in nature. This algorithm (CO) uses three principal prey-hunting strategies: searching, sitting and waiting, and attacking. The possibility of leaving the prey and returning home during the chase is included in the hunting process. The CO algorithm's performance prevents local optima in the OPF solution and ensures a balance between the exploration and exploitation phases. As part of a research study, intensive tests were carried out on 14 CEC-2005 compensation benchmark functions to evaluate the performance of the proposed CO algorithm. In addition, the CEC2010 and CEC2013 benchmarks were used in the evaluation. The proposed algorithm was also tested to solve the economic load dispatch problem, one of the most complex engineering problems.

IV.7. 2. 1. CO inspiration

The cheetah is one of the most recognizable cats in the world, itis known for its speed (120 km per hour), starts its hunt from a high place; and moves towards its prey slowly (gazelles, zebras, impalas, etc.). The hunt takes about half a minute with an average

distance of 173 m. The cheetah stumbles its prey and bites it in the throat. However, if the hunt takes too long, it gives up. Biological studies have shown that the cheetah's flexibility allows it to change direction swiftly; its long tail serves as a balance (seeFigure IV. 10). Its flexible spine allows it to "glide" between two leaps while pursuing prey.

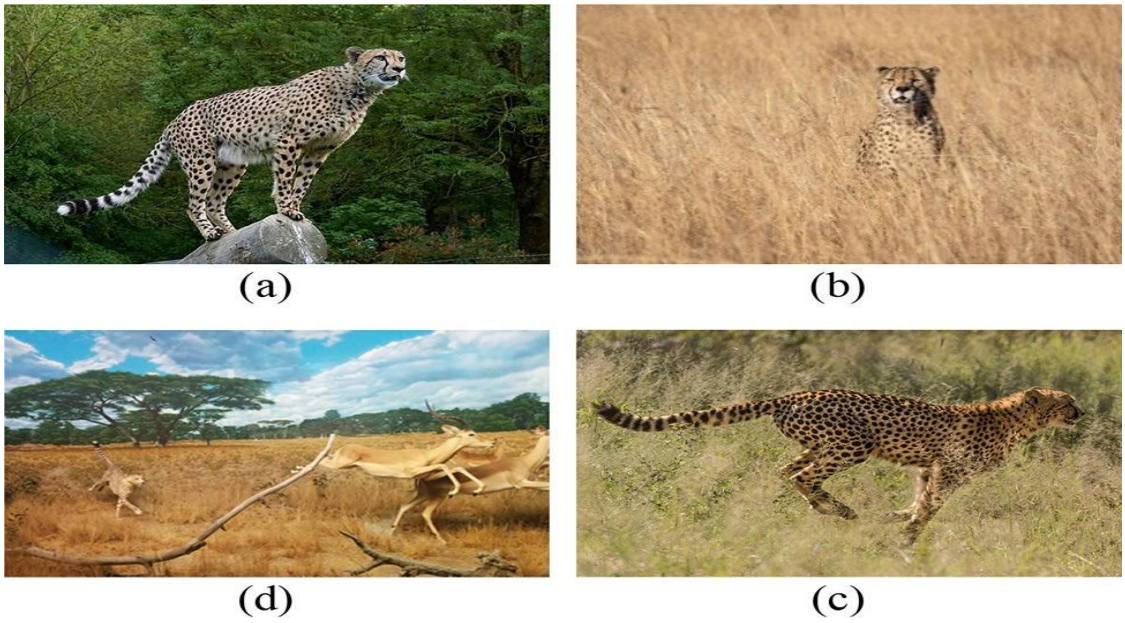

Figure IV. 10. Hunting behaviour of cheetahs: (**a**) searching for prey (scanning mode), (**b**) sitting-and-waiting (hiding), (**c**) rushing and (**d**) capturing.

IV. 7. 2. 2. Mathematical model of CO

The CO algorithm is based on intelligent hunting strategies, as illustrated in Figure IV.11, during the hunting phases (iterations). Each prey represents a decision variable corresponding to the best solution, and the cheetah situations make up a population. The pseudo-code for the CO algorithm to solve the OPF problem is provided in Figure IV.12. In this section, we will present the mathematical model for each hunting strategy below[44].

IV. 7. 2. 2. 1. Search strategy:

Cheetahs search for prey by scanning their territory or surroundings. It can use scanning mode (sitting or standing) or active mode. Scanning mode is preferred when there is a lot of prey in the area, while active mode is when prey is scattered and moving. This strategy, shown in Figure IV.11a, results in the following equation, which updates the cheetah's new position according to its current position during random searches:

$$X_{i,j}^{t+1} = X_{i,j}^{t} + \hat{r}_{i,j}^{-1} * \alpha_{i,j}^{t} \quad \text{(IV.15)}$$

Where, $$\alpha_{i,j}^{t} = 0.001 * t/T \quad \text{(IV.16)}$$

IV. 7. 2. 2. 3. Waiting strategy

After detecting a prey in an unsuitable situation, the cheetah sits and waits for the prey to approach its side; if not, it will choose a better situation. This strategy is illustrated in Figure IV.11b. This is expressed mathematically as follows:

$$X_{i,j}^{t+1} = X_{i,j}^{t} \tag{IV.17}$$

IV. 7. 2. 2. 4. Attack strategy

The two fundamental steps of this strategy and its mathematical equations are as follows:

a) Rushing: The cheetah, which decided to attack, accelerates its speed to catch its prey, as shown in Figure IV.11c.

b) Capturing: The Cheetah attacks and quickly captures its prey using its speed and agility, as shown in Figure IV.11d.

$$X_{i,j}^{t+1} = X_{B,j}^{t} + \check{r}_{i,j} . \beta_{i,j}^{t} \tag{IV.18}$$

Where,

$$\check{r}_{i,j} = |r_{i,j}|^{exp\left(r_{i,j}/2\right)} \sin(2\pi r_{i,j}) \tag{IV.19}$$

IV. 7. 2. 2. 5. Abandoning the prey and returning home:

This strategy comprises the following two stages:

a) Impossibility of hunting prey: If the cheetah cannot hunt its prey for a certain period, it will move on to the last available prey.

b) Unsuccessful hunt for prey: If the hunt for prey is unsuccessful, the cheetah must change location or return home.

IV. 7. 2. 3. CO exploration and exploitation phases

The evolution of random solutions in the iterative process of the CO algorithm fosters a balanced approach between exploration and exploitation. Exploration allows the algorithm to conduct a global search, while exploitation enables focused local searches in regions identified during the initial phase.

The proposed CO method needs a small number of equations, while the hunting strategies try to model the hunting process. These strategies create a suitable trade-off between the exploration and exploitation searches and prevent premature convergence in the different optimization problems.

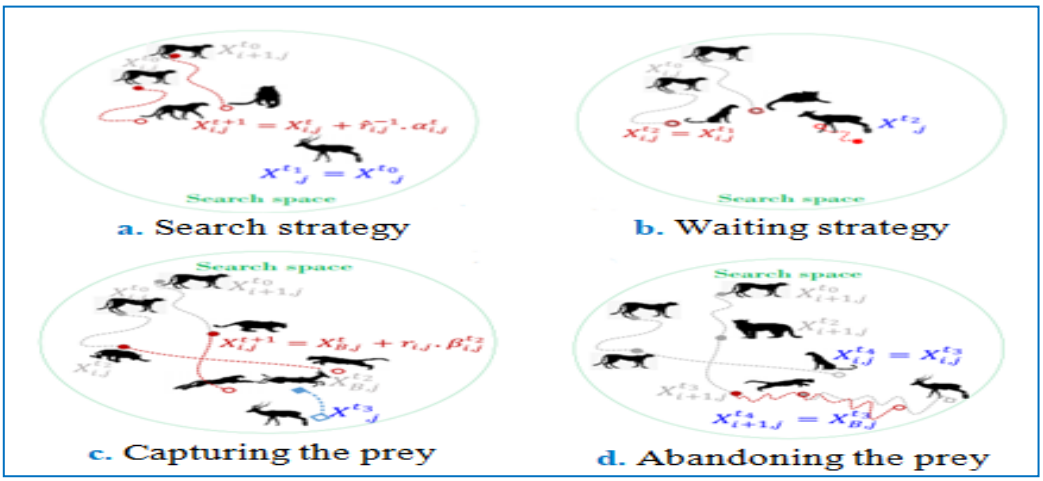

Figure IV. 11. Schematic representation of CO hunting strategies.

1. Define the problem data, dimension (D), and the initial population size(n)
2. Generate the initial population of cheetahs $X_i(i = 1,2,\ldots,n)$ and evaluate the fitness of each cheetah
3. Initialize the population's home, leader, and prey solutions
4. $t \leftarrow 0$
5. $it \leftarrow 1$
6. *MaxIter* ←desired maximum number of iterations
7. T← 60 x [D/10]
8. **while** $it \leq$ *MaxIter* **do**
9. Select m ($2 \leq m \leq n$)members of cheetahs randomly
10. **for** each member $i \in m$ **do**
11. Define the neighbour agent of member i
12. **for** each arbitrary arrangement $j \in \{1,2,\ldots, D\}$ **do**
13. Calculate $\hat{r}$, $\check{r}$, α, β , and H
14. $\boldsymbol{r}_2, \boldsymbol{r}_3 \leftarrow$random number is chosen uniformly from 0 to 1
15. **if** $\boldsymbol{r}_2 \leq \boldsymbol{r}_3$ **then**
16. $\boldsymbol{r}_4 \leftarrow$ a random number is chosen uniformly from 0 to 3
17. **if** $H \geq \boldsymbol{r}_4$ **then**
18. Calculate the new position of member i in arrangement j using Eq.(IV.15)/**Search**
19. **Else**
20. Calculate the new position of member i in arrangement j using Eq.(IV.18)/**Attack**
21. **End**
22. **Else**
23. Calculate the new position of member i in arrangement using Eq.(IV.17)/ **Sit-and-wait**
24. **End**
25. **End**
26. Update the solutions of member and the leader
27. **End**
28. $t \leftarrow t+1$
29. **if** $t >$ *rand* x T and the leader position doesn't change for a time, **then** /**Leave the prey and go back home**
30. Implement the leave the prey and go back home strategy and change the leader position
31. Substitute the position of member by the prey position
32. $t \leftarrow 0$
33. **End**
34. $it \leftarrow it+1$
35. Update the prey (global best) solution
36. **End**

Figure IV. 12. Pseudo-code of CO algorithm

IV. 8. Optimal power flow (OPF) problem

The Optimal Power Flow (OPF) problem is a nonlinear minimisation equation with equality and inequality constraints introduced by Carpentier in 1962 and has since become an important and studied research subject in power systems. The objective of solving the OPF problem is to find the optimal values of the decision variables that guarantee the minimum value of the objective function while respecting all equality and inequality constraints[3,5].

IV. 8. 1. OPF formulation problem without wind power

In mathematical terms, the OPF can be described as a single-objective optimisation problem, as follows[3,74].

$$\text{Minimize} \quad \{f(x,u)\} \tag{IV.20}$$

$$\text{Subject to}: \begin{cases} g_i(x,u) = 0, i = 1,2,\dots,m & \text{(IV.21)} \\ h_i(x,u) \leq 0, i = 1,2,\dots,p & \text{(IV.22)} \end{cases}$$

Where **f (x, u)** is the objective function to be minimized, **x** is the state vector, **u** is the control vector, **g_i (x, u)** represents equality constraints, **h_i (x, u)** represents inequality constraints, **m** and **p** are the equality and inequality constraints numbers, respectively.

IV.8.2.Design variables

IV.8.2.1. Control (decision) variables

The decision variables are all the system parameters whose value can be adjusted or controlled during the optimisation process to obtain optimal solutions, including the active power production P_{Gi} on the PV buses, excluding the slack bus, the generator voltages V_{Gi}, the injected powers VAR or the wind sources Q_C and the transformer settings T. The vector control variables **u** of the power system can be expressed as follows:

$$\mathbf{u} = \left[P_{G_2} \dots P_{G_{N_G}}, V_{G_1} \dots V_{G_{N_G}}, Q_{C_1}, \dots . Q_{C_{Nc}}, T_1, \dots T_{N_T}\right]^T \tag{IV.23}$$

IV.8.2.2. State variables:

These variables describe the changes in the system state induced by the control variables. They include the active power generated by the slack bus P_{G1}, the voltage modules of the load bus V_{Li}, the reactive powers of the generators Q_{Gi} and the line loads (apparent powers) S_{Li}. The vectors of state variables **x** in the power system can be defined as follows:

$$\mathbf{x} = \left[P_{G_1}, V_{L_1}, \dots, V_{L_{N_L}}, Q_{G_1}, \dots, Q_{G_{N_G}}, S_{l_1}, \dots, S_{l_{nl}}\right] \quad \text{(IV.24)}$$

IV.8.2.3. Perturbation variables

The demand (load) variables P_D and Q_D are not controllable because they depend only on the power demanded by the customer. The following vector P gives the disturbance variables of the electrical system [57] .

$$\mathbf{P} = \left[P_{D_1}, P_{D_2}, \dots, P_{D_n}, Q_{D_1}, Q_{D_2}, \dots, Q_{D_n}\right]^T \quad \text{(IV.25)}$$

IV.8.3.Objective functions

The main goal of optimal power flow problems is to find the steady-state operating point of the generation and transmission network that minimises a given function, known as the objective function. The most important objective functions in power systems are[75,76]:

IV. 8.3.1. Quadratic total fuel cost function

For each power plant, the fuel cost is described as a quadratic function in ($/hr) for the generated active power and hence, the quadratic total fuel cost function can be evaluated in the following form:

$$\mathbf{F_C} = \sum_{i=1}^{N_G} a_i + b_i P_{Gi} + c_i P_{Gi}^2 \quad \text{(IV.26)}$$

IV. 8.3.2. Total fuel cost with valve point loading effect function

In the realistic modelling of fuel cost in power plants using multi-valve steam turbines, a sinusoidal component is added to the quadratic fuel cost function, which is presented in the following form:

$$\mathbf{F_{Cval}} = \sum_{i=1}^{N_G} a_i + b_i P_{Gi} + c_i P_{Gi}^2 + |d_i \sin\left(e_i\left(P_{Gi}^{min} - P_{Gi}\right)\right) \quad \text{(IV.27)}$$

IV.8.3.3. Total active power losses function

The total active power losses in the power system are expressed as the sum of active power losses for all transmission lines. It can be written in the following form:

$$\mathbf{F_{APL}} = \sum_{i=1}^{n_l} \left(\mathbf{G_{ij}} \left(V_i^2 + V_j^2 - 2V_i V_j \cos \delta_{ij} \right) \right) \quad \text{(IV.28)}$$

IV.8.3.4. Total gas emission function

The Kyoto Protocol is an international treaty signed in 1997 to reduce all-natural greenhouse gas emissions caused by human activities and power plants when burning fossil fuels (coal, oil, and natural gas) to produce electric power. This reduction helps to keep a clean and unpolluted atmosphere**.** The emission function describing the number of various gases is expressed below:

$$\mathbf{F_{Em}} = \sum_{i=1}^{N_G} \alpha_i + \beta_i P_{Gi} + \lambda_i P_{Gi}^2 + \xi_i e^{(\theta_i P_{Gi})} \quad \text{(IV.29)}$$

IV.8.3.5. Voltage stability enhancement index function

Improving the system voltage stability for each bus is a fundamental measure to ensure a safe and stable power system using voltage stability (L-index). Its value varies between **0** and **1** (**0** corresponds to a zero load situation, while **1** means a voltage drop). The L-index is evaluated by:

$$\mathbf{L_j} = \left| 1 - \sum_{i=1}^{N_G} F_{ji} \frac{V_i}{V_j} \right|, \quad \text{where} \quad j = 1,2, \ldots \ldots, N_L \quad \text{(IV.30)}$$

$$\mathbf{F_{ji}} = -[Y_{LL}]^{-1} * [Y_{LG}] \quad \text{(IV.31)}$$

where $\mathbf{V_i}$ is a complex voltage of generator bus **i**, $\mathbf{V_j}$ is a complex voltage of load bus **j**, and the sub-matrices $\mathbf{Y_{LL}}$ and $\mathbf{Y_{LG}}$ have been obtained from the $\mathbf{Y_{BUS}}$ matrix after rearranging nodal current injections for nodal voltages.

$$\begin{bmatrix} I_L \\ I_G \end{bmatrix} = \begin{bmatrix} Y_{LL} Y_{LG} \\ Y_{GL} Y_{GG} \end{bmatrix} * \begin{bmatrix} V_L \\ V_G \end{bmatrix} \quad \text{(IV.32)}$$

The maximum value of $\mathbf{L_j}$ among all load buses is a system stability indicator that can be considered as an objective function presented in the following expression :

$$\mathbf{F_{Lmax}} = \max(L_j), \quad \text{where} \quad j = 1,2, \ldots \ldots, N_L \quad \text{(IV.33)}$$

IV.8.3.6. Voltage deviation function

The voltage profile is one of the most effective measures to ensure a safe power system and hence improve power system security. This improvement is achieved by reducing the load voltage deviation from **1.0** p.u. (nominal value) as the main security objective function is defined as follows:

$$\mathbf{F_{VD}} = \left(\sum_{i=1}^{NL} |V_{Li} - 1.0| \right) \tag{IV.34}$$

IV.8.3.7. Total fuel cost and voltage deviation function

Minimizing both total fuel cost in Eq. (IV.26) and voltage deviation in Eq. (IV.34) to achieve the economical and secure state of the power system, these two functions are introduced in one objective function as stated in :

$$\mathbf{F_{CVD}} = \left(\sum_{i=1}^{N_G} a_i + b_i P_{Gi} + c_i P_{Gi}^2 \right) + \boldsymbol{\Upsilon_{VD}} * F_{VD} \tag{IV.35}$$

II.5.3.8. Total fuel cost and voltage stability index function

In the aim to reduce total fuel cost and improve system voltage stability simultaneously, the two objective functions in Eq. (IV.26) and Eq. (IV.33) are implemented into a single objective function as formulated in:

$$\mathbf{F_{CLm}} = \left(\sum_{i=1}^{N_G} a_i + b_i P_{Gi} + c_i P_{Gi}^2 \right) + \boldsymbol{\Upsilon_{L}} * F_{Lmax} \tag{IV.36}$$

IV.8.3.9. Total fuel cost and active power losses function

In this case, the total fuel costs in equations (IV.26) and (IV.28) are at the same time reduced to the minimum and reflect an objective function described as follows:

$$\mathbf{F_{CAPL}} = \left(\sum_{i=1}^{N_G} a_i + b_i P_{Gi} + c_i P_{Gi}^2 \right) + \boldsymbol{\Upsilon_{PL}} * \mathbf{F_{APL}} \tag{IV.37}$$

Where $\boldsymbol{\Upsilon_{L}}$, $\boldsymbol{\Upsilon_{VD}}$ and $\boldsymbol{\Upsilon_{PL}}$ are the weight factors.

IV.8.4. Constraints

IV.8.4.1. Equality Constraints

These constraints are formulated by power flow equations to reflect the balance between generation and load powers (for both active and reactive powers) given as:

$$P_{Gi} - P_{Di} - V_i \sum_{j=1}^{N_B} V_j \left[G_{ij} \cos \delta_{ij} + B_{ij} \sin \delta_{ij} \right] = 0 \quad \text{(IV.38)}$$

$$Q_{Gi} - Q_{Di} - V_i \sum_{j=1}^{N_B} V_j \left[G_{ij} \sin \delta_{ij} - B_{ij} \cos \delta_{ij} \right] = 0 \quad \text{(IV.39)}$$

IV.8.4.2.Inequality Constraints

OPF inequalities represent the operating limits of electrical system devices as follows:

a) Generation constraints: The active and reactive outputs, as well as the voltages of the generators in the power station, are constrained by specific upper and lower limits.

$$V_{Gi,min} \leq \mathbf{V_{Gi}} \leq V_{Gi,max} \ , \qquad i = 1,2, \dots, N_G \quad \text{(IV.40)}$$

$$P_{Gi,min} \leq \mathbf{P_{Gi}} \leq P_{Gi,max}, \qquad i = 1,2, \dots, N_G \quad \text{(IV.41)}$$

$$Q_{Gi,min} \leq \mathbf{Q_{Gi}} \leq Q_{Gi,max} \ , \qquad i = 1,2, \dots, N_G \quad \text{(IV.42)}$$

b) Transformer constraints: the settings for the transformer tap and phase shifter are limited by the lower and upper limits, as follows:

$$T_{i,min} \leq \mathbf{T_i} \leq T_{i,max}, \qquad i = 1,2, \dots, N_{tap} \quad \text{(IV.43)}$$

$$P_{Si,min} \leq \mathbf{P_{Si}} \leq P_{Si,max}, i = 1,2, \dots, N_{phase} \quad \text{(IV.44)}$$

c) Security constraints: the constraints of the voltage amplitudes at load buses and the loads of the transmission lines must be limited within their limits as follows:

$$V_{Li,min} \leq \mathbf{V_{Li}} \leq V_{Li,max} \ , \ i = 1,2, \dots, N_L \quad \text{(IV.45)}$$

$$S_{li,min} \leq \mathbf{S_{li}} \leq S_{li,max} \ , \qquad i = 1,2, \dots, n_l \quad \text{(IV.46)}$$

d) VAR sources constraints: the components of the shunt power injection compensator are expressed as follows:

$$Q_{Ci,min} \leq \mathbf{Q_{Ci}} \leq Q_{Ci,max} \ , \ i = 1,2, \dots, N_C \quad \text{(IV.47)}$$

IV.8.4.3. Handling of technical constraints

The equality constraints defined by equations (IV.38) and (IV.39) are ensured through the power flow program, based on the Newton-Raphson method. Meanwhile, the inequality constraints are incorporated into the augmented objective function to maintain the dependent variables within their reasonable limits. The augmented objective function (fitness function), including the penalty function, can be defined as[62]:

$$\mathbf{f_{aug}(x,u) = f(x,u)} + \text{Penality} \tag{IV.48}$$

$$\textbf{Penality} = \lambda_p(\Delta P_{G1})^2 + \lambda_V \sum_{i=1}^{N_{PQ}} (\Delta V_{Li})^2 + \lambda_Q \sum_{i=1}^{N_{PV}} (\Delta Q_{Gi})^2 + \boldsymbol{\lambda_S} \sum_{i=1}^{n_l} (\Delta S_{li})^2 \tag{IV.49}$$

Where, $\boldsymbol{\lambda_Q}$, $\boldsymbol{\lambda_S}$and$\boldsymbol{\lambda_V}$ are the penalty factors.

$$\Delta P_{G1} = \begin{cases} (P_{G1} - P_{G1}^{max}) P_{G1} > P_{G1}^{max} \\ (P_{G1} - P_{G1}^{min}) P_{G1} < P_{G1}^{min} \\ 0 \quad P_{G1}^{min} < P_{G1} < P_{G1}^{max} \end{cases} \tag{IV.50}$$

$$\Delta V_{Li} = \begin{cases} (V_{Li} - V_{Li}^{max}) V_{Li} > V_{Li}^{max} \\ (V_{Li} - V_{Li}^{min}) V_{Li} < V_{Li}^{min} \\ 0 \quad V_{Li}^{min} < V_{Li} < V_{Li}^{max} \end{cases} \tag{IV.51}$$

$$\Delta Q_{Gi} = \begin{cases} (Q_{Gi} - Q_{Gi}^{max}) Q_{Gi} > Q_{Gi}^{max} \\ (Q_{Gi} - Q_{Gi}^{min}) Q_{Gi} < Q_{Gi}^{min} \\ 0 \quad Q_{Gi}^{min} < Q_{Gi} < Q_{Gi}^{max} \end{cases} \tag{IV.52}$$

$$\Delta S_{li} = \begin{cases} (S_{li} - S_{li}^{max}) S_{li} > S_{li}^{max} \\ 0 \quad S_{li}^{min} < S_{li} < S_{li}^{max} \end{cases} \tag{IV.53}$$

IV.9. OPF formulation problem considering wind power

In this work, the main objective of the optimal power flow OPF problem in the presence of renewable energies is the minimization of the total cost of active power generated by generation units, while satisfying the equality and the inequality constraints of a power system.The OPF problem in the presence of wind power is as follows[13,77]:

$$\begin{cases} \text{Min} & F(x,u); & \text{(IV.54)} \\ \text{Subject to} & g(x,u) = 0; & \text{(IV.55)} \\ & h(x,u) \leq 0; & \text{(IV.56)} \end{cases}$$

Where F(x, u) is the optimised objective function, x and u are the vectors of the state variables (dependent variables) and the control variables (independent variables), respectively.

IV.9.1. State and control variables

The state and control variables of the power system are as follows[65,78]:

$$\mathbf{x} = \left[P_{G_{slack}}, Q_{G_1}, \dots Q_{G_{N_G}}, Q_{W_1}, \dots Q_{W_{N_W}}, V_{L_1}, \dots V_{L_{N_L}}, S_{l_1}, \dots S_{l_{nl}}\right]^{T} \quad \text{(IV.57)}$$

$$\mathbf{u} = \left[P_{G_2} \dots P_{G_{N_G}}, P_{W_1} \dots P_{W_{N_W}}, V_{G_1} \dots V_{G_{N_G}}, Q_{C_1}, \dots Q_{C_{Nc}}, T_1, \dots T_{N_T}\right]^{T} \quad \text{(IV.58)}$$

IV.9.2. Equality and inequality constraints

a) Equality constraints

$$P_{Gi} + P_{Wi} - P_{Di} - V_i \sum_{j=1}^{N_B} V_j \left[G_{ij} \cos \delta_{ij} + B_{ij} \sin \delta_{ij}\right] = 0 \quad \text{(IV.59)}$$

$$Q_{Gi} + Q_{Wi} - Q_{Di} - V_i \sum_{j=1}^{N_B} V_j \left[G_{ij} \sin \delta_{ij} - B_{ij} \cos \delta_{ij}\right] = 0 \quad \text{(IV.60)}$$

b) Inequality constraints

OPF inequalities represent the operating limits of power system devices as follows[65,78]:

$$\begin{cases} P_{Gi,min} \le P_{Gi} \le P_{Gi,max}, & i = 1,2,\dots,N_G \\ P_{Wi,min} \le P_{Wi} \le P_{Wi,max}, & i = 1,2,\dots,N_W \\ Q_{Gi,min} \le Q_{Gi} \le Q_{Gi,max}, & i = 1,2,\dots,N_G \\ Q_{Wi,min} \le Q_{Wi} \le Q_{Wi,max}, & i = 1,2,\dots,N_W \\ V_{i,min} \le V_i \le V_{i,max}, & i = 1,2,\dots,N_G \\ T_{i,min} \le T_i \le T_{i,max}, & i = 1,2,\dots,N_{tap} \\ Q_{SVCi,min} \le Q_{SVCi} \le Q_{SVCi,max}, & i = 1,2,\dots,N_{SVC} \\ S_{li,min} \le S_{li} \le S_{li,max}, & i = 1,2,\dots,n_l \end{cases} \quad \text{(IV.61)}$$

IV.9.3. Objective functions

The objective function to be minimised includes the active production costs of the thermal and wind power plants as follows[65]:

$$\text{Min } F_{CT} = \sum_{i=1}^{N_G} F_{CTG} + \sum_{i=1}^{N_W} F_{CTW} \quad \text{(IV.62)}$$

IV.9.3.1. Fuel cost function

The quadratic function cost for thermal generators is as follows:

$$F_{CTG} = \sum_{i=1}^{N_G} a_i + b_i P_{Gi} + c_i P_{Gi}^2 \tag{IV.63}$$

IV.9.3.2.Wind cost function

The operating cost of wind power has three terms due to the impact of wind power uncertainty on the power system. These are the direct cost ($C_{d.W}$), the underestimated imbalance cost ($C_{un.wi}$), and the overestimated imbalance cost ($C_{ov.wi}$). Therefore, the total cost of wind energy is given by Eq. (IV.64), which has been derived and implemented in the wind energy analysis. All terms are detailed below[79]:

$$F_{CTW} = \sum_{i=1}^{N_W} C_{d.wi} + \sum_{i=1}^{N_W} C_{un.wi} + \sum_{i=1}^{N_W} C_{ov.wi} \tag{IV.64}$$

IV.9.3.2.1.The direct cost function

Electricity grid operators buy wind energy from wind farm owners and operators based on a power purchase agreement, which details the direct cost of the energy. The direct cost ($/h) of the *i*th wind power unit can be modelled as:

$$C_{d.w} = \sum_{i=1}^{N_W} d_{w,i} * P_{ws,i} \tag{IV.65}$$

IV.9.3.2.2.Cost function due to the underestimation

The cost of underestimating wind power occurs when actual production is greater than the scheduled wind power ($P_{wa,i} > P_{ws,i}$). In this case, the excess energy is wasted, and the utility operator is penalised for not using it. The mathematical model for the penalty cost of underestimating available wind energy is as follows[39,42]:

$$C_{un.wi} = \sum_{i=1}^{N_W} C_{pw,i} * \left(P_{wa,i} - P_{ws,i}\right) \tag{IV.66}$$

$$\begin{aligned} C_{pw,i} * \left(P_{wa,i} - P_{ws,i}\right) &= K_{Pw,i} * \left(P_{wa,i} - P_{ws,i}\right) \\ &= K_{pw,i} \int_{P_{ws,i}}^{P_{wr,i}} \left(P_w - P_{ws,i}\right) f_w(P_w) dp_w \end{aligned} \tag{IV.67}$$

IV.9.3.2.3.Cost function due to the overestimation

Overestimation costs arise when the actual wind power output is less than the estimated value ($P_{wa,i} < P_{ws,i}$). In this situation, the system operator must purchase electricity from other expensive reserves to meet demand. The penalty cost function for overestimating the available wind power is as follows:

$$C_{ov.wi} = \sum_{i=1}^{N_W} C_{rw,i} * \left(P_{ws,i} - P_{wa,i}\right) \tag{IV.68}$$

$$C_{rw,i} * \left(P_{ws,i} - P_{wa,i}\right) = K_{rw,i} * \left(P_{ws,i} - P_{wa,i}\right) = K_{rw,i} \int_{O}^{P_{ws,i}} \left(P_{ws,i} - P_w\right) f_w(P_w) dp_w \tag{IV.69}$$

- Where **f_w (P_w)** represents the probability density function (PDF) for the discrete and continuous portions of the wind power production, respectively given in equations (III.12 -III.13) and (III.14) in chapter III, respectively.

IV.9.3.3. Wind power penetration function

In this optimisation problem, the power penetration rate for each wind farm and the power output of conventional units are the control variables. The objective is to minimise the total cost of electricity generation, with a wind power penetration rate of 20% in the transmission network. In this study, three wind farms have been selected. The optimal power production per wind farm is determined as follows[78,80]:

$$P_{Wi} = \beta_i^{\circ} * P_D \tag{IV.70}$$

$$\sum_{i=1}^{N_W} \beta_i^{\circ} = \beta \tag{IV.71}$$

- Where **β_i°** is the optimal factor of the wind power penetration from the i-th wind farm, and **β** is the total factor of wind power penetration. The different power percentages of the wind source with their penetration limits are considered an additional inequality constraint.

IV.10.Conclusion

This chapter provides an overview of different optimisation methods for solving the optimal power flow problem considering wind resources. These include exact and metaheuristic approaches such as Henry Gas Solubility Optimisation (HGSO) and the Cheetah Optimiser (CO). These methods are used to minimise the main objective functions in power systems. In this study, the stochastic wind power function considers the penalty cost due to underestimation and the reserve cost due to overestimating the available wind power. Additionally, planning the penetration of wind energy is examined in this section. The next chapter will provide a detailed discussion of the simulation results and the evaluation of the proposed algorithms for solving the OPF problems.

CHAPTER : V

Results and Simulation

V .1.Introduction

In this chapter, we analyze the results obtained using the proposed algorithms: Henry's Gas Solubility Optimization (HGSO) and the Cheetah Optimizer (CO). These methods were tested on the IEEE 30 and IEEE 57 test systems, as well as the Algerian DZ 114 bus electricity transmission network, to address 16 cases of optimal power flow problems (OPFP). The results and simulations are organised into two main sections. First, we will examine the OPF using metaheuristic methods (HGSO and CO) without integrating wind energy. Following that, we will conduct a technical-economic study on electricity production from four selected wind turbines installed at three sites in the Algerian highlands. The results confirm that the Gamesa G114 wind turbine is the most suitable option for all sites, particularly for El Bayadh, as it ensures the lowest unit energy cost (UEC) compared to other types of wind turbines. Second, we will explore OPF with wind energy integration into the grid using the HGSO metaheuristic technique, applied to the IEEE 30-bus standard test system and the Algerian DZ 114 bus electrical system, to solve four OPFP cases. All simulations in this study were performed using MATLAB software.

V .2.OPF using HGSO and CO methods without including wind power

This study uses the IEEE 30-bus and IEEE 57-bus standard test systems, as well as the Algerian DZ 114-bus transmission system, to demonstrate the effectiveness and robustness of the CO and HGSO algorithms for solving optimal power flow (OPF) problems. The parameters of the HGSO and CO algorithms are depicted in Tables V.1 and V.2, respectively. In addition, Table V.3 presents 12 case studies that address OPF problems without the integration of wind farms. Appendices A, B, C, and D show the single-line diagrams of three power systems, their line and bus data, wind farms and their characteristics.

Table V.1. Characteristics of the HGSO algorithm

Parameters	IEEE 30/57/DZ 114-Bus Power Systems
Gases number	N = 100/200/200-500
Cluster number	n = 10
Constants values	M_1= 0.1, M_2 = 0.2,β = 1, α = 1, K = 1,ε =0.05
Constant values fixed for engineering problems	l_1= 1, l_2 =10, l3 =1
Constant values fixed for optimal flow problems	l_1= 0.5, l_2 =15, l_3 =0.5
Number of iterations	Niter = 200/500/300

Table V.2. Characteristics of the CO algorithm

Parameters	IEEE 30-Bus Power System
Population size	n = 180
Number of search agents in a group	N = 60
Optimization problem dimension	D=25
Number of iterations	MaxIt = 200
Random numbers r_1 ; r_2 and r_3	[0 1]
Random number r_4	[0 3]
Random value($H \geq r_4$)	$H = e^{2(1-t/T)}(2_{r1} - 1)$
Runtime	T=1

Table V.3. Summary of studied cases

Cases	Objective Function	Power Systems	Algorithm	
Case 1	Total fuel cost	IEEE 30 bus	HGSO CO	Without integration wind farms
Case 2	Fuel cost with valve point loading effect	√		
Case 3	Active power losses	√		
Case 4	Gas emission level	√		
Case 5	Fuel cost with voltage deviation	√		
Case 6	Fuel cost with voltage stability	√		
Case 7	Total fuel cost	IEEE 57 bus	HGSO	
Case 8	Fuel cost with voltage deviation	√		
Case 9	Fuel cost with voltage stability	√		
Case 10	Total fuel cost	DZ114-bus		
Case 11	Active power losses	√		
Case 12	Fuel cost with active power losses	√		
Case 13	Total fuel cost	IEEE 30 bus	HGSO	With the integration of wind farms
Case 14	Fuel cost with valve point loading effect	√		
Case 15	Total fuel cost	DZ114-bus		
Case 16	Active power losses	√		

V.2.1.The IEEE 30-bus power system

The first study was conducted on the IEEE 30-bus power system[81], which includes six generators, 41 transmission lines, 4 power transformers, and 9 VAR compensators, as detailed in Appendix A (Figure A.1, Tables A.2, and A.3). The goal was to evaluate the effectiveness of the HGSO and CO approaches in solving the OPF problem. The total power demand of this network is 283.4 MW + j 126.2 MVAR. A parametric analysis was carried out to determine the optimal values of l1, l2, and l3 related to the HGSO algorithm in solving the OPF problem. For each variant (setting of l1, l2 and l3), the HGSO algorithm was executed 30 times to obtain the minimum, average, and maximum of the optimal total fuel cost (Opt_Fc) for the IEEE 30-bus network, as shown in Table V.4.The characteristics of the system [5] are given in Tables A.1. The fuel cost coefficients considering the total fuel cost function are shown in [5, 68], while the gas emission coefficients for each generator are sourced from [62]

(refer to Tables A.4, A.5 and A.6). Tables V.5 and V.6 present the compiled simulation results for six objective function cases (refer to Table V.3), showing the optimal values of control variables determined by the HGSO and CO methods, respectively. Figures V.1, V.2, and V.3, illustrating the voltage profile using the CO method and the convergence curves of the objective functions for the four cases using the HGSO and CO algorithms, respectively. A comparison of the proposed methods (HGSO and CO) with other metaheuristic approaches reported in the literature is depicted in Table V.7.

Table V.4. The parametric analysis of HGSO ($l1_; l_2$ and l_3)

Parameters	Min(Opt_Fc)	Mean(Opt_Fc)	Max(Opt_Fc)
l_1= 1 ; l_2= 5 ; l_3= 1	800.3173	802.8481	808.3119
l_1= 1 ; l_2= 10; l_3= 1	800.2708	802.4661	808.2772
l_1= 1 ; l_2= 15; l_3= 1	800.1183	802.2749	811.6888
l_1= 1.5 ; l_2= 5 ;l_3= 1.5	800.1183	802.2749	811.6888
l_1= 0.5 ; l_2= 15; l_3= 0.5	799.3707	801.1301	807.3279

A. Simulation results

Table V.5. Optimal results for solving OPFP using HGSO algorithm for IEEE 30-bus system

Variables	**Min**	**Case 1**	**Case 2**	**Case 3**	**Case 4**	**Case 5**	**Case 6**	**Max**
P_{G1} (MW)	50	176.1889	199.6137	51.3410	63.6321	175.4477	166.7923	200
P_{G2} (MW)	20	48.1301	20.0000	80.0000	67.9369	48.2901	45.4294	80
P_{G5} (MW)	15	21.4909	20.5194	50.0000	50.0000	22.5002	22.1110	50
P_{G8} (MW)	10	21.6251	25.7989	35.0000	35.0000	21.8267	18.1433	35
P_{G11} (MW)	10	12.5713	14.7308	30.0000	30.0000	11.3734	19.8197	30
P_{G13} (MW)	12	12.0038	12.2326	40.0000	40.0000	13.7153	19.3828	40
V_{G1} (p.u)	0.95	1.1000	1.0997	1.1000	1.1000	1.0463	1.1000	1.1
V_{G2} (p.u)	0.95	1.0896	1.0890	1.1000	1.0957	1.0266	1.0907	1.1
V_{G5} (p.u)	0.95	1.0618	1.0726	1.0888	1.0860	1.0122	1.0921	1.1
V_{G8} (p.u)	0.95	1.0682	1.0735	1.0925	1.0896	1.0017	1.0911	1.1
V_{G11} (p.u)	0.95	1.1000	1.0989	1.1000	1.1000	1.0634	1.1000	1.1
V_{G13} (p.u)	0.95	1.0949	1.0202	1.1000	1.0501	1.0003	1.1000	1.1
T_{11} (6_9)	0.90	0.9952	1.0967	1.0181	1.1000	1.0275	1.0262	1.1
T_{12} (6_10)	0.90	1.0468	1.0474	1.0105	1.1000	0.9427	1.0502	1.1
T_{15} (4_12)	0.90	1.0486	1.0310	1.0418	1.0829	0.9332	0.9664	1.1
T_{36} (28_27)	0.90	0.9702	1.0269	1.0249	1.0381	0.9580	0.9352	1.1
Q_{C10} (MVar)	0	3.8673	4.3038	3.1543	5.0000	3.1501	5.0000	5
Q_{C12} (MVar)	0	3.7557	4.1979	3.6054	2.6928	2.7295	5.0000	5
Q_{C15} (MVar)	0	4.9319	4.9851	2.9722	3.5711	2.5341	5.0000	5
Q_{C17} (MVar)	0	4.9910	2.7406	4.4374	3.8769	1.1206	5.0000	5
Q_{C20} (MVar)	0	4.7268	2.9233	4.9508	3.6891	3.8965	5.0000	5
Q_{C21} (MVar)	0	5.0000	1.4140	5.0000	4.9063	4.2959	5.0000	5
Q_{C23} (MVar)	0	5.0000	3.9821	3.6297	5.0000	1.2620	5.0000	5
Q_{C24} (MVar)	0	2.6794	4.9861	5.0000	3.6064	4.1597	5.0000	5
Q_{C29} (MVar)	0	4.9659	4.9508	4.5653	2.9496	3.0192	2.7059	5
F_C ($/h)	-	**799.3707**	**918.3128**	967.2832	944.8241	**803.8981**	**804.7259**	-
F_{Em}(Ton/h)	-	0.3633	0.4402	0.2072	**0.2047**	0.3608	0.3353	-
F_{APL}(MW)	-	8.6100	9.4954	**2.9410**	3.1690	9.7534	8.2787	-
F_{VD}(p.u)	-	1.4523	0.5740	1.5624	0.7146	**0.1461**	2.0191	-
F_{Lmax}	-	0.1184	0.1303	0.1220	0.1305	0.1370	**0.1108**	-

Table V.6. Optimal results for solving OPFP using CO algorithm for IEEE 30-bus system

Variables	Min	Case 1	Case 2	Case 3	Case 4	Case 5	Case 6	Max
P_{G1} (MW)	50	178.0793	149.7507	52.2776	63.7276	174.2740	177.3620	200
P_{G2} (MW)	20	48.3974	51.9888	79.4892	67.9677	48.5704	49.2206	200
P_{G5} (MW)	15	21.2856	23.3656	49.9444	49.9815	22.4919	20.9048	80
P_{G8} (MW)	10	20.0822	30.2051	34.9390	34.9897	20.4547	21.2306	35
P_{G11} (MW)	10	12.2660	19.0750	29.9797	29.9852	13.9446	11.1129	35
P_{G13} (MW)	12	12.0264	16.8154	39.7262	39.9661	13.5086	12.2985	40
V_{G1} (p.u)	0.95	1.0996	1.0509	1.0897	1.0717	1.0383	1.0996	1.1
V_{G2} (p.u)	0.95	1.0859	1.0289	1.0841	1.0650	1.0244	1.0857	1.1
V_{G5} (p.u)	0.95	1.0604	1.0010	1.0640	1.0427	1.0202	1.0560	1.1
V_{G8} (p.u)	0.95	1.0685	0.9998	1.0706	1.0547	1.0068	1.0627	1.1
V_{G11} (p.u)	0.95	1.0985	1.0412	1.0967	1.0679	1.0202	1.0987	1.1
V_{G13} (p.u)	0.95	1.0977	1.0586	1.0990	1.0936	0.9986	1.0992	1.1
T_{11} (6_9)	0.90	0.9983	1.0178	1.0021	1.0513	1.0227	1.0448	1.1
T_{12} (6_10)	0.90	1.0065	0.9870	0.9414	0.9229	0.9002	0.9188	1.1
T_{15} (4_12)	0.90	1.0361	1.0260	0.9889	1.0034	0.9590	0.9939	1.1
T_{36} (28_27)	0.90	0.9810	0.9837	0.9691	0.9919	0.9623	0.9506	1.1
Q_{C10} (MVar)	0	2.8030	4.2491	4.4691	3.7358	3.4524	4.9408	5
Q_{C12} (MVar)	0	3.6956	3.1405	4.5957	0.4191	2.7200	4.9198	5
Q_{C15} (MVar)	0	4.3801	3.1065	4.3531	1.1912	4.4617	4.7867	5
Q_{C17} (MVar)	0	4.6096	2.1573	4.0590	3.9948	0.2268	3.8658	5
Q_{C20} (MVar)	0	3.0708	2.3468	4.7039	3.0672	4.2538	4.8061	5
Q_{C21} (MVar)	0	4.6254	4.0631	4.7850	3.9376	4.3933	4.3449	5
Q_{C23} (MVar)	0	2.0134	2.6013	3.7095	3.0393	4.5662	3.5754	5
Q_{C24} (MVar)	0	4.7441	4.6717	4.5367	4.8298	4.5584	4.7766	5
Q_{C29} (MVar)	0	3.4895	2.4736	3.3497	4.9514	2.4291	4.4795	5
F_C ($/h)	-	**799.2530**	**809.2989**	965.1057	944.7781	**815.1045**	**810.8296**	-
F_{Em}(Ton/h)	-	0.3687	0.3002	0.2071	**0.2048**	0.3572	0.3672	-
F_{APL}(MW)	-	8.7368	7.8005	**2.9561**	3.2177	9.8442	8.7294	-
F_{VD}(p.u)	-	1.3935	0.2322	1.7735	1.0774	**0.1052**	1.7397	-
F_{Lmax}	-	0.1217	0.1405	0.1177	0.1259	0.1371	**0.1153**	-

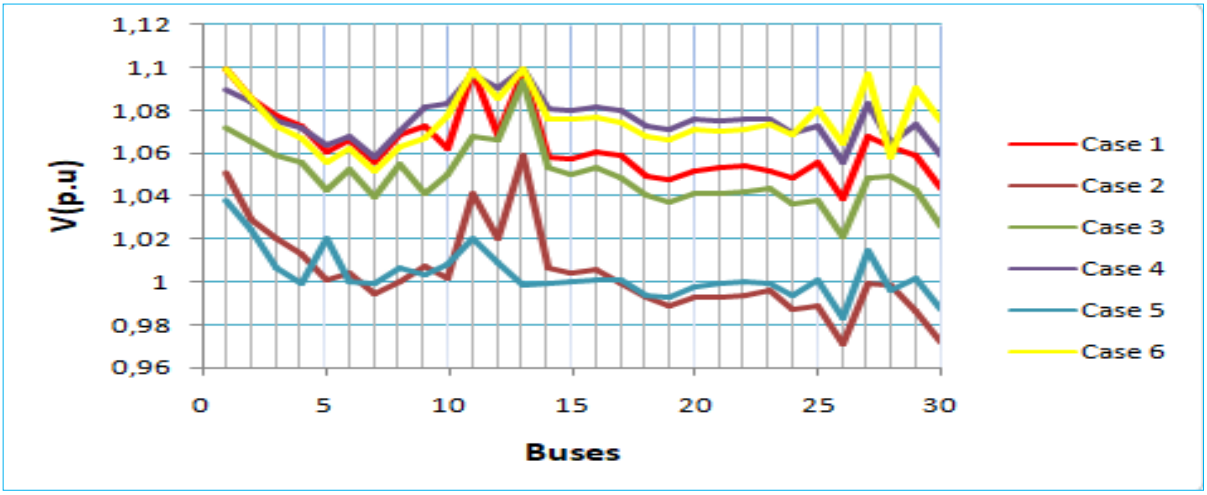

Figure V.1. Voltage profile for six cases using CO method.

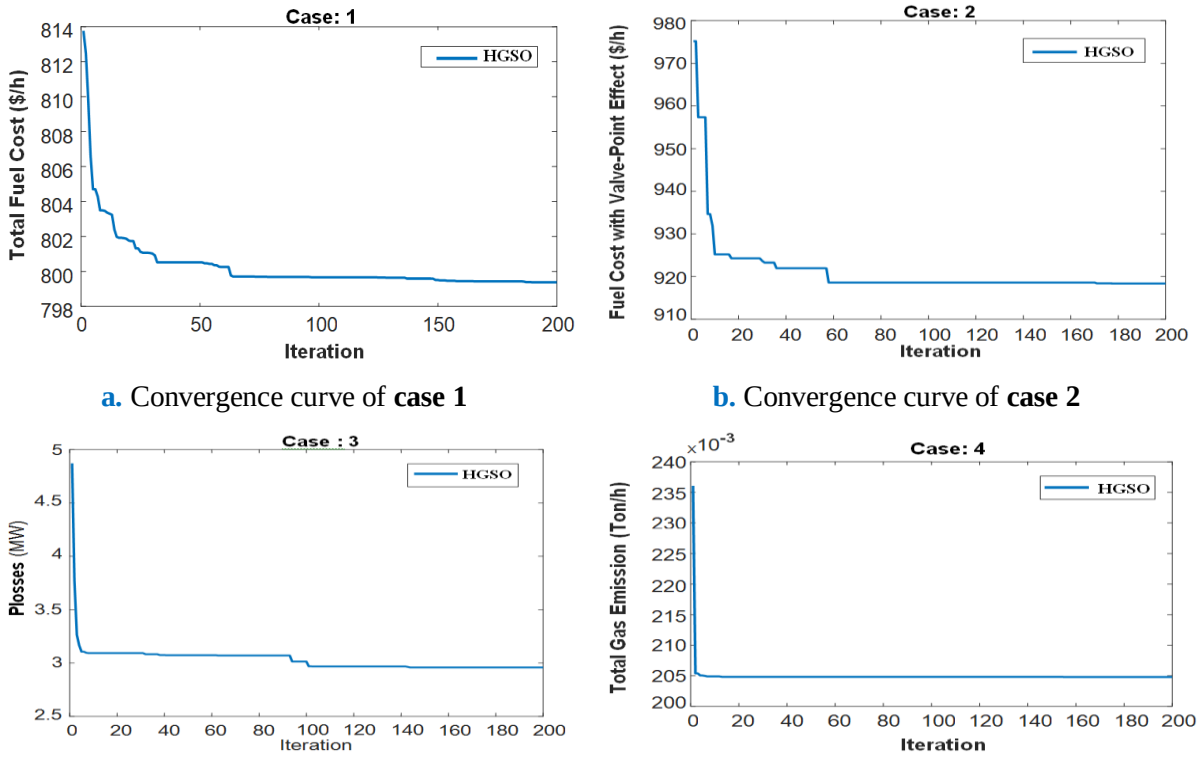

a. Convergence curve of **case 1**

b. Convergence curve of **case 2**

c. Convergence curve of **case 3**

d. Convergence curve of **case 4**

Figure V.2. Convergence curves of OPFP by HGSO: from case **1** to case **4 (**IEEE 30-bus)

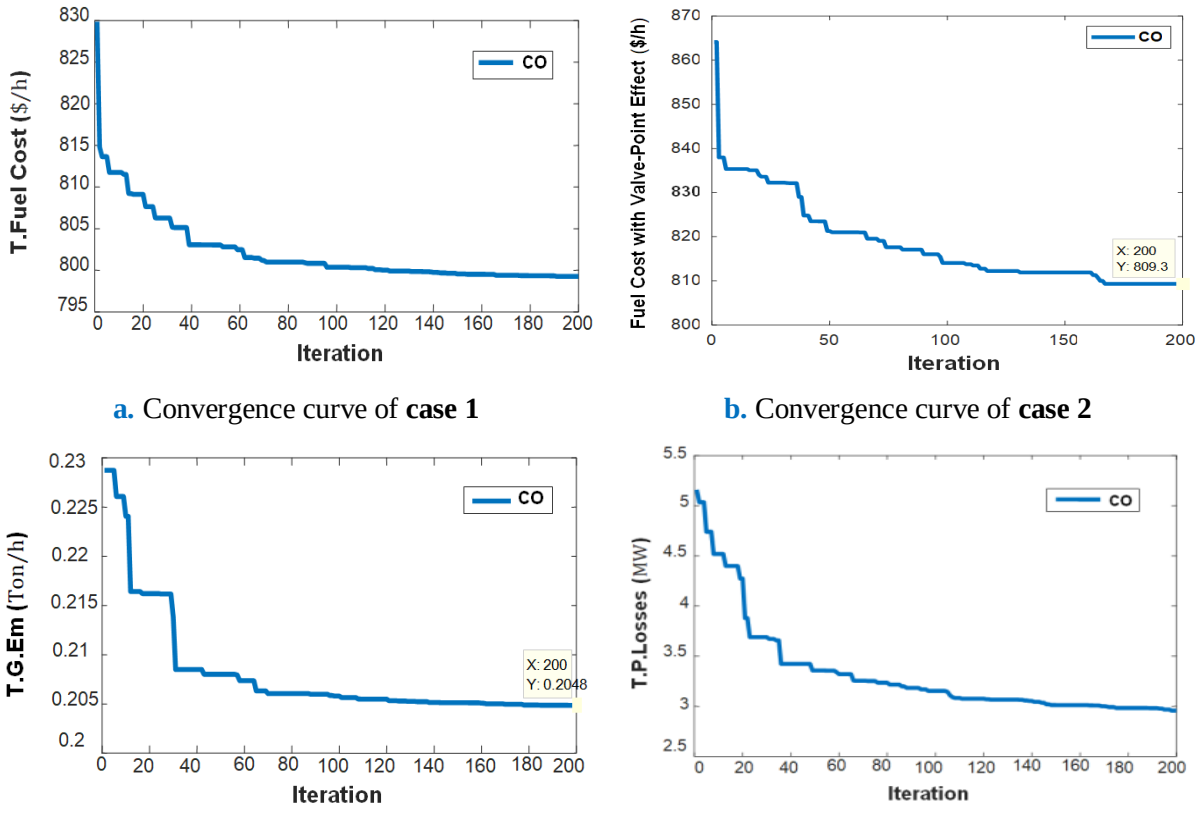

a. Convergence curve of **case 1**

b. Convergence curve of **case 2**

c. Convergence curve of **case 3**

d. Convergence curve of **case 4**

Figure V.3. Convergence curves of OPFP by CO: from case **1** to case **4 (**IEEE 30-bus)

Table V.7. Comparison of HGSO and CO with other methods for six **Cases**

Cases	**Methods**	**Fc**($/h)	**Em**(Ton/h)	**APL**(MW)	**VD** (p.u)	**Lmax**
Case1	NBA [68]	801.8442	-	9.1983	-	-
	SFLA [59]	801.8280	-	-	-	-
	PSO [69]	801.2300	0.3690	9.2600	1.0600	0.1560
	JFO [71]	801.0200	0.3673	9.2026	0.5320	0.1383
	CSA [61]	800.9886	-	-	-	-
	TLBO [58]	800.6740	0.3668	9.0198	0.9120	-
	MSA [70]	800.5099	0.3664	9.0345	0.9035	0.1383
	MGOA [64]	800.4744	0.3649	8.9882	0.8851	0.1295
	IMFO [62]	800.3848	0.3658	8.9990	0.9035	0.1274
	CO [61]	**799.2530**	0.3687	8.7368	1.3935	0.1217
	HGSO	**799.3707**	0.3633	8.6100	1.4523	0.1184
Case 2	CSA [61]	931.1146	-	-	-	-
	MSA [70]	930.7441	0.4349	13.1378	0.4492	0.1567
	JFO [71]	922.4800	0.4395	10.4660	0.4706	0.1433
	HHO [66]	920.5094	0.3738	9.6692	0.8844	-
	CO [61]	**809.2989**	0.3003	7.8005	0.2322	0.1405
	HGSO	**918.3128**	0.4402	9.4954	0.5740	0.1303
Case 3	PSO [69]	968.0800	0.2070	3.278	0.800	0.1410
	IMFO [62]	944.2572	0.2048	3.2601	0.8881	0.1276
	HHO [66]	932.4159	0.2176	3.2561	0.8679	-
	MSA [70]	944.5003	0.2048	3.2358	0.8739	0.1388
	JFO [71]	945.1000	0.2048	3.2320	1.1740	0.1260
	TLBO [58]	967.7195	0.2072	3.1104	0.8821	-
	CO [61]	965.1057	0.2071	**2.9561**	1.7735	0.1177
	HGSO	967.2832	0.2072	**2.9410**	1.5624	0.1220
Case 4	MOALO[74]	826.4556	0.2642	5.7727	1.2560	-
	HHO [66]	965.1211	0.2212	3.1069	0.8676	-
	IMFO [62]	967.5900	0.2073	3.0905	0.9192	0.1274
	TLBO [58]	967.7195	0.2072	3.1104	0.8821	-
	MSA [70]	967.6636	0.2072	3.1005	0.8886	0.1385
	PSO [69]	948.4700	0.2050	4.5300	0.8900	0.1290
	JFO [71]	944.3000	0.2049	3.4324	1.6486	0.1182
	CO [61]	944.7781	0.2048	3.2177	1.0774	0.1259
	HGSO	944.8241	**0.2047**	3.1690	0.7146	0.1305
Case 5	PSO [69]	830.3700	0.4430	10.410	1.6100	0.1300
	MOALO[74]	803,0611	-	-	0.3787	-
	GOA [64]	803.4488	0.3625	9.7749	0.1709	0.1353
	JFO [71]	803.5700	0.3700	9.9491	0.1480	0.1371
	CO [61]	815.1045	0.3572	9.8442	0.1052	0.1371
	HGSO	**803.8981**	0.3608	9.7534	**0.1461**	0.1370
Case 6	MSA [70]	801.2248	0.3610	8.9761	0.9265	0.1374
	PSO [69]	859.7100	0.3100	10.620	1.7800	0.1250
	MGOA [64]	800.5595	0.3695	9.1380	0.8302	0.1255
	IMFO [62]	800.4762	0.3662	9.0160	0.9086	0.1255
	CO [61]	810.8296	0.3672	8.7294	1.7397	0.1153
	HGSO	**804.7259**	0.3353	8.2787	2.0191	**0.1180**

B. Results interpretation

- The control and state variables of the HGSO and CO methods have been verified and constrained; by equality and inequality bounds, including safety constraints, within their acceptable range, as shown in Tables V.5 and V.6, respectively.

- The comparison report presented in Table V.7 confirms the ability of the HGSO and CO algorithms to achieve the best possible solutions through their smooth convergence curves, as shown in Figures V.2 and V.3.
- The voltage profile for the six-optimisation cases in the 30-bus system using the CO method is depicted in Figure V.1. It shows that the voltage levels at the load buses are within acceptable ranges.
- It is evident that the newly introduced CO and HGSO methods outperform other techniques in reducing the objective function across all six cases (see Tables V.5 and V.6), using the IEEE 30-bus power system. The comparison results, detailed in Table V.7 and discussed below, demonstrate the superior effectiveness of these methods.

Case 1: The first case aims to minimise the total fuel cost for electricity generation. The simulation results in Tables V.5 and V.6 show that the fuel costs for the HGSO and CO methods are lower (799.3707 and 799.2530$/h, respectively) than others in Table V.7.

Case 2: In this case, the valve point affects the fuel cost function by adding the absolute sinusoidal form to the quadratic fuel cost equation. The best total fuel cost obtained was 918.3128 ($/h) using the HGSO method. The CO algorithm was even better, with a lower total fuel cost of 809.29 ($/h), demonstrating its superiority (seeTableV.7).

Case 3: The total active power losses, in this case, are minimised using the HGSO and CO methods, resulting in optimum power losses of 2.9410 MW and 2.956 MW, respectively, which are lower than those obtained using the other techniques in the literature.

Case 4: The HGSO and CO algorithms successfully reduced the optimal emission levels to 0.2047 and 0.2048 tonnes per hour, respectively, compared to other optimization methods.

Case 5: The objective is to minimize both fuel cost and voltage deviation. The HGSO method delivered optimal results with a fuel cost of 803.8981($/h) and a voltage deviation of 0.1461 p.u. In comparison, the CO method achieved a slightly higher fuel cost of 815.1045 ($/h) but excelled in voltage deviation, reducing it to 0.105 p.u., outperforming other techniques.

Case 6: This case aims to reduce the total fuel cost and the maximum L-index simultaneously. The HGSO method achieved lower values of 804.7259 ($/h) and 0.1180 (p.u.), outperforming other techniques, while the CO method also delivered competitive results with optimal values of 810.8296 ($/h) and 0.1052 (p.u.) as shown in Table V.7.

V.2.2.The IEEE 57-bus power system

The second test system, the IEEE 57-bus power system[3],comprises seven generators, 80

transmission lines, 17 transformers, and 3 VAR compensators. This system is used to assess the effectiveness of the HGSO method in addressing OPF problem. Detailed technical characteristics and a single-line diagram of this system are available in Appendix B (Figure B.1, and Tables B. 1, B. 2, B. 3 and B. 4). The total power demand is 1250.8 MW + j336.4 MVAR. The optimal values of control variables and objective functions are depicted in Table V.8. At the same time, the comparison of HGSO with other algorithms is given in Table V.9. Three optimisation cases using the HGSO method from case 7 to case 9 (refer to Table V. 3) are investigated.

A.Simulation results

Table V.8. Optimal results for solving OPFP using HGSO algorithm for IEEE 57-bus system

Variables	Min	Case 7	Case 8	Case 9	Max
$P_{G1\ (MW)}$	00	149.9183	143.8809	145.0980	575.88
$P_{G2\ (MW)}$	00	72.8250	71.0921	80.9257	100
$P_{G3\ (MW)}$	00	45.9372	45.2785	44.3142	140
$P_{G6\ (MW)}$	00	87.7951	99.2248	91.5566	100
$P_{G8\ (MW)}$	00	469.8666	460.2303	470.3573	550
$P_{G9\ (MW)}$	00	76.9162	85.7701	74.3983	100
$P_{G12\ (MW)}$	00	362.4702	362.1430	359.6229	410
$V_{G1\ (p.u)}$	0.95	1.0915	1.0380	1.0990	1.1
$V_{G2\ (p.u)}$	0.95	1.0885	1.0327	1.0974	1.1
$V_{G3\ (p.u)}$	0.95	1.0840	1.0248	1.0942	1.1
$V_{G6\ (p.u)}$	0.95	1.0992	1.0380	1.0994	1.1
$V_{G8\ (p.u)}$	0.95	1.1000	1.0541	1.0996	1.1
$V_{G9\ (p.u)}$	0.95	1.0787	1.0189	1.0777	1.1
$V_{G12\ (p.u)}$	0.95	1.0836	1.0130	1.0837	1.1
$T_{19\ (4\_18)}$	0.90	0.9938	1.0057	1.0039	1.1
$T_{20\ (4\_18)}$	0.90	1.0069	0.9833	1.0383	1.1
$T_{31\ (21\_20)}$	0.90	0.9273	0.9965	0.9532	1.1
$T_{35\ (24\_25)}$	0.90	0.9786	0.9626	0.9297	1.1
$T_{36\ (24\_25)}$	0.90	1.0513	1.0595	1.0628	1.1
$T_{37\ (24\_26)}$	0.90	0.9630	0.9821	0.9644	1.1
$T_{41\ (7\_29)}$	0.90	0.9725	1.0106	1.0052	1.1
$T_{46\ (34\_32)}$	0.90	0.9935	0.9004	0.9952	1.1
$T_{54\ (11\_41)}$	0.90	0.9941	0.9283	1.0133	1.1
$T_{58\ (15\_45)}$	0.90	0.9657	0.9202	1.0091	1.1
$T_{59\ (14\_46)}$	0.90	0.9902	0.9722	1.0195	1.1
$T_{65\ (10\_51)}$	0.90	0.9733	0.9621	0.9680	1.1
$T_{66\ (13\_49)}$	0.90	0.9651	0.9525	0.9777	1.1
$T_{71\ (11\_43)}$	0.90	1.0215	0.9736	1.0203	1.1
$T_{73\ (40\_56)}$	0.90	0.9981	1.0018	0.9907	1.1
$T_{76\ (39\_57)}$	0.90	1.0246	1.0258	1.0825	1.1
$T_{80\ (9\_55)}$	0.90	1.0044	0.9780	1.0131	1.1
$Q_{C18\ (MVar)}$	0	0.0597	0.0756	0.0377	20
$Q_{C25\ (MVar)}$	0	0.2209	0.1228	0.2689	20
$Q_{C53\ (MVar)}$	0	0.1769	0.1001	0.1407	20
$\mathbf{F_C}$ ($/h)	-	**41. 670.0000**	**41. 753.0000**	**41. 680.0000**	-
$\mathbf{F_{APL}}$(MW)	-	14.9285	16.8198	15.4730	-
$\mathbf{F_{VD}}$ (p.u)	-	2.9837	**0.2539**	2.4241	-
$\mathbf{F_{Lmax}}$	-	0.2127	0.8750	**0.2127**	-

Table V.9. Comparison of HGSO with other methods for three cases

Cases	Methods	F_C($/h)	F_{APL}(MW)	F_{VD}(p.u)	F_{Lmax}
Case7	SFLA [59]	41.872.9000	-	-	-
	NBA [68]	41.838.2081	18.6718	-	-
	TLBO [58]	41.679.8910	15.1530	1.6510	-
	MSA [70]	41.673.7231	15.0526	1.5508	0.2839
	MGOA [64]	41.671.0980	15.0094	1.5297	0.2460
	HGSO	**41.670.0000**	14.9285	2.9837	0.2127
Case 8	MOALO [74]	41.747.8223	-	0.9444	-
	MGOA [64]	41.697.9735	15.7451	0.7381	1.3475
	IMFO [62]	41. 692.7178	15.7552	0.7182	0.2425
	MSA [70]	41.714.9851	15.9214	0.6781	0.2953
	HGSO	**41.753.0000**	16.8198	**0.2539**	0.8750
Case 9	MSA [70]	41.675.9948	15.0026	1.7236	0.2748
	MGOA [64]	41.682.4031	15.2633	1.3333	0.2297
	HGSO	**41.680.0000**	15.4730	2.4241	**0.2127**

B. Results interpretation

The HGSO method outperformed other algorithms in all three cases (see Tables V.8), delivering superior results in fuel cost, voltage deviation, and voltage stability (see Tables V.9). In **case 7**, the optimal total fuel cost of 41,670.00 ($/h) was lower than other techniques, indicating the superior performance of the HGSO method. In the minimisation of fuel cost with voltage deviation in **case 8**, the HGSO method reduced the voltage deviation to 0,2539 (p.u.), demonstrating its efficiency compared to recent algorithms in the literature. While in **case 9**, the HGSO method yielded an L-index of 0.2127 (p.u.) and a fuel cost of 41,680.00($/h), which were the best values compared to other methods, cited above.

V.2.3.The Algerian DZ114-bus electrical transmission network

The third system tested is Algeria's large electricity transmission network [25], to evaluate the effectiveness of the HGSO algorithm. It is shown on a map published by Sonelgaz in 2007 (see Figure C.1) and comprises 15 generators, 175 lines and 16 tap changers on lines 160 to 175, as well as 12 VAR compensators. Its total electricity demand is 3727 MW + j 2070 MVAR, with technical details provided in [74]. Three optimisation cases are treating using the HGSO method, from case 10 to case 12 (in Table V.3). The bus and line data with the fuel cost coefficients [60] are in Appendix C (Tables C.1, C.2, C.3, C.4, and C.5). The optimal results obtained by the HGSO method are summarised in Table V.10. The comparison of HGSO with others for three cases in Table V.11 .The convergence curve of the proposed HGSO algorithm for the first two cases is plotted in Figure V.4. While the voltage profile of the Algerian power system in Figure V.5.

A.Simulation results

Table V.10. Optimal results for solving OPFP using HGSO algorithm for the Algerian DZ 114 bus

Variables	Min	Case 10	Case 11	Case 12	Max
$P_{G4\,(MW)}$	135.0000	348.3765	355.4595	608.9816	1350.0000
$P_{G5\,(MW)}$	135.0000	467.5035	542.9554	311.2254	1350.0000
$P_{G11\,(MW)}$	10.0000	100.0000	98.3618	100.0000	100.0000
$P_{G15\,(MW)}$	30.0000	188.4769	192.0580	235.6576	300.0000
$P_{G17\,(MW)}$	135.0000	518.2787	529.3234	512.3014	1350.0000
$P_{G19\,(MW)}$	34.5000	220.0679	188.5006	281.3769	345.0000
$P_{G22\,(MW)}$	34.5000	175.2057	183.4193	118.8408	345.0000
$P_{G52\,(MW)}$	34.5000	158.6728	160.8692	131.3275	345.0000
$P_{G80\,(MW)}$	34.5000	183.1605	247.0336	261.6869	345.0000
$P_{G83\,(MW)}$	30.0000	167.1790	246.2296	200.4776	300.0000
$P_{G98\,(MW)}$	30.0000	198.1002	278.4689	115.4165	300.0000
$P_{G100\,(MW)}$	60.0000	596.6675	286.0773	600.0000	600.0000
$P_{G101(MW)}$	20.0000	200.0000	173.9237	167.3948	200.0000
$P_{G109\,(MW)}$	10.0000	96.4511	99.5077	34.4145	100.0000
$P_{G111\,(MW)}$	10.0000	168.9493	194.6771	121.9808	200.0000
V_{G4} (p.u)	0.90	1.1000	1.0978	1.0841	1.1
V_{G5} (p.u)	0.90	1.0987	1.0940	1.0741	1.1
V_{G11} (p.u)	0.90	1.1000	1.0876	1.0245	1.1
V_{G15} (p.u)	0.90	1.1000	1.0975	1.0543	1.1
V_{G17} (p.u)	0.90	1.0929	1.0993	1.0158	1.1
V_{G19} (p.u)	0.90	1.0987	1.0553	0.9848	1.1
V_{G22} (p.u)	0.90	1.0801	1.0755	1.0266	1.1
V_{G52} (p.u)	0.90	1.0378	1.0500	1.0220	1.1
V_{G80} (p.u)	0.90	1.0514	1.0965	1.0667	1.1
V_{G83} (p.u)	0.90	1.0718	1.1000	1.0178	1.1
V_{G98} (p.u)	0.90	1.0981	1.0876	1.0111	1.1
V_{G100} (p.u)	0.90	1.1000	1.0932	0.9912	1.1
V_{G101} (p.u)	0.90	1.1000	1.0761	1.0034	1.1
V_{G109} (p.u)	0.90	1.0747	1.0772	1.0070	1.1
V_{G111} (p.u)	0.90	1.1000	1.1000	0.9945	1.1
$\mathbf{T_{160}}$ (80-88)	0.90	1.0272	1.0916	0.9161	1.1
$\mathbf{T_{161}}$ (81-90)	0.90	1.1000	1.0752	0.9964	1.1
$\mathbf{T_{162}}$ (86-93)	0.90	1.1000	1.0689	0.9662	1.1
$\mathbf{T_{163}}$ (41-42)	0.90	1.0565	1.0562	1.0653	1.1
$\mathbf{T_{164}}$ (57-58)	0.90	1.0297	1.0554	1.0204	1.1
$\mathbf{T_{165}}$ (43-44)	0.90	1.1000	1.0430	1.0020	1.1
$\mathbf{T_{166}}$ (59-60)	0.90	1.1000	1.0679	0.9479	1.1
$\mathbf{T_{167}}$ (63-64)	0.90	1.1000	1.0595	0.9673	1.1
$\mathbf{T_{168}}$ (71-72)	0.90	1.0867	1.0834	0.9600	1.1
$\mathbf{T_{169}}$ (17-18)	0.90	1.1000	1.0447	0.9506	1.1
$\mathbf{T_{170}}$ (20-21)	0.90	1.1000	1.0397	0.9744	1.1
$\mathbf{T_{171}}$ (26-27)	0.90	1.0936	1.0786	0.9598	1.1
$\mathbf{T_{172}}$ (26-28)	0.90	1.1000	1.0852	0.9743	1.1
$\mathbf{T_{173}}$ (30-31)	0.90	1.0735	1.0691	0.9514	1.1
$\mathbf{T_{174}}$ (47-48)	0.90	1.0825	1.0808	0.9989	1.1
$\mathbf{T_{175}}$ (74-76)	0.90	1.0181	1.0609	0.9215	1.1
$Q_{C41\,(MVar)}$	3	19.9330	19.5710	11.4201	20
$Q_{C43\,(MVar)}$	3	14.4175	16.8581	14.0053	20
$Q_{C50\,(MVar)}$	3	20.0000	18.9466	9.9930	20
$Q_{C66\,(MVar)}$	3	12.7807	19.2152	12.3902	20
$Q_{C67\,(MVar)}$	3	16.2197	18.1566	8.8092	20
$Q_{C68\,(MVar)}$	3	20.0000	17.6083	8.3920	20
$Q_{C69\,(MVar)}$	3	15.3815	18.7583	5.2522	20
$Q_{C70\,(MVar)}$	3	12.0233	16.4676	7.5048	20
$Q_{C77\,(MVar)}$	3	18.3710	13.6874	10.6600	20
$Q_{C89\,(MVar)}$	3	12.6754	18.5778	17.6067	20
$Q_{C92\,(MVar)}$	3	9.3146	17.0296	12.8221	20
$Q_{C93\,(MVar)}$	3	15.7228	18.9097	9.8242	20
$\mathbf{F_C}$ ($/h)	-	**18.998.8900**	20.689.0000	**20.397.3000**	-
$\mathbf{F_{APL}}$ (MW)	-	60.0894	**49.8652**	74.0823	-

Table V.11. Comparison of HGSO with other methods for three cases

Cases	Methods	F_C($/h)	F_{APL}(MW)
Case10	MOALO [74]	19.355.8595	-
	PSO [60]	19.235.0000	87.9052
	DEA [60]	19.203.3400	89.2570
	GA [67]	19.201.3290	89.2570
	GOA [65]	19.178.8180	75.0552
	GWO [63]	19.171.9582	75.1879
	SMA [65]	19.170.2050	74.9442
	ALO [63]	19.141.7714	76.3446
	HGSO	**18.998.8900**	**60.0894**
Case 11	SSA [67]	-	93.6440
	HGSO	**20.689.0000**	**49.8652**
Case 12	MOALO [74]	20.600.7073	66.0278
	HGSO	**20.397.3000**	**74.0823**

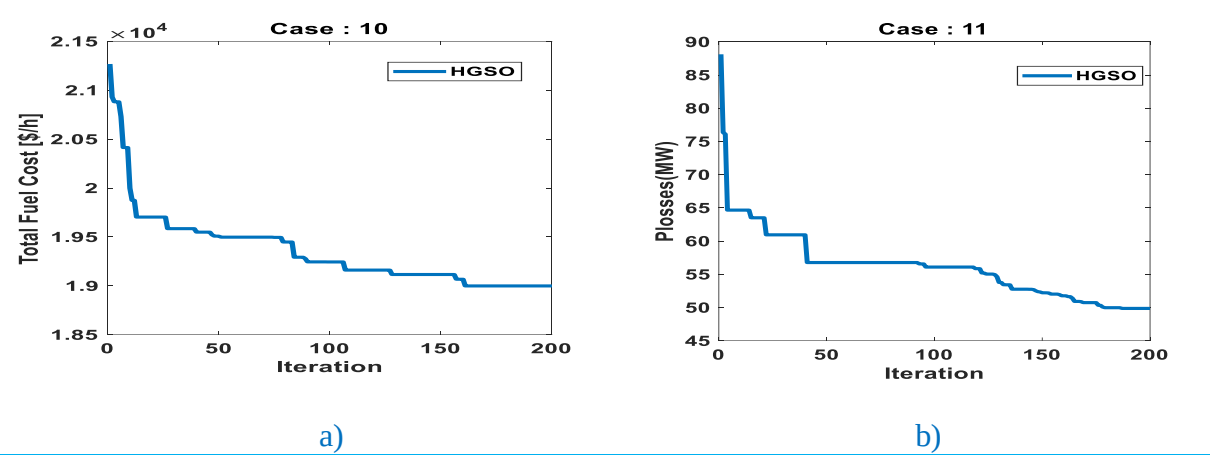

Figure V.4. Convergence curves of the OPFP for cases 10 and 11 of the Algerian DZ114-bus

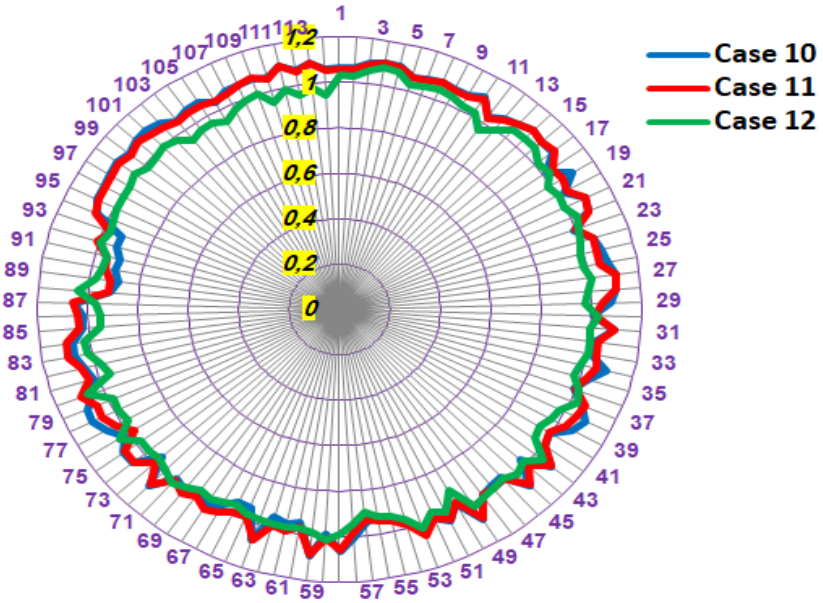

Figure V.5. Algerian electricity network voltage profile (114 JB)

B. Results interpretation

- A summary of the optimisation cases using the HGSO method is provided in Table V.10. The comparison of the optimal results with other methods for the three cases is presented in Table V.11.

Case 10: Minimization of fuel cost

The objective in this case is to minimize the total fuel cost. The HGSO method achieved a total cost of 18,998.89$/h (Table V.10), representing a significant improvement over results from other methods reported in the literature (see Table V.11).

Case 11: Minimization of active power losses

For this case, the focus is on minimising total active power losses. The HGSO method resulted in optimal active power losses of 49.8652 MW, outperforming the SAA method, which recorded losses of 93.644 MW.

Case 12: Minimization of fuel cost and active power losses

This case aims simultaneously to reduce fuel costs and active power losses. The HGSO method achieved a 6.4% reduction in total fuel cost compared to the MOALO method, although it resulted in an 18% increase in active power losses compared to MOALO.

- Figure V.5 illustrates the voltage profile of the Algerian DZ114-bus system for three cases of OPF problems: case 10, case 11, and case 12. This shows that the load bus voltages are within the acceptable range. For buses, 49 (TENES), 56 (MEDEA), 88 (EHADJAR), 89 (SOUK AHRAS), 90 (AL AWINT) and 91 (TEBESSA), the voltage magnitudes are close to the minimal permissible voltage (V≈ 0.9 p.u). To prevent voltage drops in these buses and avoid critical situations in the network operation due to the increase in load demand, the insertion of reactive power compensators in these nodes that will improve the voltage magnitudes, ensuring both the stability and the security of the DZ114 Algerian electrical network.

V.2.4. Principal advantages of the HGSO and CO method

The main advantages of the proposed methods, HGSO and CO, are summarised below:

V.2.4.1.Advantages of the HGSO method

- The exploration and exploitation mechanisms are managing by controlling the randomness rate to escape from local optima, and to cover the whole search. This task is accomplished by tuning the three principal parameters: Sij, γ, and F.

- Updating each solution (gas i in its cluster j) is based on the global solution (best gas position in all clusters) and the best gas position in each cluster, which allows the HGSO algorithm to achieve the best balance between exploration and exploitation factors, and avoid the local optimal as shown by the convergence curves in Figures V.2 and V.4.

- The values of the control and state variables obtained by the HGSO method have been checked and bounded by equality and inequality limits, including safety constraints, which are within their permissible ranges, as presented in Tables V.5, V.8, V.10, and Figure V.5.

- The comparison report confirms the ability of the HGSO algorithms to achieve the best solution as illustrated in in Tables V.7, V.9 and V.11**.**

V. 2.4.2. Advantages of the CO method

- The strategies of the hunting process create a good balance between the exploration and exploitation phases and prevent premature convergence or avoidance of local solutions, as shown in Figure V.3.

- The control and state variables of the CO method are verified and constrained by both equality and inequality bounds, including safety constraints, within their acceptable range, as shown in Table V.6 and Figure V.1.

- The comparison report highlights the ability of the CO algorithm to achieve the best optimal values, as indicated in Table V.7.

V.3. OPF using the HGSO method with wind power integration

In this study, we will discuss the results and simulation of OPF using the metaheuristic technique with wind power integration in two sections. First, a techno-economic study was used to determine the cost of wind power, and second, a metaheuristic method was used to determine the optimal cost of producing electricity from thermal stations with wind farms.

V.3.1.Wind energy cost based on a techno-economic study

In this section, we chose three sites in the highland region of Algeria to calculate the Weibull parameters and the annual mean wind speed for various turbine hub heights. The Weibull parameters for the selected sites at a height of 10 m, the technical characteristics of the wind turbines and the turbine-specific costs are given in Tables III. 5, III. 6, and III. 7 for Chapter III. Lastly, we discuss the cost optimization of wind power.The following are the results and simulations of this work:

V.3.1.1.Weibull parameters and wind speed extrapolation

- Table V.12 shows the annual Weibull parameter results for different hub heights of the selected turbines. Eqs (III. 8), (III. 9), and (III. 10) were used to estimate the shape factors, scale factors, power coefficients, and mean wind speeds at different hub heights of the turbines.

Table V.12. Weibull parameters extrapolation at hub height turbines in chosen sites

Wind turbines	h_i(m)	v_i(m/s)	k_i	c_i(m/s)	z_i	Sites
Vestas V-80	67	4.5416	2.1000	6.8861	0.301	Setif
SuzlonS-82	78.5	4.6456	2.1358	7.2990	0.306	
EnerconE-58	89	4.7298	2.1656	7.6547	0.310	
Gamesa G-114	93	4.7596	2.1760	7.7857	0.311	
Vestas V-80	67	5.1453	2.2353	7.6264	0.287	Djelfa
SuzlonS-82	78.5	5.2632	2.2739	8.0626	0.292	
EnerconE-58	89	5.3586	2.3050	8.4375	0.296	
Gamesa G-114	93	5.3924	2.3161	8.5753	0.297	
Vestas V-80	67	6.2348	2.4605	8.9081	0.266	El Bayadh
SuzlonS-82	78.5	6.3776	2.5024	9.3802	0.271	
EnerconE-58	89	6.4932	2.5367	9.7845	0.275	
Gamesa G-114	93	6.5341	2.5489	9.9328	0.276	

- The average wind speed increases with the hub height of the wind turbines and the Weibull parameters for each site, as shown in Figure V.6. El Bayadh is the windiest site among the selected regions.

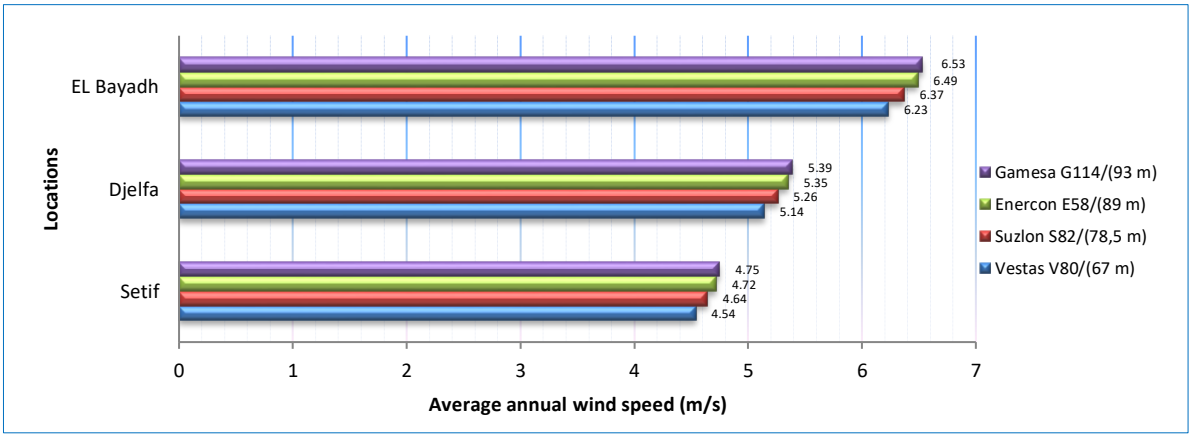

Figure V.6.Average wind speed extrapolation for different hub height turbines

V.3.1.2.Electrical power output and cost analysis

- The capacity factor (C_f), annual energy production (AEP), total lifetime energy production of the wind turbine (TEP), present value cost (PVC), and unit cost of energy (UCE) for each type of wind turbine installed at each selected site were determined using the following Eqs. (III.15), (III.17), (III.18), (III.19), and (III.21) respectively, as detailed

in Table V.13. The average cost of each turbine (C_{wind}) was determined by Eq. (III.20), based on the rated power of the turbine and the specific costs given in Table III. 7. So, as shown in Table V.13, the Gamesa model achieved the highest annual energy production value among these four types of wind turbines, including the capacity factor, at the El Bayadh site.

Table V.13. Results of the techno-economic study for wind power production

Parameters	Sites			Wind turbines	C_{wind} ($)	PVC
	Setif	Djelfa	EL Bayadh			
C_f (%)	13.03	15.67	20.93	Vestas V-80	000.2600	3.4343e+006
P_{out}(KW)	260.5781	313.4757	418.6693			
AEP (GWh)	2.2827	2.7460	3.6675			
TEP (GWh)	45.653	54.921	73.351			
UCE ($/KWh)	0.0752	0.0625	0.0468			
C_f (%)	19.76	23.76	31.44	Suzlon S-82	1950.000	2.5757e+006
P_{out}(KW)	296.4327	356.4531	471.6535			
AEP (GWh)	2.5968	3.1225	4.1317			
TEP (GWh)	935.51	62.451	82.634			
UCE ($/KWh)	0.0496	0.0412	0.0312			
C_f (%)	33.00	38.15	47.51	Enercon E-58	1300.000	1.7172e+006
P_{out}(KW)	330.0285	381.5316	475.0813			
AEP (GWh)	2.8910	3.3422	4.1617			
TEP (GWh)	57.821	66.844	83.234			
UCE ($/KWh)	0.0297	0.0257	0.0206			
C_f (%)	45.18	51.40	61.68	Gamesa G-114	000.2600	3.4343e+006
P_{out}(KW)	903.5591	1.0280e+003	1.2336e+03			
AEP (GWh)	7.9152	9.0052	10.806			
TEP (GWh)	158.30	180.10	216.12			
UCE ($/KWh)	0.0217	0.0191	0.0159			

- The annual energy production AEP obtained by the wind turbine models used at each site is depicted in Table V.13 and Figure V.7. AEP production ranges from 2.28 GWh in Sétif (using the Vesta V80) to 10.8 GWh in El Bayadh (using the Gamesa G114). El Bayadh generates the most energy across all turbine types.

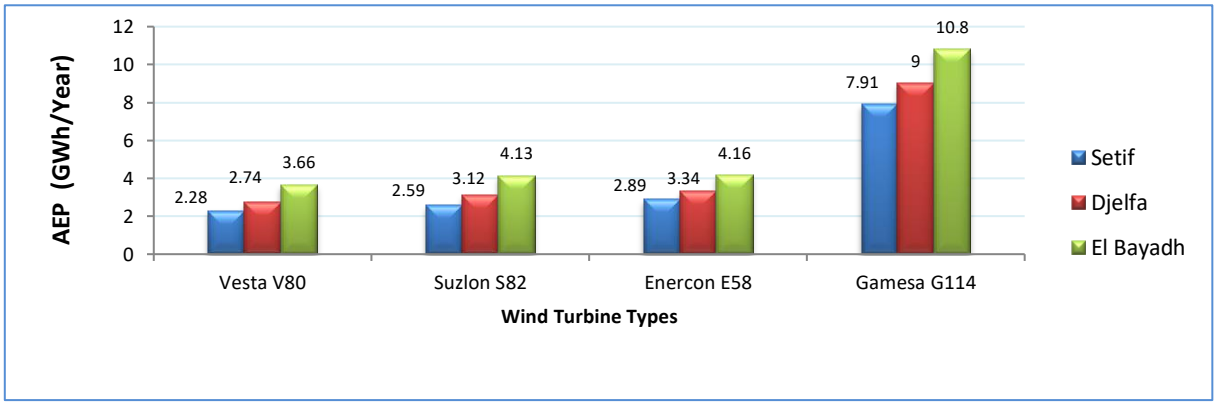

Figure V.7. Annual energy production per turbine type at each location.

- Figure V.8 displays the capacity factors of the selected wind turbines. The Gamesa G114 type has the highest capacity factor, ranging from 45.18% in Sétif to 51.4% in Djelfa and 61.68% in El Bayadh, respectively. In contrast, the Vestas V80 model has the lowest capacity factor in all these locations.

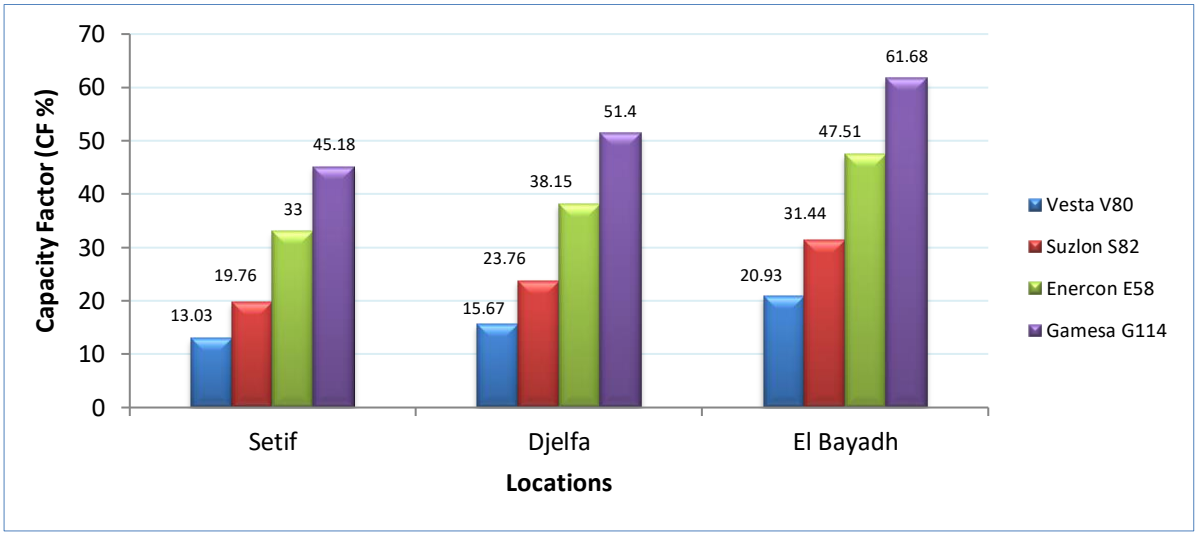

Figure V.8.The capacity factor per turbine type at each location

- In addition, the unit energy cost UCE using the PVC method for the selected wind turbine is in Table V.13, and illustrated in Figure V.9. The UCE ranges from about 0.0752 ($/KWh) in Sétif for the Vesta V80 model to 0.0159 ($/KWh) in El Bayadh for the Gamesa G114 model. It should be noted that the El Bayadh site has the lowest unit energy cost compared to the other sites, while the highest energy cost is recorded in Setif with the Vesta V80 model.

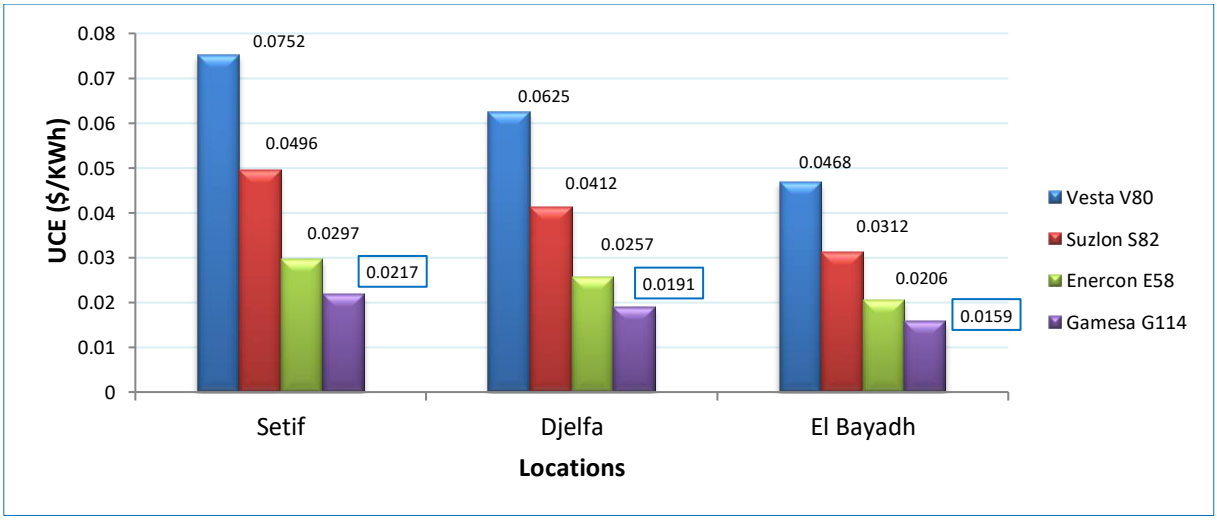

Figure V.9.Unit energy cost (UEC) per turbine type at each location

V.3.2.Optimal cost of electricity generation

This study analyses and discusses the simulation results of optimising the total electricity production cost by integrating thermal power plants with wind farms using the HGSO metaheuristic method to solve four cases of objective functions given in Table V.3. The standard IEEE 30-bus test system and the Algerian DZ 114-bus transmission network are considered for this test, using the Gamesa G-114 turbine, as studied in our previous study [1]. This section examines network performance before and after installing a wind turbine generator, enabling a comparative evaluation of its impact on system dynamics and efficiency.

V.3.2.2 Modified IEEE 30 bus system with wind power

This section addresses the OPF problem for a hybrid power system combining conventional thermal generators with stochastic wind power, as illustrated in Figure D.1 (Appendix D). In this scenario, three wind farms are integrated at load buses 10, 24, and 30, contributing to a total wind power penetration rate of 20% of the overall electricity demand. Each wind farm consists of 20 wind turbines, with a total rated capacity of 40 MW (each turbine rated at 2 MW). Adjusted data for the IEEE 30-bus system, cost coefficients, and wind farm characteristics are given in Tables D.1, D.2, and D.3, respectively (Appendix D). This study analyses two specific cases: the quadratic fuel cost (F_C) and the fuel cost considering the valve point load effect (F_{Cvalv}), which are referred to as cases 13 and 14 in Table V.3. The convergence curves and optimal simulation results for these two objective functions are in Figures V.10 and Table V.14, respectively. Figures V.11 and V.12 show the optimal output active powers.

A.<u>Simulation results</u>

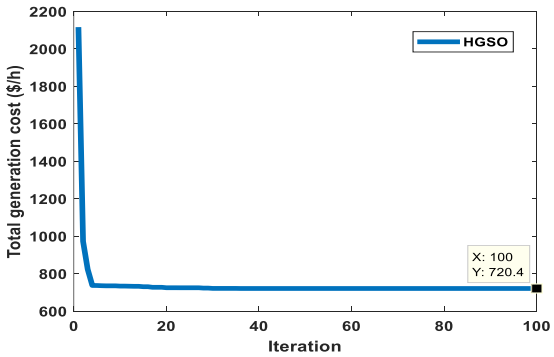

a) Case 13

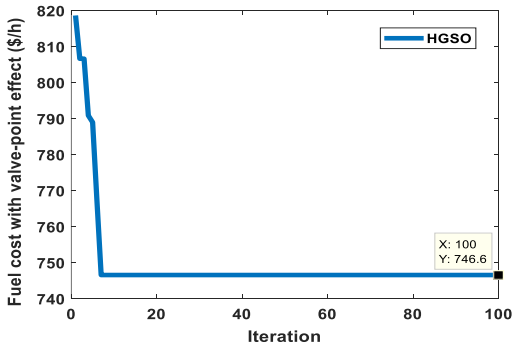

b) Case 14

Figure V.10. Convergence characteristics of OPFP by HGSO with wind power (IEEE 30-bus)

Table V.14. Optimal results for solving OPFP using HGSO with wind farms (IEEE 30-bus)

Variables	Min	Case 13	Case 14	Max
P_{G1} (MW)	50	135.9128	151.4882	200
P_{G2} (MW)	20	36.6317	20.0000	80
P_{G5} (MW)	15	18.5327	18.7885	50
P_{G8} (MW)	10	17.2107	21.3089	35
P_{G11} (MW)	10	11.8035	12.2034	30
P_{G13} (MW)	12	14.3277	12.0000	40
P_{W10} (MW)	0	16.3388	9.6566	40
P_{W24} (MW)	0	20.2015	20.6311	40
P_{W30} (MW)	0	20.1397	26.3923	40
V_{G1} (p.u)	0.95	0.9850	1.0081	1.1
V_{G2} (p.u)	0.95	0.9674	0.9732	1.1
V_{G5} (p.u)	0.95	0.9706	0.9671	1.1
V_{G8} (p.u)	0.95	0.9567	0.9501	1.1
V_{G11} (p.u)	0.95	0.9657	0.9767	1.1
V_{G13} (p.u)	0.95	0.9562	0.9706	1.1
V_{W10} (p.u)	0.95	0.9633	0.9618	1.1
V_{W24} (p.u)	0.95	0.9578	0.9500	1.1
V_{W30} (p.u)	0.95	1.0046	0.9593	1.1
T_{11} (6_9)	0.90	0.9198	0.9407	1.1
T_{12} (6_10)	0.90	0.9433	0.9072	1.1
T_{15} (4_12)	0.90	0.9201	0.9000	1.1
T_{36} (28_27)	0.90	0.9232	0.9042	1.1
Q_{C10} (MVar)	0	0.2080	0.6881	5
Q_{C12} (MVar)	0	0.2591	0.0011	5
Q_{C15} (MVar)	0	1.8188	0.3102	5
Q_{C17} (MVar)	0	0.6268	2.2340	5
Q_{C20} (MVar)	0	1.1817	0.3493	5
Q_{C21} (MVar)	0	0.2895	0.7909	5
Q_{C23} (MVar)	0	0.4714	0.6881	5
Q_{C24} (MVar)	0	0.5901	0.0011	5
Q_{C29} (MVar)	0	0.5334	0.3102	5
Thermal generation cost $\mathbf{F_{CTG}}$ ($/h)	-	614.0980	630.3768	-
Wind generation cost $\mathbf{F_{CTW}}$ ($/h)	-	106.2636	116.2043	-
Total generation cost $\mathbf{F_{CT}}$ ($/h)	-	**720.3616**	**746.5811**	-
F_{APL}(MW)	-	7.6991	9.0690	-
(p.u)F_{VD}	-	0.8666	0.9418	-
β_{10} (%)	-	5.77	3.41	-
β_{24} (%)	-	7.13	7.28	-
β_{30} (%)	-	7.11	9.31	-

- As demonstrated in Table V.14, the simulation results for the two objective function cases show that the optimal values of the control variables, as determined by the HGSO method, remain within their allowable limits, ensuring compliance with system constraints.

- The smooth convergence curves for the two cases, shown in Figure V.10, indicate that the HGSO method efficiently reaches the global optimal value by the fourth iteration in case 13. In case 14, convergence occurs at the sixth iteration, proving the algorithm's effectiveness.

- To analyse the effects of wind integration on the IEEE 30-bus network, wind farms were added to load nodes 10, 24 and 30, as shown in Figure V.11.The total integration rate (β %) was set at 20% of the total power demanded by the loads to ensure network stability. In this scenario, the optimal integration rates for each wind farm (PW10, PW24 and PW30) are 5.77%, 7.13% and 7.11%, corresponding to capacities of 16.33 MW, 20.20 MW and 20.13 MW, respectively. In addition, the active power generated (PG) by the integrated plants in Case 13 (PG1, PG2, PG5, PG8 and PG11) was lower than that produced by the six conventional plants in Case 1(without wind power).

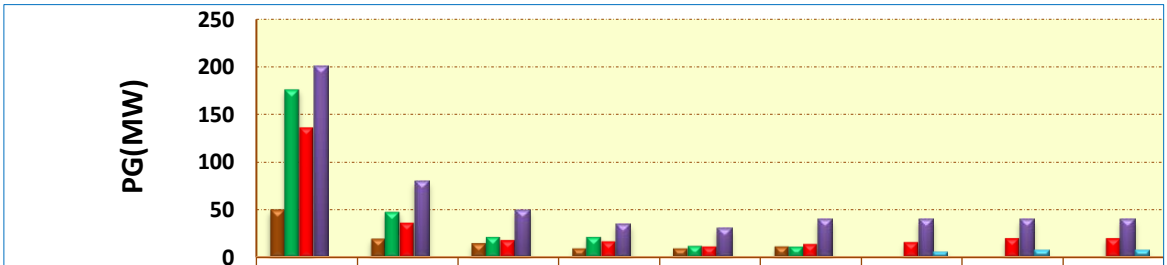

	PG1	PG2	PG5	PG8	PG11	PG13	PW10	PW24	PW30
PG min	50	20	15	10	10	12	0	0	0
PG without PW	176.18	48.13	21.49	21.62	12.57	12	0	0	0
PG with PW	135.91	36.63	18.53	17.21	11.8	14.32	16.33	20.2	20.13
PG max	200	80	50	35	30	40	40	40	40
β(%) case 13	0	0	0	0	0	0	5.77	7.13	7.11

Figure V. 11. Active power variation in Cases 1 and 13 (F_C)

- As shown in Figure V.12, the optimal integration rates for each wind farm in Case 14 were determined to be 3.41%, 7.28% and 9.31%. These rates correspond to capacities of 9.65 MW, 20.63 MW and 26.39 MW, respectively. In addition, the optimal active power (P_G), including the wind farms in Case 14, was lower than that of six conventional power stations in Case 2, underlining the benefits of integrating wind power into the grid.

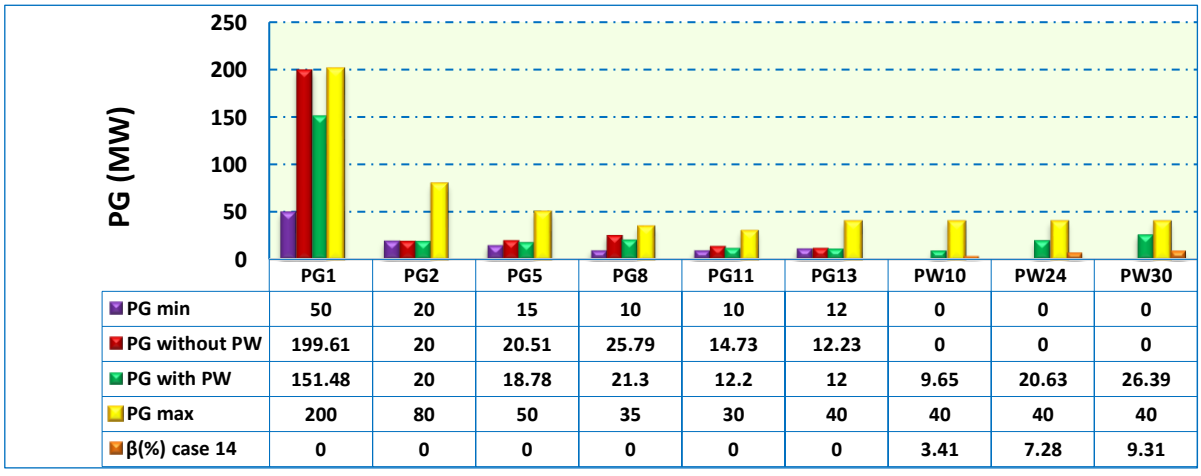

	PG1	PG2	PG5	PG8	PG11	PG13	PW10	PW24	PW30
PG min	50	20	15	10	10	12	0	0	0
PG without PW	199.61	20	20.51	25.79	14.73	12.23	0	0	0
PG with PW	151.48	20	18.78	21.3	12.2	12	9.65	20.63	26.39
PG max	200	80	50	35	30	40	40	40	40
β(%) case 14	0	0	0	0	0	0	3.41	7.28	9.31

Figure V.12. Active power variation in Cases 2 and 14 (F_{Cvalv})

Case 13: Minimisation of the total cost of fuel and wind power

The total cost of fuel and wind energy using the HGSO method, as shown in Table V.14, is 720.3616 ($/h), which is significantly lower than the 799.3707 ($/h) obtained in the scenario without wind integration (see Case 1 in Table V.5). In addition, the integration of wind farms has not reduced only overall costs but also active power losses and voltage deviations within the network.

Case 14: Minimization of the total cost of fuel with valve point effect and wind power

In this case, as shown in Table V.14, the total fuel cost, including the valve point load effect, optimised by the HGSO method is 746.58 ($/h), which is much lower compared to the 918.31 ($/h) without wind integration (see Case 2, Table V.5). This demonstrates that integrating wind power into the grid effectively reduces energy production costs and losses, proving the superiority of the HGSO method in solving optimal power flow (OPF) problems.

V. 2.2.2 Algerian grid DZ 114 bus with wind farms

In this project, we propose the addition of two wind farms located in the Algerian highlands, specifically in Setif and Djelfa, based on our technical and economic study [1]. Each wind farm has a rated power of 50 MW/60 kV and is equipped with 25 wind turbines, each with a capacity of 2 MW. The wind farms are connected to buses 99 and 107 of the Algerian electricity grid, with two SVC devices linked. The direct cost coefficient $\mathbf{d_{w,\,i}}$ ($/kWh) for each wind turbine at each site was calculated in our previous research [1] using equation (III.21) in Chapter III, which involves determining the direct cost $\mathbf{C_{d.w}}$ ($/h) of the i-th wind power unit, as outlined in equation (IV.65) in Chapter IV. This network's technical characteristics are in Appendix D. Two cases are examined: the quadratic fuel cost F_C and the active power losses ATL (cases 15 and 16 in Table V.3). Simulation results are summarised in Tables V.15 and V.16. Figures V.13, V.14, V.15, V.16, V.17 and V.18 illustrate the convergence curve in case 15, the optimal active power generation in cases 10 and 15, the optimal reactive power generation in case 15, the convergence curve for case 16, the optimal active power generation in cases 11 and16, and the voltage profile of the Algerian electrical network respectively.

A.Simulation and results interpretation

Case 15: Minimising total fuel and wind energy costs

In this scenario, the objective is to minimise the total cost of electricity production (F_{CT}). Applying the HGSO method, the combined energy cost of 17 power plants (15 traditional power stations and 02 wind farms)amounts to19,925.00 ($/h), as detailed in Table V.15.

Although this cost is slightly higher than the 18,998.89 ($/h) obtained with the 15 thermal plants (Table V.10), the HGSO method adds 0.926($/h) to the total cost of fuel and wind power, demonstrating its effectiveness in generating both financial and economic benefits.

Table V.15. Optimal results for solving OPFP using HGSO with wind farms in case **15** (DZ114 bus)

Variables	Min	Max	Case 15	Variables	Min	Max	Case 15
P_{G4} (MW)	135.0000	1350.0000	397.1607	V_{G4} (p.u)	0.90	1.1	1.0863
P_{G5} (MW)	135.0000	1350.0000	498.6662	V_{G5} (p.u)	0.90	1.1	1.0757
P_{G11} (MW)	10.0000	100.0000	37.1217	V_{G11} (p.u)	0.90	1.1	1.0764
P_{G15} (MW)	30.0000	300.0000	219.9376	V_{G15} (p.u)	0.90	1.1	1.0896
P_{G17} (MW)	135.0000	1350.0000	406.1528	V_{G17} (p.u)	0.90	1.1	1.0838
P_{G19} (MW)	34.5000	345.0000	258.2110	V_{G19} (p.u)	0.90	1.1	1.0239
P_{G22} (MW)	34.5000	345.0000	113.2332	V_{G22} (p.u)	0.90	1.1	1.0041
P_{G52} (MW)	34.5000	345.0000	203.0498	V_{G52} (p.u)	0.90	1.1	0.9960
P_{G80} (MW)	34.5000	345.0000	239.0936	V_{G80} (p.u)	0.90	1.1	1.0640
P_{G83} (MW)	30.0000	300.0000	188.8714	V_{G83} (p.u)	0.90	1.1	1.0952
P_{G98} (MW)	30.0000	300.0000	145.6234	V_{G98} (p.u)	0.90	1.1	1.0881
P_{W99} (MW)	0	50.0000	38.1233	V_{G99} (p.u)	0.90	1.1	1.0814
P_{G100} (MW)	60.0000	600.0000	599.7059	V_{G100} (p.u)	0.90	1.1	1.1000
P_{G101} (MW)	20.0000	200.0000	199.7107	V_{G101} (p.u)	0.90	1.1	1.0968
P_{W107} (MW)	0	50.0000	34.3463	V_{G107} (p.u)	0.90	1.1	1.0399
P_{G109} (MW)	10.0000	100.0000	87.8218	V_{G109} (p.u)	0.90	1.1	0.9995
P_{G111} (MW)	10.0000	200.0000	124.6355	V_{G111} (p.u)	0.90	1.1	1.0773
T_{160} (80-88)	0.90	1.1	1.0281	Q_{C41} (MVar)	3	20	16.2511
T_{161} (81-90)	0.90	1.1	0.9453	Q_{C43} (MVar)	3	20	12.4253
T_{162} (86-93)	0.90	1.1	1.0620	Q_{C50} (MVar)	3	20	12.8530
T_{163} (41-42)	0.90	1.1	1.0242	Q_{C66} (MVar)	3	20	15.9071
T_{164} (57-58)	0.90	1.1	0.9630	Q_{C67} (MVar)	3	20	6.5234
T_{165} (43-44)	0.90	1.1	1.0980	Q_{C68} (MVar)	3	20	15.8275
T_{166} (59-60)	0.90	1.1	1.0979	Q_{C69} (MVar)	3	20	8.3700
T_{167} (63-64)	0.90	1.1	0.9363	Q_{C70} (MVar)	3	20	14.9833
T_{168} (71-72)	0.90	1.1	1.0833	Q_{C77} (MVar)	3	20	3.6900
T_{169} (17-18)	0.90	1.1	1.0344	Q_{C89} (MVar)	3	20	9.7608
T_{170} (20-21)	0.90	1.1	1.0115	Q_{C92} (MVar)	3	20	5.0161
T_{171} (26-27)	0.90	1.1	1.0145	Q_{C93} (MVar)	3	20	6.2749
T_{172} (26-28)	0.90	1.1	0.9887	F_{CT} ($/h)	-	-	19.925.00
T_{173} (30-31)	0.90	1.1	0.9909	F_{CTG} ($/h)	-	-	18.883.00
T_{174} (47-48)	0.90	1.1	0.9948	F_{CTW} ($/h)	-	-	1.042.00
T_{175} (74-76)	0.90	1.1	1.0124	F_{APL} (MW)	-	-	64.4646

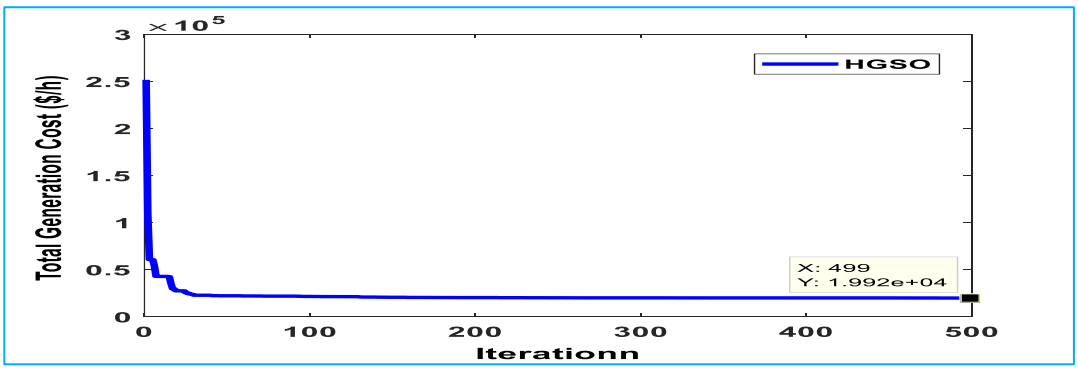

Figure V.13. Convergence curve of OPFP by HGSO with wind power in case **15** (DZ 114 bus)

- The results shown in Table V.15 confirm that the optimal values of the control variables for minimising total fuel and wind energy cost using the HGSO method remain within the permissible bounds. This ensures that the system constraints are effectively satisfied, demonstrating the method's reliability and compliance with operational requirements.

- The proposed method converges significantly faster in the first iterations, allowing the optimal solution to be found efficiently at 499 iterations, as shown in Figure V.13, thus proving its performance.

- As shown in Figure V.14, the electricity production of the power plants integrated with the wind farms varies between the decrease in production of the conventional power plants (case 10) and the increase in energy production of the wind farms (case 15); specifically, for PG4, PG5, PG15, PG19, PG52, PG80, PG83 and PG100. In addition, the optimal active power of the wind farms PW 99 and PW 107 in case 15 are 38.12 MW and 34.34 MW, respectively. These results indicate that integrating wind power not only enhances electricity production but also leads to reductions in fuel consumption, production costs, and CO2 emissions.

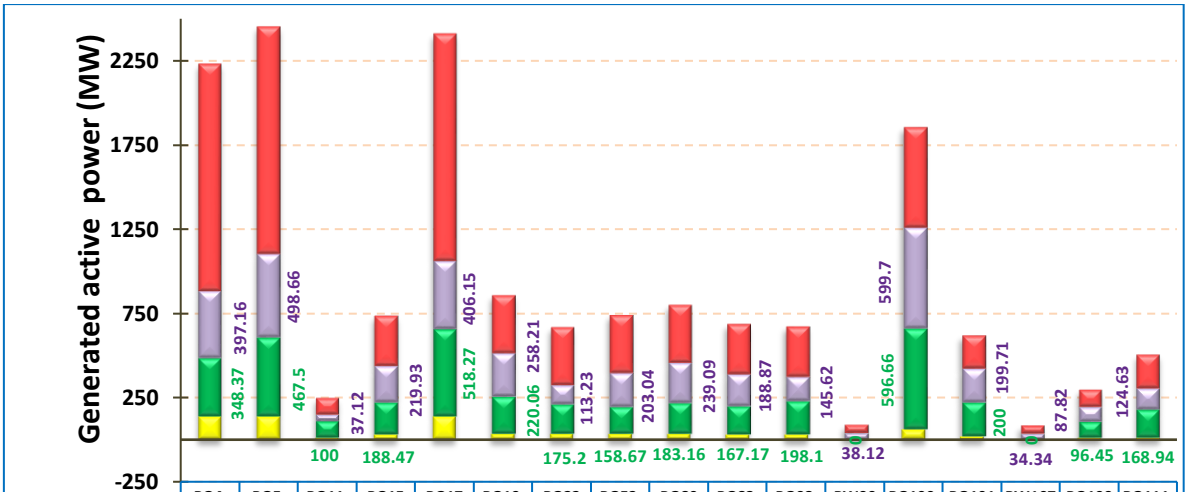

	PG4	PG5	PG11	PG15	PG17	PG19	PG22	PG52	PG80	PG83	PG98	PW99	PG100	PG101	PW107	PG109	PG111
PG max	1350	1350	100	300	1350	345	345	345	345	300	300	50	600	200	50	100	200
PG with PW	397.16	498.66	37.12	219.93	406.15	258.21	113.23	203.04	239.09	188.87	145.62	38.12	599.7	199.71	34.34	87.82	124.63
PG without PW	348.37	467.5	100	188.47	518.27	220.06	175.2	158.67	183.16	167.17	198.1	0	596.66	200	0	96.45	168.94
PG min	135	135	10	30	135	34	34	34	34	30	30	0	60	20	0	10	10

Figure V.14. Optimal active power generation in cases 10 and 15

- Figure V.15 shows the optimal reactive power from the power plants, which includes two wind farms at buses 99 and 107, is within acceptable limits.The reactive powers generated by the SVCs at theses buses are 21.18 MVar and 18.03 MVar, respectively.

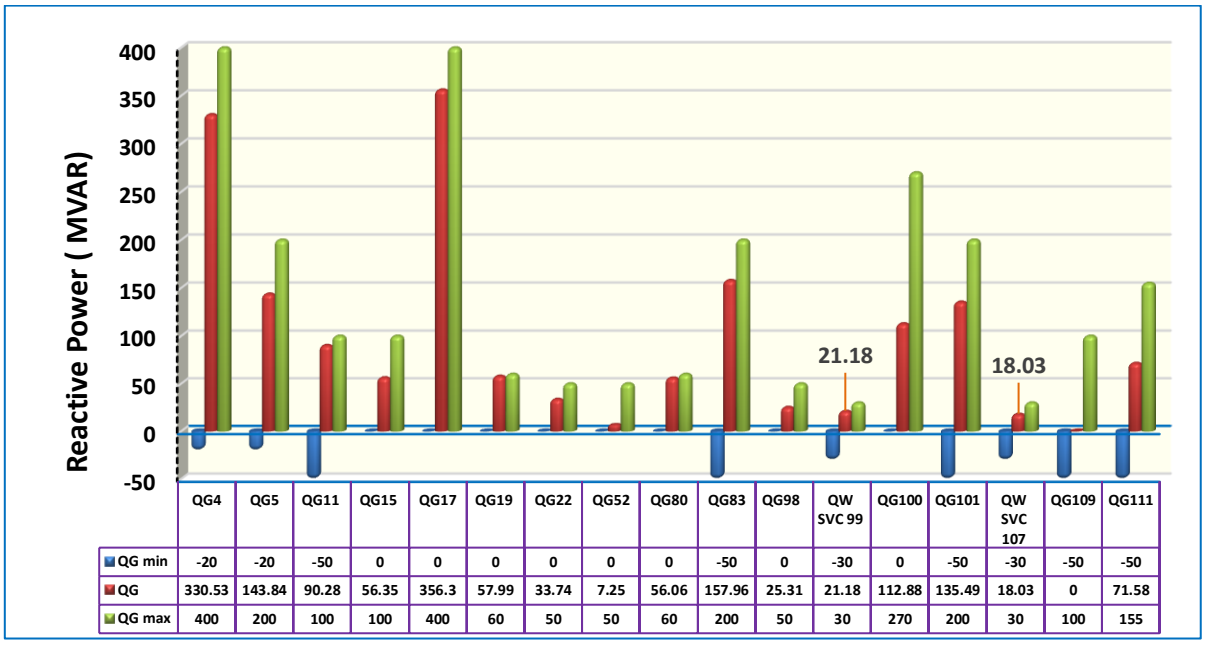

	QG4	QG5	QG11	QG15	QG17	QG19	QG22	QG52	QG80	QG83	QG98	QW SVC 99	QG100	QG101	QW SVC 107	QG109	QG111
QG min	-20	-20	-50	0	0	0	0	0	0	-50	0	-30	0	-50	-30	-50	-50
QG	330.53	143.84	90.28	56.35	356.3	57.99	33.74	7.25	56.06	157.96	25.31	21.18	112.88	135.49	18.03	0	71.58
QG max	400	200	100	100	400	60	50	50	60	200	50	30	270	200	30	100	155

Figure V.15. Optimal reactive power generation in case 15

Case 16: Minimization of active power losses

In this case, the objective is to minimize the total active power losses (APL) in the power system integrated with wind farms. Using the HGSO method, the optimal active power losses were reduced to 49.14 MW (Table V.16), compared to 49.8652 MW in the scenario without wind farms (Table V.10). The total APL convergence curve is shown in Figure V.16.

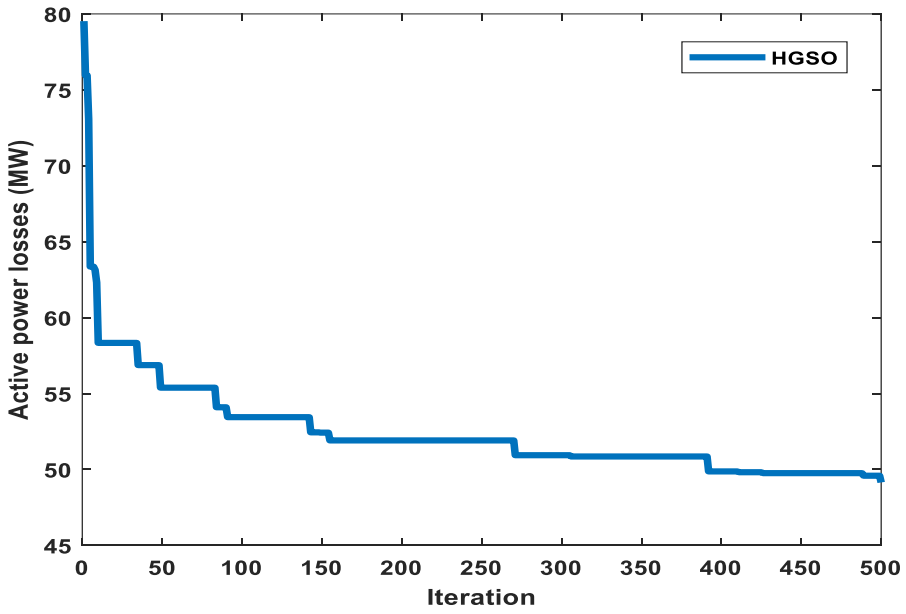

Figure V.16. Convergence curve of OPFP by HGSO with wind power in case **16** (DZ 114 bus)

Table V.16. Optimal results for solving OPFP using HGSO with wind farms in case **16** (DZ114 bus)

Variables	Min	Max	Case 16	Variables	Min	Max	Case 16
P_{G4} (MW)	135.0000	1350.0000	458.5764	V_{G4} (p.u)	0.90	1.1	1.0997
P_{G5} (MW)	135.0000	1350.0000	47.2169	V_{G5} (p.u)	0.90	1.1	1.0880
P_{G11} (MW)	10.0000	100.0000	98.5698	V_{G11} (p.u)	0.90	1.1	1.0865
P_{G15} (MW)	30.0000	300.0000	53.9067	V_{G15} (p.u)	0.90	1.1	1.0861
P_{G17} (MW)	135.0000	1350.0000	404.4767	V_{G17} (p.u)	0.90	1.1	1.0964
P_{G19} (MW)	34.5000	345.0000	234.5023	V_{G19} (p.u)	0.90	1.1	1.0777
P_{G22} (MW)	34.5000	345.0000	215.3450	V_{G22} (p.u)	0.90	1.1	1.0971
P_{G52} (MW)	34.5000	345.0000	152.1502	V_{G52} (p.u)	0.90	1.1	1.0466
P_{G80} (MW)	34.5000	345.0000	264.0466	V_{G80} (p.u)	0.90	1.1	1.0868
P_{G83} (MW)	30.0000	300.0000	133.2775	V_{G83} (p.u)	0.90	1.1	1.0905
P_{G98} (MW)	30.0000	300.0000	160.0311	V_{G98} (p.u)	0.90	1.1	1.0959
P_{W99} (MW)	0	50.0000	46.1475	V_{G99} (p.u)	0.90	1.1	1.0954
P_{G100} (MW)	60.0000	600.0000	403.4224	V_{G100} (p.u)	0.90	1.1	1.0967
P_{G101} (MW)	20.0000	200.0000	195.5995	V_{G101} (p.u)	0.90	1.1	1.0888
P_{W107} (MW)	0	50.0000	44.8868	V_{G107} (p.u)	0.90	1.1	1.0890
P_{G109} (MW)	10.0000	100.0000	92.3762	V_{G109} (p.u)	0.90	1.1	1.0903
P_{G111} (MW)	10.0000	200.0000	171.6153	V_{G111} (p.u)	0.90	1.1	1.0559
T_{160} (80-88)	0.90	1.1	1.0752	Q_{C41} (MVar)	3	20	19.51
T_{161} (81-90)	0.90	1.1	1.0599	Q_{C43} (MVar)	3	20	19.34
T_{162} (86-93)	0.90	1.1	1.0791	Q_{C50} (MVar)	3	20	18.36
T_{163} (41-42)	0.90	1.1	1.0846	Q_{C66} (MVar)	3	20	18.46
T_{164} (57-58)	0.90	1.1	1.0790	Q_{C67} (MVar)	3	20	18.97
T_{165} (43-44)	0.90	1.1	1.0465	Q_{C68} (MVar)	3	20	17.59
T_{166} (59-60)	0.90	1.1	1.0836	Q_{C69} (MVar)	3	20	18.67
T_{167} (63-64)	0.90	1.1	1.0045	Q_{C70} (MVar)	3	20	19.00
T_{168} (71-72)	0.90	1.1	1.0823	Q_{C77} (MVar)	3	20	18.71
T_{169} (17-18)	0.90	1.1	1.0518	Q_{C89} (MVar)	3	20	16.81
T_{170} (20-21)	0.90	1.1	1.0623	Q_{C92} (MVar)	3	20	15.45
T_{171} (26-27)	0.90	1.1	1.0364	Q_{C93} (MVar)	3	20	18.88
T_{172} (26-28)	0.90	1.1	1.0813	$\mathbf{F_{CT}}$ ($/h)	-	-	20.715.00
T_{173} (30-31)	0.90	1.1	1.0432	$\mathbf{F_{CTG}}$ ($/h)	-	-	19.664.00
T_{174} (47-48)	0.90	1.1	1.0915	$\mathbf{F_{CTW}}$ ($/h)	-	-	1.071.00
T_{175} (74-76)	0.90	1.1	1.0860	$\mathbf{F_{APL}}$ (MW)	-	-	49.14

- The results shown in Table V.16 indicate the optimal values of the control variables for minimizing total active losses in the 114-bus network, considering the integration of wind energy through the HGSO method while staying within the permitted limits. This demonstrates that the system constraints are effectively satisfied, confirming the reliability of the method and its compatibility with the operational requirements.

- In Case 16, as depicted in Figure V.17, the optimal power output from the PW99 and PW107 wind farms is 46.14 MW and 44.88 MW, respectively. The total power generated by the plants integrated with these wind farms (PG4, PG19, PG22, PG80, PG100 and PG101) exceeds the output of the conventional power plants in Case 11. This integration effectively reduces fuel consumption by traditional power plants and significantly lowers gas emissions.

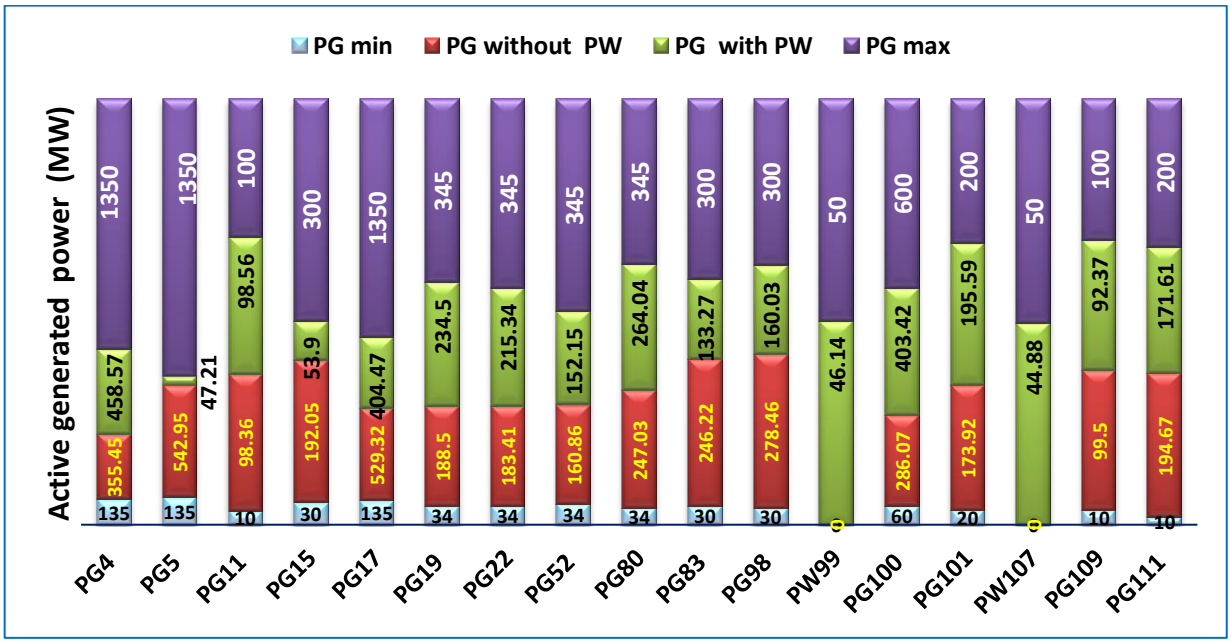

Figure V. 17. Optimal active power generation in cases 11 and 16

- As shown in Figure V.18, the voltage profiles of the electricity network (DZ 114 bus), which includes the wind farms connected to buses 99 and 107 in cases 15 (F_{CT}) and 16 (APL), indicate that the load bus voltages stay within the system's acceptable limits.

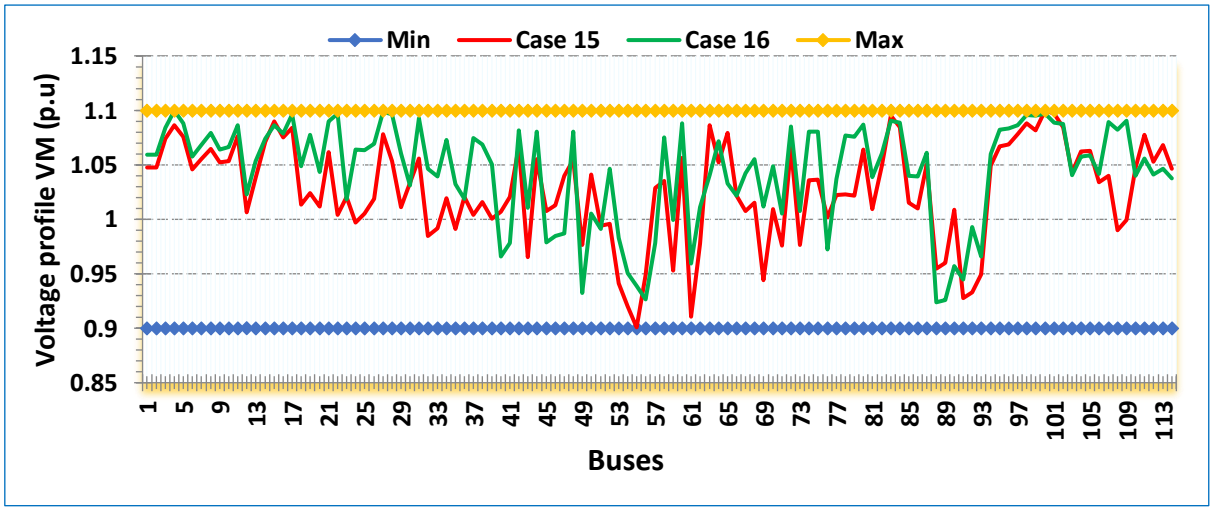

Figure V.18. Voltage profile in cases 15 and 16 of Algerian DZ114-bus

V.4.Conclusion

In this chapter, we validated two metaheuristic methods (HGSO and CO), through various OPF cases using the IEEE 30-bus, IEEE 57-bus, and an Algerian DZ114-bus transmission network. MATLAB simulations demonstrate that the proposed techniques consistently outperform other well-known metaheuristic methods, proving their superior efficiency and

robustness. Furthermore, the optimal results achieved using the HGSO method in cases 15 and 16, reveal that integrating wind farms into the Algerian DZ114-bus system, based on a technical and economic study of wind farm implementation, has yielded significant financial, technical, and economic benefits for the electricity network. This integration also addresses various environmental and technical challenges, including increased electricity production, decreased production costs, reduced CO2 emissions, conservation of fossil fuels, and improved overall electricity quality. Thus, the findings confirm the superiority of the HGSO method for solving the OPF problem across all 16 cases.

CHAPTER: VI

General Conclusion

VI.1. Summary and Conclusion

The management of energy systems (including the production, transmission, and distribution of electrical energy)has become increasingly complex due to the rising electricity demand. This increase poses major challenges for modern power networks. One proposed solution is the integration of renewable energy sources into electricity grids, which addresses issues like the depletion of fossil fuel resources and greenhouse gas emissions from conventional power plants. However, this integration introduces new complexities in solving the Optimal Power Flow (OPF) problem, primarily due to the uncertainties related to the operational constraints of renewable energy sources. Traditional methods for solving the OPF problem are not well suited to the practical considerations of optimal energy management. Therefore, there is a need to explore meta-heuristic methods. This research aims to develop a robust tool for solving the optimal power flow problem using new meta-heuristic techniques to address the practical constraints associated with integrating renewable energy sources.

The main objective of this thesis is to achieve optimal power management in power systems that incorporate renewable energy sources, with a specific focus on stochastic wind energy. Due to the inherent intermittency of wind, this energy source introduces significant uncertainty into the system. To address this challenge, meta-heuristic methods are used to solve Optimal Power Flow problems(OPFP) in systems integrating wind energy.To effectively model and describe the wind speed distribution, the Weibull probability density function is used, which more accurately captures the variability and stochastic nature of the wind.In this work, we have proposed two innovative meta-heuristic approaches to solve the OPFP: the Henry Gas Solubility Optimization (HGSO) algorithm; inspired by physical processes, and the Cheetah Optimizer (CO); inspired by natural phenomena. These methods optimise several key objective functions, including total fuel cost (with or without wind integration), total active power losses, emissions, stability index, and voltage deviation at the load bus level, while ensuring that system equality and inequality constraints are satisfied. In addition, the objective function takes into account the minimisation of total costs associated with both conventional power generation and stochastic wind power generation, including penalty costs for underestimating and reserve costs for overestimating available wind power.

The effectiveness of the proposed methods is evaluated across sixteen OPF cases using the IEEE 30-bus, IEEE 57-bus, and Algerian DZ114-bus transmission systems. MATLAB simulations show that the proposed techniques consistently outperform other well-known meta-heuristic methods, demonstrating greater efficiency and robustness. In addition, the HGSO method significantly reduces total fuel and wind energy costs compared to scenarios that do not integrate wind energy. This demonstrates that integrating wind power into the grid can reduce production costs and bring financial, technical, and economic benefits. Thus, it proves the superiority of the HGSO method in solving OPFP in 16 cases.

A techno-economic analysis of site-specific wind farms has shown that wind energy can become economically advantageous, in line with Algeria's renewable energy objectives. The study evaluates the cost of generating electricity from wind at three high-potential sites in the Algerian highlands: El-Beidh, Sétif, and Djelfa. Wind data from the Algerian National Meteorological Office was analysed to evaluate the performance of four wind turbine models at each site. The results indicated that:

- Highland wind speeds at 10m height vary per location: Sétif - 3.46m/s, Djelfa - 3.92m/s, El Bayadh - 4.75m/s.
- The analysis of wind speed extrapolation at various turbine hub heights (67 m, 78.5 m, 89 m, and 93 m) in different locations showed that El Bayadh is the windiest site among the selected regions. The average wind speed varied from 4.54 m/s to 6.53 m/s, depending on the turbine height. This suggests that wind speed increases with turbine hub height and the corresponding Weibull parameters for each site.
- After evaluating four turbines (Vestas V-80, Suzlon S-82, Enercon E-58, and Gamesa G-114) with powers from 1 to 2 MW, the Gamesa G-114 proved to be the most appropriate for all selected sites based on its technical characteristics.
- Annual energy production from wind turbines varies between 2.28 GWh (Vesta V80 in Setif) and 10.8 GWh (Gamesa G114 in El Bayadh).
- The capacity factors of the selected wind turbines show that the Gamesa G-114 has the highest capacity factor among the selected types; it varies between 45.18%, 51.4% and 61.68% at Sétif, Djelfa and El Bayadh respectively, while the Vestas V80 has the lowest capacity factor at all these sites.

- The unit cost energy (UCE) using the PVC method for each selected wind turbine was approximately 0.0752 ($/KWh) in Setif with the Vesta V80 and 0.0159 ($/KWh) GWh in El Bayadh with the Gamesa G114.
- The Gamesa G 114 turbine has shown exceptional performance in the Unit Cost of Energy (UCE), making it an advantageous option for wind energy projects. El Beidh is an optimal location for planning a wind farm project due to its favourable conditions.Moreover, the competitive unit cost of energy from wind sources in selected locations makes wind farm installations economically viable.
- The integration of wind farms; based on techno-economic analysis in the specific locations; will make the wind energy price competitive to implement Algeria's renewable energy program, which calls for the installation of 5,010 MW of wind power to improve the performance of the electrical transmission grid DZ-114 bus.
- In addition to their positive environmental impact in terms of cleanliness, wind farms also contribute to reducing the energy production of thermal power plants, leading to a decrease in toxic gas emissions.
- This study offers significant economic benefits for market actors in the Algerian energy sector by reducing the consumption of fossil resources such as natural gas, coal, and gasoline.
- Improve administrative facilities and incentivise foreign capital for investment and partnerships in the renewable energy sector.

VI.2. Future work

- In future work, the sizing limits of wind farms in terms of active power production (injection from wind farms) and reactive power (injection or absorption) using OAPF and ORPF, respectively, can be determined in perspective, considering Gamesa G 114 industrial turbine and the three selected wind farms locations Sétif, Djelfa and El Bayadh.

- The wind farms integrated into the Algerian DZ-114 bus transmission network can enhance the power quality at minimal wind energy cost by optimising the reactive and active power flow using ORPF and OAPF, leading to a more efficient and reliable electric power system. This task can be reserved for future simulation works.

APPENDIX

Appendix A : Standard IEEE-30 buses test system data

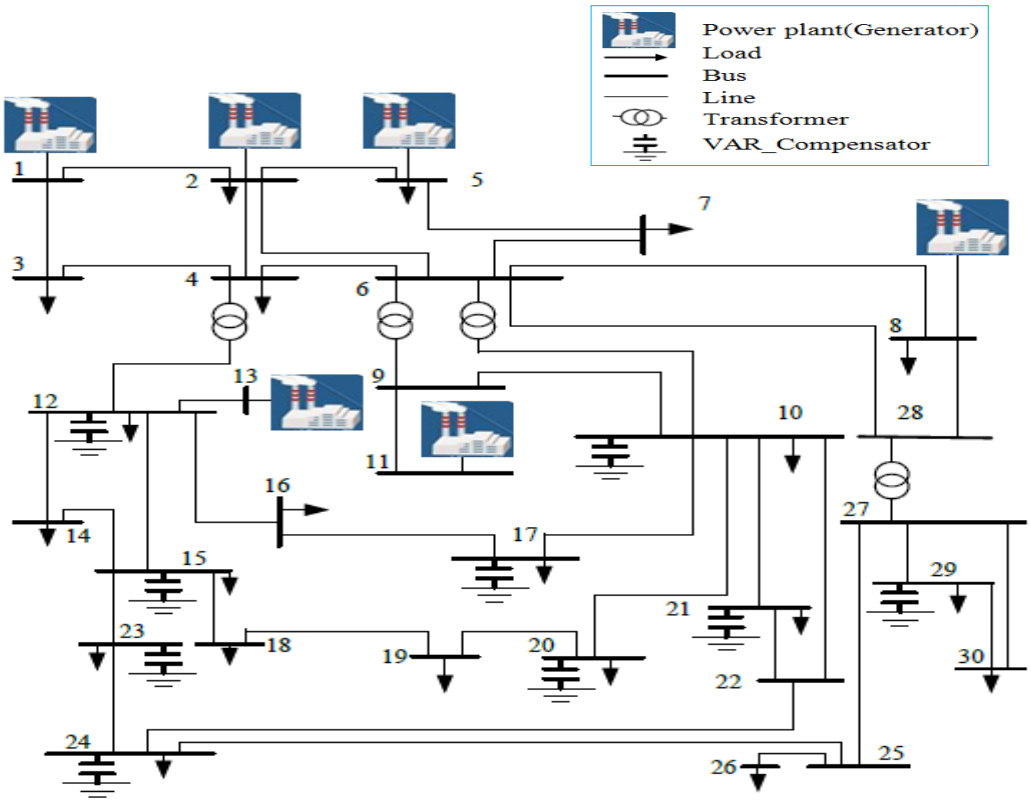

Figure A.1.IEEE 30-bus system single-line diagram

Table A.1. Electrical system parameters (IEEE 30 bus network)

Characteristics IEEE 30-bus system	N°	Details
Buses	30	[5,81]
Branches	41	[5,81]
Generators	6	Buses: **1 (swing)**, 2, 5, 8, 11 and 13
Shunt VAR compensators	9	Buses: 10, 12, 15, 17, 20, 21, 23, 24. and 29
Transformer with tap changer	4	Branches: 11, 12, 15 and 36
Control variables	25	-
Load bus voltage limits	24	[0.95 – 1.05] p.u
Generator voltage limits	-	[0.95–1.1] p.u
Setting of the tap changer in transformer	-	[0.9 –1.1] p.u
VAR compensation limits	-	[0–5] MVAR
Active demand	-	2834 MW
Reactive demand	-	1262 MVAR
S. Base	-	100 MVA

Table A.2. Bus data (IEEE 30 bus network)

Bus_i	Type	Vsp (p.u)	Theta (°)	P_{Gi} MW	Q_{Gi} MVar	P_{Li} MW	Q_{Li} MVar	Q_{min} MVar	Q_{max} MVar	Qc MVar
1	1	1,06	0	99,24	0	0	0	-20	200	0
2	2	1,045	0	80	0	21,7	12,7	-20	100	0
3	3	1	0	0	0	2,4	1,2	0	0	0
4	3	1	0	0	0	7,6	1,6	0	0	0
5	2	1,01	0	50	0	94,2	19	-15	80	0
6	3	1	0	0	0	0	0	0	0	0
7	3	1	0	0	0	22,8	10,9	0	0	0
8	2	1,01	0	20	0	30	30	-15	60	0
9	3	1	0	0	0	0	0	0	0	0
10	3	1	0	0	0	5,8	2	0	0	0
11	2	1,082	0	20	0	0	0	-10	50	0
12	3	1	0	0	0	11,2	7,5	0	0	0
13	2	1,071	0	20	0	0	0	-15	60	0
14	3	1	0	0	0	6,2	1,6	0	0	0
15	3	1	0	0	0	8,2	2,5	0	0	0
16	3	1	0	0	0	3,5	1,8	0	0	0
17	3	1	0	0	0	9	5,8	0	0	0
18	3	1	0	0	0	3,2	0,9	0	0	0
19	3	1	0	0	0	9,5	3,4	0	0	0
20	3	1	0	0	0	2,2	0,7	0	0	0
21	3	1	0	0	0	17,5	11,2	0	0	0
22	3	1	0	0	0	0	0	0	0	0
23	3	1	0	0	0	3,2	1,6	0	0	0
24	3	1	0	0	0	8,7	6,7	0	0	0
25	3	1	0	0	0	0	0	0	0	0
26	3	1	0	0	0	3,5	2,3	0	0	0
27	3	1	0	0	0	0	0	0	0	0
28	3	1	0	0	0	0	0	0	0	0
29	3	1	0	0	0	2,4	0,9	0	0	0
30	3	1	0	0	0	10,6	1,9	0	0	0

Bus Types

- Slack bus(1)
- PV bus (2)
- PQ bus (3)

Table A.3. Line data (IEEE 30 bus network)

Line	Bus i From - To	R (pu)	X (pu)	B/2 (pu)	X'mer TAP (a)
1	1-2	0,0192	0,0575	0	1
2	1-3	0,0452	0,1652	0	1
3	2-4	0,057	0,1737	0	1
4	3-4	0,0132	0,0379	0	1
5	2-5	0,0472	0,1983	0	1
6	2-6	0,0581	0,1763	0	1
7	4-6	0,0119	0,0414	0	1
8	5-7	0,046	0,116	0	1
9	6-7	0,0267	0,082	0	1
10	6-8	0,012	0,042	0	1
11	6-9	0	0,208	0	0,99801053
12	6-10	0	0,556	0	0,99807573
13	9-11	0	0,208	0	1
14	9-10	0	0,11	0	1
15	4-12	0	0,256	0	1,03622401
16	12-13	0	0,14	0	1
17	12-14	0,1231	0,2559	0	1
18	12-15	0,0662	0,1304	0	1
19	12-16	0,0945	0,1987	0	1
20	14-15	0,221	0,1997	0	1
21	16-17	0,0824	0,1923	0	1
22	15-18	0,1073	0,2185	0	1
23	18-19	0,0639	0,1292	0	1
24	19-20	0,034	0,068	0	1
25	10-20	0,0936	0,209	0	1
26	10-17	0,0324	0,0845	0	1
27	10-21	0,0348	0,0749	0	1
28	10-22	0,0727	0,1499	0	1
29	21-22	0,0116	0,0236	0	1
30	15-23	0,1	0,202	0	1
31	22-24	0,115	0,179	0	1
32	23-24	0,132	0,27	0	1
33	24-25	0,1885	0,3292	0	1
34	25-26	0,2544	0,38	0	1
35	25-27	0,1093	0,2087	0	1
36	28-27	0	0,396	0	0,97637713
37	27-29	0,2198	0,4153	0	1
38	27-30	0,3202	0,6027	0	1
39	29-30	0,2399	0,4533	0	1
40	8-28	0,0636	0,2	0	1
41	6-28	0,0169	0,0599	0	1

Table A.4: Thermal power generation limits and cost coefficients

Generators	a ($/hr)	b ($/MW.hr)	c ($/MW².hr)	P_{Gmin} (MW)	P_{Gmax} (MW)	Q_{Gmin} (MVar)	Q_{Gmax} (MVar)
G1	0	2	0.00375	50	200	-20	200
G2	0	1.75	0.0175	20	80	-20	100
G5	0	1	0.0625	15	50	-15	80
G8	0	3.25	0.00834	10	35	-15	60
G11	0	3	0.025	10	30	-10	50
G13	0	3	0.025	12	40	-15	60

Where, a_i, b_i and c_i are the fuel cost coefficients for each generatorin power production.

Table A.5. Fuel cost coefficients considering the valve-point effects

Generators	a ($/hr)	b ($/MW.hr)	c ($/MW².hr)	d ($/hr)	e (rad/MW)	P_{Gmin} (MW)	P_{Gmax} (MW)	Q_{Gmin} (MVAR)	Q_{Gmax} (MVAR)
G1	150	2.00	0.0016	50.00	0.0630	50	200	-20	200
G2	25	2.50	0.0100	40.00	0.0980	20	80	-20	100

Where,a_i, b_i, c_i, d_i and e_i are the fuel cost factors for each power production unit.

Table A. 6. Emission coefficients of thermal power plant

Generators	α (ton/hr)	β (ton/MW.hr)	λ (ton/MW².hr)	ξ (ton/ hr)	θ (1/MW)
G1	4.091	-5.554	6.490	0.0002	2.857
G2	2.543	-6.047	5.638	0.0005	3.333
G5	4.258	-5.094	4.586	0.000001	8
G8	5.326	-3.550	3.380	0.002	2
G11	4.258	-5.094	4.586	0.000001	8
G13	6.131	-5.555	5.151	0.00001	6.667

Where, α_i,β_i,λ_i, d_i, $\xi_i$and θ_i are emission coefficients for each power plant.

Appendixe B: Standard IEEE-57 buses test system data

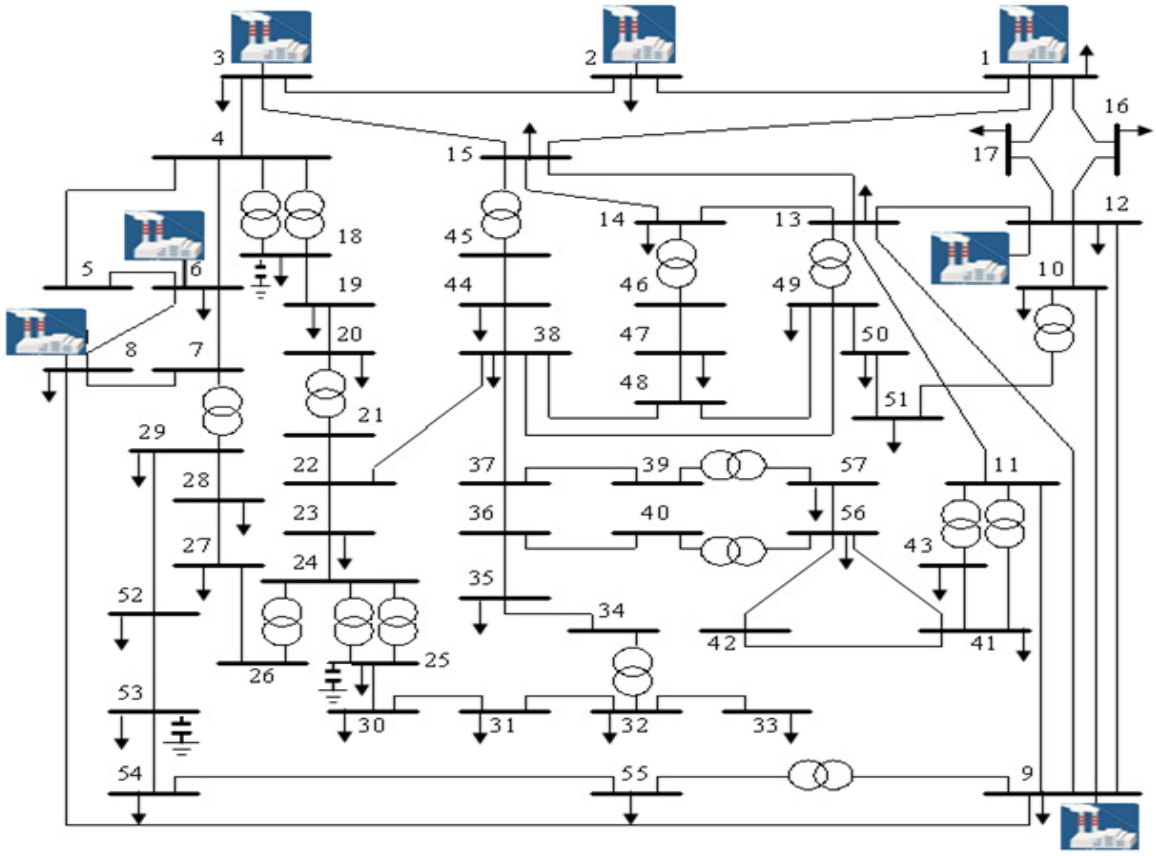

Figure.B.1.IEEE 57 bus system single-line diagram

Table B.1. Electrical system parameters (IEEE 57 bus network)

IEEE 57-bus System Characteristics	N°	Details
Buses	57	[62,82]
Branches	80	[62,82]
Generators	7	Buses: **1 (swing)**,2, 3, 6, 8, 9 and 12
Shunt VAR compensators	3	Buses: 18, 25 and 53
Transformer with tap changer	17	Branches: 19, 20, 31, 35, 36, 37, 41, 46, 54, 58, 59, 65, 66, 71, 73, 76 and 80
Control variables	34	-
Load bus voltage limits	50	[0.94-1.08] p.u.
Generator voltage limits	-	[0.95–1.1] p.u
Setting of the tap changer in the transformer	-	[0.9 –1.1] p.u
VAR compensation limits	-	[0–20] MVAR
Active demand	-	12.508 MW
Reactive demand	-	3.364 MVAR
S. Base	-	100 MVA

Table B.2. Bus data (IEEE 57 bus network)

Bus_i	Type	Vsp (p.u)	Theta (°)	P_{Gi} MW	Q_{Gi} MVar	P_{Li} MW	Q_{Li} MVar	Q_{min} MVar	Q_{max} MVar	Qc MVar
1	1	1,04	0	478,9	-16,1	0	0	-200	300	0
2	2	1,01	0	4	-0,8	3	88	-17	50	0
3	2	0,985	0	42	-1	41	21	-10	60	0
4	3	0,981	0	0	0	10	5	0	0	0
5	3	0,976	0	0	0	13	4	0	0	0
6	2	0,98	0	76	0,8	75	2	-8	25	0
7	3	0,984	0	0	0	10	5	0	0	0
8	2	1,005	0	160	62,1	150	22	-140	200	0
9	2	0,98	0	130	2,2	121	26	-3	9	0
10	3	0,986	0	0	0	5	2	0	0	0
11	3	0,974	0	0	0	10	5	0	0	0
12	2	1,015	0	400	128,5	377	24	-150	155	0
13	3	0,979	0	0	0	18	2,3	0	0	0
14	3	0,97	0	0	0	10,5	5,3	0	0	0
15	3	0,988	0	0	0	22	5	0	0	0
16	3	1,013	0	0	0	43	3	0	0	0
17	3	1,017	0	0	0	42	8	0	0	0
18	3	1,001	0	0	0	27,2	9,8	0	0	0
19	3	0,97	0	0	0	3,3	0,6	0	0	0
20	3	0,964	0	0	0	2,3	1	0	0	0
21	3	1,008	0	0	0	10	2	0	0	0
22	3	1,01	0	0	0	10	0	0	0	0
23	3	1,008	0	0	0	6,3	2,1	0	0	0
24	3	0,999	0	0	0	5	0	0	0	0
25	3	0,982	0	0	0	6,3	3,2	0	0	0
26	3	0,959	0	0	0	0	0	0	0	0
27	3	0,982	0	0	0	9,3	0,5	0	0	0
28	3	0,997	0	0	0	4,6	2,3	0	0	0
29	3	1,01	0	0	0	17	2,6	0	0	0
30	3	0,962	0	0	0	3,6	1,8	0	0	0
31	3	0,936	0	0	0	5,8	2,9	0	0	0
32	3	0,949	0	0	0	1,6	0,8	0	0	0
33	3	0,947	0	0	0	3,8	1,9	0	0	0
34	3	0,959	0	0	0	0	0	0	0	0
35	3	0,966	0	0	0	6	3	0	0	0
36	3	0,976	0	0	0	0	0	0	0	0
37	3	0,985	0	0	0	0	0	0	0	0
38	3	1,013	0	0	0	14	7	0	0	0
39	3	0,983	0	0	0	0	0	0	0	0
40	3	0,973	0	0	0	0	0	0	0	0
41	3	0,996	0	0	0	6,3	3	0	0	0
42	3	0,966	0	0	0	7,1	4,4	0	0	0
43	3	1,01	0	0	0	2	1	0	0	0
44	3	1,017	0	0	0	12	1,8	0	0	0
45	3	1,036	0	0	0	0	0	0	0	0
46	3	1,05	0	0	0	0	0	0	0	0

47	3	1,033	0	0	0	29,7	11,6	0	0	0
48	3	1,027	0	0	0	0	0	0	0	0
49	3	1,036	0	0	0	18	8,5	0	0	0
50	3	1,023	0	0	0	21	10,5	0	0	0
51	3	1,052	0	0	0	18	5,3	0	0	0
52	3	0,98	0	0	0	4,9	2,2	0	0	0
53	3	0,971	0	0	0	20	10	0	0	0
54	3	0,996	0	0	0	4,1	1,4	0	0	0
55	3	1,031	0	0	0	6,8	3,4	0	0	0
56	3	0,968	0	0	0	7,6	2,2	0	0	0
57	3	0,965	0	0	0	6,7	2	0	0	0

Table B. 3. Linedata (IEEE 57 bus network)

Line	Bus i From - To	R (pu)	X (pu)	B/2 (pu)	X'mer TAP (a)
1	1-2	0,0083	0,028	0,0645	1
2	2-3	0,0298	0,085	0,0409	1
3	3-4	0,0112	0,0366	0,019	1
4	4-5	0,0625	0,132	0,0129	1
5	4-6	0,043	0,148	0,0174	1
6	6-7	0,02	0,102	0,0138	1
7	6-8	0,0339	0,173	0,0235	1
8	8-9	0,0099	0,0505	0,0274	1
9	9-10	0,0369	0,1679	0,022	1
10	9-11	0,0258	0,0848	0,0109	1
11	9-12	0,0648	0,295	0,0386	1
12	9-13	0,0481	0,158	0,0203	1
13	13-14	0,0132	0,0434	0,0055	1
14	13-15	0,0269	0,0869	0,0115	1
15	1-15	0,0178	0,091	0,0494	1
16	1-16	0,0454	0,206	0,0273	1
17	1-17	0,0238	0,108	0,0143	1
18	3-15	0,0162	0,053	0,0272	1
19	4-18	0	0,555	0	0,97
20	4-18	0	0,43	0	0,978
21	5-6	0,0302	0,0641	0,0062	1
22	7-8	0,0139	0,0712	0,0097	1
23	10-12	0,0277	0,1262	0,0164	1
24	11-13	0,0223	0,0732	0,0094	1
25	12-13	0,0178	0,058	0,0302	1
26	12-16	0,018	0,0813	0,0108	1
27	12-17	0,0397	0,179	0,0238	1
28	14-15	0,0171	0,0547	0,0074	1
29	18-19	0,461	0,685	0	1
30	19-20	0,283	0,434	0	1
31	21-20	0	0,7767	0	1,043
32	21-22	0,0736	0,117	0	1
33	22-23	0,0099	0,0152	0	1

34	23-24	0,166	0,256	0,0042	1
35	24-25	0	1,182	0	1
36	24-25	0	1,23	0	1
37	24-26	0	0,0473	0	1,043
38	26-27	0,165	0,254	0	1
39	27-28	0,0618	0,0954	0	1
40	28-29	0,0418	0,0587	0	1
41	7-29	0	0,0648	0	0,967
42	25-30	0,135	0,202	0	1
43	30-31	0,326	0,497	0	1
44	31-32	0,507	0,755	0	1
45	32-33	0,0392	0,036	0	1
46	34-32	0	0,953	0	0,975
47	34-35	0,052	0,078	0,0016	1
48	35-36	0,043	0,0537	0,0008	1
49	36-37	0,029	0,0366	0	1
50	37-38	0,0651	0,1009	0,001	1
51	37-39	0,0239	0,0379	0	1
52	36-40	0,03	0,0466	0	1
53	22-38	0,0192	0,0295	0	1
54	11-41	0	0,749	0	0,955
55	41-42	0,207	0,352	0	1
56	41-43	0	0,412	0	1
57	38-44	0,0289	0,0585	0,001	1
58	15-45	0	0,1042	0	0,955
59	14-46	0	0,0735	0	0,9
60	46-47	0,023	0,068	0,0016	1
61	47-48	0,0182	0,0233	0	1
62	48-49	0,0834	0,129	0,0024	1
63	49-50	0,0801	0,128	0	1
64	50-51	0,1386	0,22	0	1
65	10-51	0	0,0712	0	0,93
66	13-49	0	0,191	0	0,895
67	29-52	0,1442	0,187	0	1
68	52-53	0,0762	0,0984	0	1
69	53-54	0,1878	0,232	0	1
70	54-55	0,1732	0,2265	0	1
71	11-43	0	0,153	0	0,958
72	44-45	0,0624	0,1242	0,002	1
73	40-56	0	1,195	0	0,958
74	56-41	0,553	0,549	0	1
75	56-42	0,2125	0,354	0	1
76	39-57	0	1,355	0	0,98
77	57-56	0,174	0,26	0	1
78	38-49	0,115	0,177	0,003	1
79	38-48	0,0312	0,0482	0	1
80	9-55	0	0,1205	0	0,94

Table B.4. Thermal power generation limits and cost coefficients

Generators	a ($/hr)	b ($/MW.hr)	c ($/MW².hr)	P_{Gmin} (MW)	P_{Gmax} (MW)	Q_{Gmin} (MVAR)	Q_{Gmax} (MVAR)
G1	0	20	0.0775795	0	575.88	-140	200
G2	0	40	0.01	0	100	-17	50
G3	0	20	0.25	0	140	-10	60
G6	0	40	0.01	0	100	-8	25
G8	0	20	0.0222222	0	550	-140	200
G9	0	40	0.01	0	100	-3	9
G12	0	20	0.0322581	0	410	-150	155

Appendix C: Algerian Power System DZ114-bus data

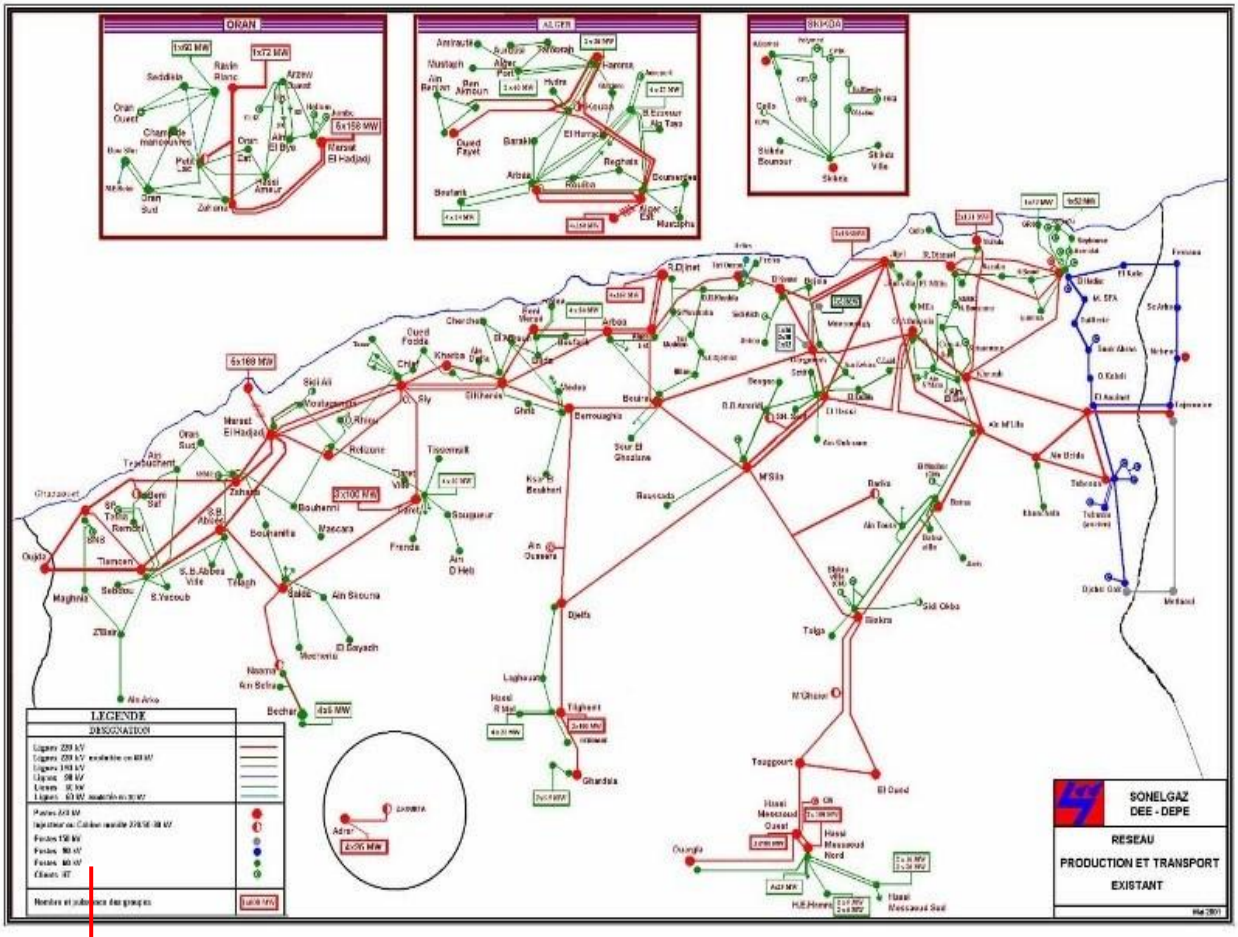

Figure C.1. Algerian 114-bus electrical network topology

The table depicted in Figure C.1 [25] is described in detail below (Table C.1):

TableC.1. Voltage level code on lines and substations

Designation	Voltage level code
Power lines 220 KV	
220 KV power line operated at 60 KV	
Power lines 150KV	
Power lines 90KV	
Power lines 60KV	
60 KV power lines operated at 30KV	
220 KV substations	
220/60-30KV injector or mobile cabin	
150KV substations	
90KV substations	
60KV substations	
Customer HT	
Number of generator outputs	1*600 MW

Table C.2. Electrical system parameters (DZ114-bus)

Algerian Power System DZ114-bus Characteristics	N°	Details
Buses	114	[25,60,74]
Branches	175	[25,60,74]
Generators	15	Buses: **4 (swing)**, 5,11,15,17,19,22,52,80,83,98,100,101, 109 and 111
Shunt VAR compensation	12	Buses: 41,43, 50,66,67,68,69,70, 77,89,92,and 93
Transformer with tap changer	16	Branches: 160,161, 162,163,164,165,166,167,168, 169, 170,171,172,173, 174 and 175
Control variables	58	-
Load bus voltage limits	99	[0.90–1.05]p.u
Generator voltage limits	-	[0.90–1.1]p.u
Setting of the tap changer in the transformer	-	[0.90–1.1]p.u
VAR compensation limits	-	[3–20] MVAR
Active demand	-	3727 MW
Reactive demand	-	2070 MVAR
S. Base	-	100 MVA

Table C.3. Bus data (Algerian Electric PowerDZ114-bus)

Bus N°	Bus Name	Bus Type	Voltage Mag. V(p.u)	Angle Deg. θ(°)	Load		Generator		Injected		
					PLi MW	QLi MVar	PGi MW	QGi MVar	Qmin MVar	Qmax MVar	Qc MVar
1	OUJDA	3	1	0	0	0	0	0	0	0	0
2	GHAZAOUET	3	1	0	36	17	0	0	0	0	0
3	ZAHANA	3	1	0	64	31	0	0	0	0	0
4	MERSATEL HADJADJ1	1	1,0773	0	125	94	685,7288	6,93	-20	400	0
5	MERSAT EL HADJADJ2	2	1,05	0	335	250	300	6,93	-20	200	0
6	TLEMCEN	3	1	0	78	37	0	0	0	0	0
7	SIDIBELABES	3	1	0	55	26	0	0	0	0	0
8	RELIZANE	3	1	0	50	24	0	0	0	0	0
9	BENISAF	3	1	0	40	19	0	0	0	0	0
10	SAIDA	3	1	0	42	21	0	0	0	0	0
11	TIARET	2	1	0	96	47	160	19	-50	100	0
12	BECHAR	3	1	0	31	15	0	0	0	0	0
13	AIN-SEFRA	3	1	0	13	6	0	0	0	0	0
14	PETITLAC1	3	1	0	136	65	0	0	0	0	0
15	RAVINBLANC	2	1,03	0	0	0	60	7,7	0	100	0
16	PETITLAC2	3	1	0	0	0	0	0	0	0	0
17	ALGEREST1	2	1,0282	0	0	0	640	6,93	0	400	0
18	ALGEREST2	3	1	0	0	0	0	0	0	0	0
19	ALGERPORT	2	0,95	0	11	5	100	7,7	0	60	0
20	LARBAA1	3	1	0	14	9	0	0	0	0	0
21	LARBAA2	3	1	0	70	52	0	0	0	0	0
22	BABEZZOUAR	2	0,96	0	42	25	60	15,12	0	50	0
23	BENAKNOUN	3	1	0	23	11	0	0	0	0	0
24	ELHARRACH	3	1	0	60	36	0	0	0	0	0
25	GLACIERE	3	1	0	17	8	0	0	0	0	0
26	ELHAMMA1	3	1	0	55	26	0	0	0	0	0
27	ELHAMMA2	3	1	0	0	0	0	0	0	0	0
28	ELHAMMA3	3	1	0	0	0	0	0	0	0	0
29	ELKOUBA	3	1	0	37	18	0	0	0	0	0
30	OULED FAYET1	3	1	0	30	15	0	0	0	0	0
31	OULED FAYET2	3	1	0	0	0	0	0	0	0	0
32	ROUIBA1	3	1	0	40	24	0	0	0	0	0
33	ROUIBA2	3	1	0	29	14	0	0	0	0	0
34	TAFOURA	3	1	0	29	14	0	0	0	0	0
35	BARAKI	3	1	0	33	16	0	0	0	0	0
36	AINBENIANE	3	1	0	17	8	0	0	0	0	0
37	AINTAYA	3	1	0	11	5	0	0	0	0	0
38	AURASSI	3	1	0	20	10	0	0	0	0	0
39	ELGOLF	3	1	0	20	10	0	0	0	0	0
40	CHLEF	3	1	0	21	10	0	0	0	0	0
41	OUEDSLY 1	3	1	0	53	32	0	0	0	0	0
42	OUEDSLY 2	3	1	0	0	0	0	0	0	0	0
43	ELKHEMIS1	3	1	0	31	18	0	0	0	0	0
44	ELKHEMIS2	3	1	0	0	0	0	0	0	0	0
45	AINDEFLA1	3	1	0	12	6	0	0	0	0	0
46	AINDEFLA2	3	1	0	0	0	0	0	0	0	0
47	KHERBA1	3	1	0	21	10	0	0	0	0	0
48	KHERBA2	3	1	0	0	0	0	0	0	0	0
49	TENES	3	1	0	13	6	0	0	0	0	0
50	OUEDELFODA	3	1	0	4	2	0	0	0	0	0

51	GHRIB	3	1	0	1	1	0	0	0	0	0
52	BOUFARIK	2	0,96	0	56	27	80	16,9	0	50	0
53	BLIDA	3	1	0	16	8	0	0	0	0	0
54	ELAFFROUN	3	1	0	21	10	0	0	0	0	0
55	CHERCHEL	3	1	0	18	9	0	0	0	0	0
56	MEDEA	3	1	0	33	20	0	0	0	0	0
57	BERROUAGHIA1	3	1	0	35	21	0	0	0	0	0
58	BERROUAGHIA2	3	1	0	0	0	0	0	0	0	0
59	BENIMERAD1	3	1	0	36	17	0	0	0	0	0
60	BENIMERAD2	3	1	0	0	0	0	0	0	0	0
61	ELKOLEA	3	1	0	27	13	0	0	0	0	0
62	BOUMERDES	3	1	0	22	11	0	0	0	0	0
63	TIZIOUZOU1	3	1	0	49	29	0	0	0	0	0
64	TIZIOUZOU2	3	1	0	0	0	0	0	0	0	0
65	FREHA	3	1	0	11	5	0	0	0	0	0
66	DRÄABEN KHEDDA	3	1	0	35	21	0	0	0	0	0
67	TIZIMEDDEN	3	1	0	10	5	0	0	0	0	0
68	S.E.DJEMÄA	3	1	0	11	5	0	0	0	0	0
69	SOR ELGHOZLANE	3	1	0	20	10	0	0	0	0	0
70	ILLITEN	3	1	0	7	3	0	0	0	0	0
71	BOUIRA1	3	1	0	36	22	0	0	0	0	0
72	BOUIRA2	3	1	0	0	0	0	0	0	0	0
73	SI MUSTAPHA	3	1	0	36	22	0	0	0	0	0
74	AINOUSSARA1	3	1	0	0	0	0	0	0	0	0
75	AINOUSSARA2	3	1	0	0	0	0	0	0	0	0
76	AINOUSSARA3	3	1	0	12	6	0	0	0	0	0
77	BOUFARIK	3	1	0	7	3	0	0	0	0	0
78	MUSTAPHA BACHA	3	1	0	13	7	0	0	0	0	0
79	ELAMIRALIA	3	1	0	14	7	0	0	0	0	0
80	ELHADJAR1	2	0,97	0	157	107	100	100	0	60	0
81	ELAOUINET1	3	1	0	0	0	0	0	0	0	0
82	ELKHROUB	3	1	0	75	36	0	0	0	0	0
83	SKIKDA	2	1	0	70	51	230	8,4	-50	200	0
84	R. DJAMEL	3	1	0	46	34	0	0	0	0	0
85	AINBEIDA	3	1	0	45	22	0	0	0	0	0
86	TEBESSA1	3	1	0	0	0	0	0	0	0	0
87	AINMLILA	3	1	0	32	15	0	0	0	0	0
88	ELHADJAR2	3	1	0	46	22	0	0	0	0	0
89	SOUKAHRAS	3	1	0	34	17	0	0	0	20	0
90	ELAOUINET2	3	1	0	18	9	0	0	0	0	0
91	TEBESSA2	3	1	0	44	21	0	0	0	0	0
92	DJEBELONK	3	1	0	10	5	0	0	0	0	0
93	TEBESSA3	3	1	0	0	0	0	0	0	0	0
94	OUED ATHMANIA	3	1	0	48	23	0	0	0	0	0
95	AKBOU1	3	1	0	35	17	0	0	0	0	0
96	AKBOU2	3	1	0	0	0	0	0	0	0	0
97	ELKSEUR	3	1	0	42	20	0	0	0	0	0
98	DARGUINA	2	1,04	0	13	6	100	14	0	50	0
99	ELHASSI	3	1	0	105	50	0	0	0	0	0
100	JIJEL	2	1,0573	0	33	16	550	9,98	0	270	0
101	M'SILA	2	1,0818	0	50	24	360	18,3	-50	200	0
102	BORDJBOU-ARRERIDJ	3	1	0	34	16	0	0	0	0	0
103	BISKRA	3	1	0	66	32	0	0	0	0	0
104	BARIKA1	3	1	0	18	9	0	0	0	0	0
105	BARIKA2	3	1	0	0	0	0	0	0	0	0

106	BATNA	3	1	0	64	31	0	0	0	0	0
107	DJELFA	3	1	0	65	37	0	0	0	0	0
108	GHARDAIA	3	1	0	22	11	0	0	0	0	0
109	TILGHEMT	2	1,0818	0	37	18	180	16,35	-50	100	0
110	M'GHAIER	3	1	0	13	6	0	0	0	0	0
111	H.MESSAOUD NORD	2	1,0909	0	94	56	200	16,35	-50	155	0
112	TOUGGOURT	3	1	0	24	12	0	0	0	0	0
113	OUARGLA	3	1	0	23	11	0	0	0	0	0
114	ELOUED	3	1	0	24	12	0	0	0	0	0

Table C.4. Line data (Algerian Electric PowerDZ114-bus)

Line	From bus i To bus j (i-j)	Resistance R(p.u)	Reactance X(p.u)	Susceptance ½ B (p.u)	= 1 for lines > 1 or < 1 for Tap.(a) at bus	Smax (KVA)	Un (KV)
1	2-1	0.0085	0.0403	0.0303	1	250	220
2	6-1	0.0122	0.0578	0.0436	1	250	220
3	2-6	0.0140	0.0498	0.0355	1	200	220
4	4-42	0.0274	0.1295	0.0976	1	250	220
5	4-42	0.0139	0.0121	0.1474	1	450	220
6	4-3	0.0033	0.0158	0.0482	1	500	220
7	5-3	0.0028	0.0189	0.0294	1	450	220
8	5-4	0.0018	0.0126	0.0197	1	450	220
9	4-7	0.0144	0.0678	0.0512	1	250	220
110	15-16	0.0038	0.0135	0.0097	1	200	220
11	16-4	0.0041	0.0144	0.0103	1	200	220
12	16-14	0.0013	0.0045	0.0032	1	200	220
13	8-42	0.0171	0.0629	0.0454	1	200	220
14	8-1	0.0184	0.0870	0.0657	1	250	220
15	10-7	0.0150	0.0709	0.0535	1	250	220
16	10-11	0.0228	0.1076	0.0811	1	250	220
17	7-6	0.0157	0.0740	0.0558	1	250	220
18	11-42	0.0170	0.0806	0.0608	1	250	220
19	6-4	0.0288	0.1012	0.0730	1	200	220
20	9-3	0.0042	0.0284	0.0442	1	450	220
21	9-4	0.0088	0.0600	0.0933	1	450	220
22	13-12	0.0501	0.2365	0.1784	1	250	220
23	10-13	0.0464	0.2190	0.1652	1	250	220
24	17-20	0.0065	0.0244	0.0176	1	200	220
25	17-21	0.0073	0.0278	0.0202	1	200	220
26	17-72	0.0197	0.0732	0.0530	1	200	220
27	17-27	0.0046	0.0237	0.1003	1	300	220
28	17-31	0.0061	0.0311	0.0617	1	350	220
29	31-28	0.0017	0.0088	0.0746	1	300	220
30	17-64	0.0198	0.0727	0.0525	1	200	220
31	21-44	0.0240	0.0861	0.0615	1	200	220
32	60-31	0.0037	0.0253	0.0393	1	450	220
33	21-60	0.0056	0.0263	0.0198	1	250	220
34	60-44	0.0122	0.0578	0.0436	1	250	220
35	58-44	0.0121	0.0569	0.0429	1	250	220
36	72-101	0.0213	0.1007	0.0760	1	250	220
37	72-58	0.0183	0.0863	0.0651	1	250	220

38	58-75	0.0148	0.0701	0.0528	1	250	220
39	75-107	0.0185	0.0876	0.0660	1	250	220
40	75-74	0.0006	0.0026	0.0026	1	250	220
41	44-42	0.0248	0.0903	0.0649	1	200	220
42	44-42	0.0183	0.0864	0.0651	1	250	220
43	42-48	0.0074	0.0506	0.0786	1	450	220
44	48-44	0.0025	0.0158	0.0245	1	450	220
45	107-101	0.0334	0.1577	0.1189	1	250	220
46	64-97	0.0178	0.0654	0.0470	1	200	220
47	72-96	0.0152	0.0540	0.0386	1	200	220
48	96-98	0.0203	0.0720	0.0515	1	200	220
49	96-95	0.0015	0.0070	0.0053	1	200	220
50	18-22	0.0290	0.1397	0.0017	1	80	60
51	18-37	0.0256	0.1233	0.0015	1	80	60
52	37-22	0.0171	0.0822	0.0010	1	80	60
53	19-26	0.0058	0.0077	0.0017	1	60	60
54	19-26	0.0058	0.0077	0.0017	1	60	60
55	19-34	0.0019	0.0126	0.0001	1	80	60
56	20-18	0.1348	0.2944	0.0013	1	50	60
57	20-24	0.0376	0.1390	0.0006	1	40	60
58	20-24	0.0368	0.1361	0.0006	1	40	60
59	20-29	0.0319	0.1178	0.0005	1	40	60
60	20-35	0.0428	0.1528	0.0006	1	40	60
61	35-29	0.0458	0.1639	0.0007	1	40	60
62	20-32	0.0708	0.2365	0.0010	1	60	60
63	22-32	0.0342	0.1142	0.0005	1	60	60
64	22-24	0.0239	0.0799	0.0003	1	60	60
65	22-24	0.0239	0.0799	0.0003	1	60	60
66	23-30	0.0239	0.0799	0.0003	1	60	60
67	23-36	0.0136	0.0457	0.0002	1	60	60
68	36-30	0.0273	0.0913	0.0004	1	60	60
69	33-18	0.0205	0.0685	0.0003	1	60	60
70	32-33	0.0239	0.0799	0.0003	1	60	60
71	26-25	0.0139	0.0517	0.0002	1	30	60
72	24-25	0.0164	0.0608	0.0003	1	60	60
73	26-34	0.0049	0.0318	0.0002	1	60	60
74	29-26	0.0119	0.0158	0.0034	1	60	60
75	29-39	0.0126	0.0820	0.0004	1	80	60
76	38-34	0.0047	0.0307	0.0002	1	80	60
77	18-73	0.1557	0.3427	0.0015	1	50	60
78	18-73	0.0854	0.3028	0.0012	1	60	60
79	62-18	0.0508	0.1941	0.0008	1	60	60
80	20-52	0.0873	0.2162	0.0011	1	50	60
81	20-52	0.0875	0.2167	0.0011	1	50	60
82	54-59	0.1188	0.3063	0.0015	1	50	60
83	52-59	0.0360	0.1014	0.0005	1	50	60
84	57-51	0.1227	0.4098	0.0018	1	60	60
85	57-77	0.1366	0.4566	0.0020	1	60	60
86	52-53	0.0937	0.1788	0.0007	1	35	60
87	53-54	0.0937	0.1788	0.0007	1	35	60
88	52-30	0.0722	0.1789	0.0009	1	50	60
89	71-70	0.1599	0.3148	0.0013	1	35	60
90	40-41	0.0586	0.1623	0.0008	1	50	60
91	40-50	0.1343	0.3645	0.0016	1	35	60

92	71-69	0.1093	0.3653	0.0016	1	60	60
93	70-68	0.1204	0.2180	0.0009	1	35	60
94	44-45	0.1025	0.3425	0.0015	1	60	60
95	51-43	0.2067	0.3556	0.0015	1	35	60
96	54-55	0.1196	0.3996	0.0018	1	60	60
97	55-43	0.1708	0.5708	0.0025	1	60	60
98	73-62	0.0410	0.1370	0.0006	1	60	60
99	73-67	0.3347	0.7007	0.0031	1	40	60
100	68-67	0.1648	0.3569	0.0015	1	40	60
101	29-26	0.0119	0.0158	0.0034	1	60	60
102	73-66	0.1623	0.5752	0.0023	1	60	60
103	63-66	0.0683	0.2283	0.0010	1	60	60
104	63-65	0.0557	0.1861	0.0008	1	60	60
105	63-65	0.0557	0.1861	0.0008	1	60	60
106	56-54	0.1025	0.3425	0.0015	1	60	60
107	57-56	0.1196	0.3996	0.0018	1	60	60
108	57-56	0.1196	0.3996	0.0018	1	60	60
109	47-50	0.1196	0.3996	0.0018	1	60	60
110	47-46	0.0342	0.1142	0.0005	1	60	60
111	67-66	0.1128	0.2794	0.0014	1	50	60
112	49-41	0.1265	0.4225	0.0019	1	50	60
113	19-78	0.0042	0.0055	0.0012	1	60	60
114	19-79	0.0105	0.0139	0.0030	1	60	60
115	59-61	0.0513	0.1816	0.0007	1	60	60
116	45-46	0.0171	0.0605	0.0002	1	60	60
117	85-87	0.0158	0.0745	0.0562	1	250	220
118	85-86	0.0139	0.0657	0.0495	1	250	220
119	85-81	0.0099	0.0467	0.0352	1	250	220
120	87-106	0.0105	0.0495	0.0373	1	250	220
121	87-82	0.0056	0.0266	0.0200	1	250	220
122	87-99	0.0322	0.1249	0.0909	1	200	220
123	103-105	0.0130	0.0613	0.0462	1	250	220
124	105-101	0.0171	0.0806	0.0608	1	250	220
125	105-104	0.0015	0.0070	0.0053	1	250	220
126	103-106	0.0208	0.0983	0.0741	1	250	220
127	81-82	0.0303	0.1075	0.0768	1	200	220
128	80-82	0.0319	0.1129	0.0807	1	200	220
129	80-84	0.0191	0.0676	0.0483	1	200	220
130	84-83	0.0051	0.0180	0.0129	1	200	220
131	82-83	0.0191	0.0676	0.0483	1	200	220
132	100-98	0.0102	0.0598	0.0754	1	250	220
133	100-97	0.0111	0.0759	0.1179	1	450	220
134	98-97	0.0121	0.0448	0.0325	1	200	220
135	99-100	0.0231	0.1089	0.0821	1	250	220
136	87-100	0.0102	0.0694	0.0105	1	450	220
137	100-84	0.0065	0.0442	0.0687	1	450	220
138	84-80	0.0074	0.0506	0.0786	1	450	220
139	86-81	0.0055	0.0379	0.0589	1	450	220
140	98-99	0.0163	0.0580	0.0414	1	200	220
141	101-102	0.0116	0.0547	0.0413	1	250	220
142	99-102	0.0116	0.0547	0.0413	1	250	220
143	99-101	0.0111	0.0759	0.1179	1	450	220
144	98-94	0.0357	0.1275	0.0918	1	200	220
145	94-82	0.0056	0.0263	0.0198	1	250	220

146	92-93	0.1624	0.4088	0.0099	1	60	90
147	93-91	0.0304	0.1074	0.0021	1	60	90
148	93-91	0.0379	0.1342	0.0027	1	60	90
149	90-89	0.0776	0.2400	0.0052	1	60	90
150	90-89	0.1354	0.4100	0.0089	1	60	90
151	90-93	0.1852	0.3189	0.0068	1	60	90
152	103-110	0.0185	0.0876	0.0660	1	250	220
153	110-112	0.0185	0.0876	0.0660	1	250	220
154	103-114	0.0419	0.1979	0.1493	1	250	220
155	109-108	0.0148	0.0701	0.0528	1	250	220
156	109-107	0.0388	0.1833	0.1382	1	250	220
157	112-114	0.0190	0.0896	0.0675	1	250	220
158	112-111	0.0297	0.1402	0.1057	1	250	220
159	113-111	0.0167	0.0787	0.0608	1	250	220
160	80-88	0.0123	0.3140	0.0	1,03	400	220
161	81-90	0.0062	0.1452	0.0	1,03	240	220
162	86-93	0.0012	0.0742	0.0	1,03	240	220
163	42-41	0.0012	0.0742	0.0	1,03	240	220
164	58-57	0.0012	0.0742	0.0	1,03	240	220
165	44-43	0.0029	0.1053	0.0	1,03	120	220
166	60-59	0.0014	0.0516	0.0	1,03	360	220
167	64-63	0.0019	0.0700	0.0	1,03	180	220
168	72-71	0.0012	0.0742	0.0	1,03	240	220
169	18-17	0.0014	0.0516	0.0	1,03	360	220
170	21-20	0.0016	0.0525	0.0	1,03	240	220
171	27-26	0.0024	0.1484	0.0	1,03	120	220
172	28-26	0.0024	0.1484	0.0	1,03	120	220
173	31-30	0.0007	0.0495	0.0	1,03	360	220
174	48-47	0.0012	0.0742	0.0	1,03	240	220
175	74-76	0,0089	0.3340	0.0	1,03	40	220

Table C.5. Thermal power generation limits and cost coefficients (DZ114-bus)

Generators	a ($/hr)	b ($/MW.hr)	c ($/MW².hr)	P_{Gmin} (MW)	P_{Gmax} (MW)	Q_{Gmin} (MVAR)	Q_{Gmax} (MVAR)
G4	0	1.5000	0.0085	135	1350	-20	400
G5	0	1.5000	0.0085	135	1350	-20	200
G11	0	2.5000	0.0170	10	100	-50	100
G15	0	2.5000	0.0170	30	300	0	100
G17	0	1.5000	0.0085	135	1350	0	400
G19	0	2.5000	0.0170	34.5	345	0	60
G22	0	2.5000	0.0170	34.5	345	0	50
G52	0	2.5000	0.0170	34.5	345	0	50
G80	0	2.5000	0.0170	34.5	345	0	60
G83	0	2.0000	0.0170	30	300	-50	200
G98	0	2.0000	0.0170	30	300	0	50
G100	0	1.5000	0.0030	60	600	0	270
G101	0	1.5000	0.0030	20	200	-50	200
G109	0	2.5000	0.0170	10	100	-50	100
G111	0	2.5000	0.0170	10	200	-50	155

Appendixe D: Integration wind farm into electrical network

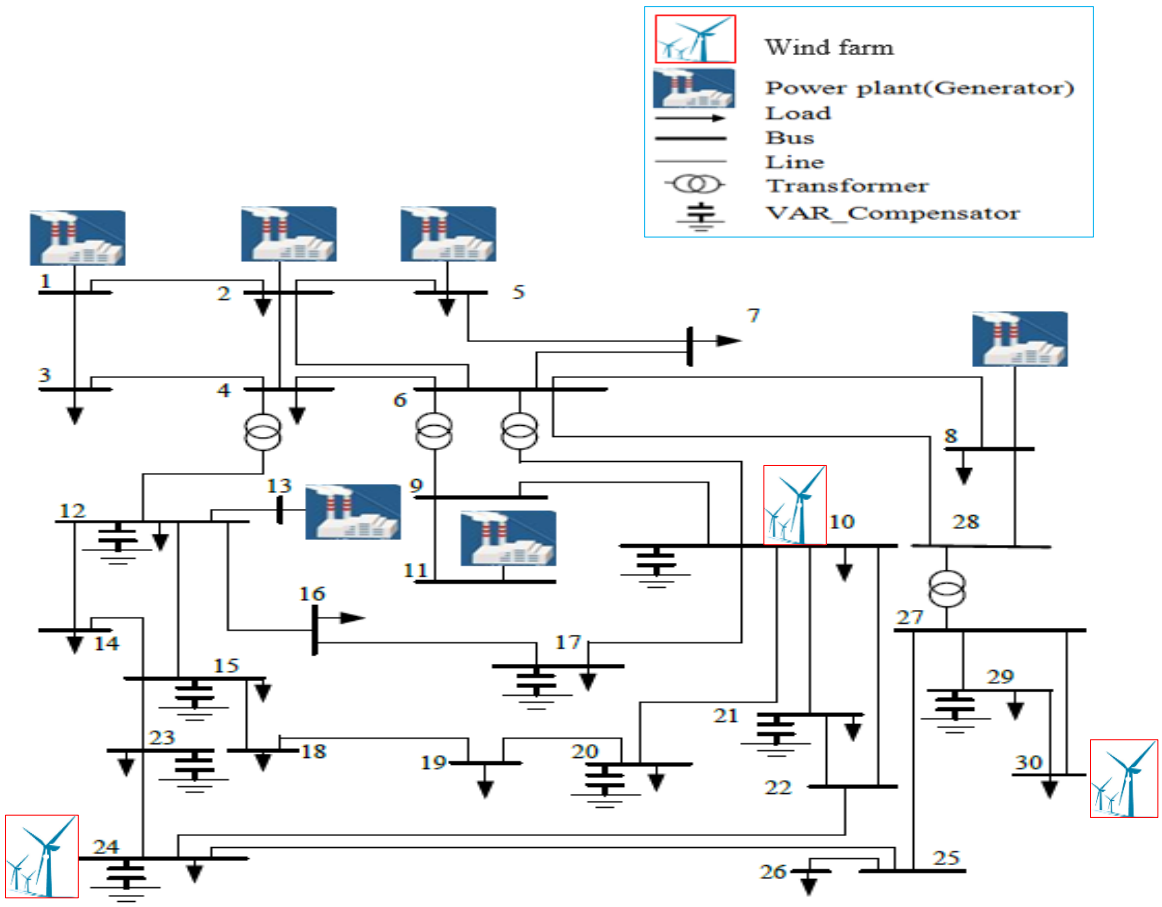

Figure D.1. Diagram of the modified IEEE 30-bus test system (with integration wind farm)

Table D.1. Wind farm characteristics (integrated into IEEE 30 bus system)

Wind Farms sites	Bus	Weibull parameters		Wind cost factors			Turbines number	Gamesa G-114[1]			
		ki	ci (m/s)	$d_{w,i}$ ($/ KWh)	$k_{pw,i}$ ($/ MWh)	$k_{rw,i}$ ($/ MWh)		P_{WR} (MW)	**Vin** (m/s)	**Vr** (m/s)	**Vout** (m/s)
1	10	2	5.6	1.12	1	1	20	2	2.5	10	25
2	24	2	5.6	1.12	1	1	20	2			
3	30	2	5.6	1.12	1	1	20	2			

Table D.2. Characteristics of modified IEEE 30 bus system

Characteristics IEEE 30-bus system	N°	Details
Buses	30	[5,81]
Branches	41	[5,81]
Generators	6	Buses: **1 (swing)**, 2, 5, 8, 11 and 13
Wind farms	3	Buses: 10, 24 and 30
Shunt VAR compensators	9	Buses: 10, 12, 15, 17, 20, 21, 23, 24. and 29
Transformer with tap changer	4	Branches: 11, 12, 15 and 36
Control variables	31	-
Load bus voltage limits	24	[0.95 – 1.05] p.u
Generator voltage limits	-	[0.95–1.1] p.u
Setting of the tap changer in the transformer	-	[0.9 –1.1] p.u
VAR compensation limits	-	[0–5] MVAR
Active demand	-	2834 MW
Reactive demand	-	1262 MVAR
S. Base	-	100 MVA

Table D.3: Power generation limits and cost coefficients (modified IEEE 30 bus)

Generators	a ($/hr)	b ($/MW.hr)	c ($/MW².hr)	P_{Gmin} (MW)	P_{Gmax} (MW)	Q_{Gmin} (MVar)	Q_{Gmax} (MVar)
G_1	0	2	0.00375	50	200	-20	200
G_2	0	1.75	0.0175	20	80	-20	100
G_5	0	1	0.025	15	50	-15	80
G_8	0	3.25	0.00834	10	35	-15	60
G_{W10}	0	0	0	0	40	-10	10
G_{11}	0	3	0.025	10	30	-10	50
G_{13}	0	3	0.025	12	40	-15	60
G_{W24}	0	0	0	0	40	-10	10
G_{W30}	0	0	0	0	40	-10	10

Table D.4. Wind farm characteristics of the Algerian Electric Power DZ114-bus

Wind farms sites	Bus	Weibull parameters		Wind cost factors			Turbines number	Gamesa G-114[1]			
		ki	ci (m/s)	$d_{w,i}$ ($/ KWh)	$K_{Pw,i}$ ($/ MWh)	$K_{rw,i}$ ($/ MWh)		P_{WT} (MW)	v_{in} (m/s)	v_r (m/s)	v_{out} (m/s)
Setif	99	2.1760	7.7857	0.0217	1.5	3	25	2	2.5	10	25
Djelfa	107	2.3161	8.5753	0.0191	1.5	3	25	2			

Table D.5. Characteristics of modified Algerian Electric PowerDZ114-bus

Algerian Power System DZ114-bus Characteristics	N°	Details
Buses	114	[25,60]
Branches	175	[25,60]
Generators	15	Buses: **4 (swing)**, 5,11,15,17,19,22,52,80,83,98,100,101, 109 and 111
Wind farms	02	Buses:99 and 107 [1]
Shunt VAR compensators	12	Buses:41,43, 50,66,67,68,69,70, 77,89,92,and 93
Transformer with tap changer	16	Branches:160,161, 162,163,164,165,166,167,168, 169, 170,171,172,173, 174 and 175
Control variables	62	-
Load bus voltage limits	99	[0.90–1.05]p.u
Generator voltage limits	-	[0.90–1.1]p.u
Setting of the tap changer in the transformer	-	[0.90–1.1]p.u
VAR compensation limits	-	[3–20] MVAR
Active demand	-	3727 MW
Reactive demand	-	2070 MVAR
S. Base	-	100 MVA

Table D.6. Power generation limits and cost coefficients of modified Algerian (DZ114-bus)

Generators	a ($/hr)	b ($/MW.hr)	c ($/MW².hr)	P_{Gmin} (MW)	P_{Gmax} (MW)	Q_{Gmin} (MVAR)	Q_{Gmax} (MVAR)
G4	0	1.5000	0.0085	135	1350	-20	400
G5	0	1.5000	0.0085	135	1350	-20	200
G11	0	2.5000	0.0170	10	100	-50	100
G15	0	2.5000	0.0170	30	300	0	100
G17	0	1.5000	0.0085	135	1350	0	400
G19	0	2.5000	0.0170	34.5	345	0	60
G22	0	2.5000	0.0170	34.5	345	0	50
G52	0	2.5000	0.0170	34.5	345	0	50
G80	0	2.5000	0.0170	34.5	345	0	60
G83	0	2.0000	0.0170	30	300	-50	200
G98	0	2.0000	0.0170	30	300	0	50
GW99	0	0	0	0	50	-30	30
G100	0	1.5000	0.0030	60	600	0	270
G101	0	1.5000	0.0030	20	200	-50	200
GW107	0	0	0	0	50	-30	30
G109	0	2.5000	0.0170	10	100	-50	100
G111	0	2.5000	0.0170	10	200	-50	155

BIBLIOGRAPHY

BIBLIOGRAPHY

[1] F.Z. Aroua, A. Salhi, O. Charrouf, D. Naimi, K. Fettah, Wind energy cost evaluation based on a techno-economic assessment in the Algerian highlands, Energy Sustain. Dev. 81 (2024) 101502. https://doi.org/10.1016/j.esd.2024.101502.

[2] Labiba Adjoudj, Contribution à l'étude de l'OPF du réseau Algérien basée sur les énergies renouvelables et les FACTS ,These de doctorat,Université Djillali Liabes de Sidi Bel Abbes, 2018.

[3] Hanna Merah, Contribution to the Optimization of Electrical Network Energy using Metaheuristic Methods in the Presence of FACTS Systems and Renewable Energies,doctoral thesis, University of Echahid Hamma Lakhdar el Oued Faculty, 2024.

[4] A. Salhi, D. Naimi, T. Bouktir, Fuzzy multi-objective optimal power flow using genetic algorithms applied to Algerian electrical network, Adv. Electr. Electron. Eng. 11 (2013) 443–454. https://doi.org/10.15598/aeee.v11i6.832.

[5] A. Salhi, D. Naimi, T. Bouktir, Optimal power flow resolution using artificial bee colony algorithm based grenade explosion method, J. Electr. Syst. 12-4. (2016) 734–756.https://creativecommons.org/licenses/by-nc/4.0/(the "License").

[6] K. Chakraborty, A. Chakrabarti, Soft Computing Techniques in Voltage Security Analysis, 2015. http://link.springer.com/10.1007/978-81-322-2307-8.

[7] John J. Grainger, William D. Stevenson,Power System Analysis, 1994th ed., n.d.Downloaded From: www.EasyEngineering.net.

[8] Mohammed Albadi, - Power Flow Analysis, in Mod. Power Syst. Anal., CRC Press, 2016: pp. 490–551. https://doi.org/10.1201/b14796-12.

[9] P. Presutto, Schaum - Outline - Electrical Power Systems. pdf, in: n.d.https://www.academia.edu/36597581/Schaum_Outline_Electrical_Power_Systems_pdf

[10] Gacem Abdelmalek., Commande Robuste d'un Dispositif FACTS par les Méthodes Métaheuristiques pour la Stabilité de Tension d'un Réseau Electrique,These de doctorat, Université Mohamed Khider Biskra, 2019.

[11] Yahiaoui. Merzoug, Contrôle optimal des puissances réactives et des tensions dans un réseau d'énergie électrique par dispositifs FACTS,These de doctorat, Université des sciences et de la Technologie Mohamed Boudiaf Oran,2014.studylibfr.com › doc › 1941715

[12] Alkhatib Hasan, Etude de la Stabilité aux Petites Perturbations dans les Grands Reseaux Electriques:Optimisation de la Regulation par une Methode Metaheuristique,These de doctorat,Université Paul Cézanne - Aix-Marseille III, 2008.

[13] Hadji Boubakeur, Contribution à l'Amélioration de l'Efficacité des Réseaux

Electriques par l'Intégration et le Contrôle Flexible de l'Energie Eolienne et des Systèmes FACTS,These de doctorat, Université Mohamed Khider Biskra, 2017.

[14] O.U. C, Power Flow Analysis of Nigerian Power Requirement for the Award of Ph . D Degree in the, (2013) 1–167.

[15] H. Saadat, Power System Analysis, 1999. http://www.mhhe.com.

[16] E. Csanyi, The Structure of Electric Power Systems(Generation,Distribution and Transmission of Energy), (n.d.). https://electrical-engineering-portal.com/electric-power-systems.

[17] A. Hubert, power plant : operating principle, history and evolution, (2023). https://www.choisir.com/energie/articles/117578/ce-quil-faut-savoir-sur-les-centrales-electriques.

[18] J.R.B. Machowski, JanZbigniew Lubosny,Janusz W. Bialek, Power System Dynamics Stability and ControlThird Edition, 2020.

[19] Sebaa Haddi, Contribution à l ' optimisation de l ' insertion des énergies renouvelables dans un réseau électrique intelligent (Smart Grid),These de doctorat, Université Ferhat Abbas Setif,2019

[20] Réseau électrique - Définition, Source Wikipédia Sous Licence CC-BY-SA 3.0. (n.d.). https://www.techno-science.net/glossaire-definition/Reseau-electrique.html.

[21] IEA, Renewables 2021 Analysis and Forecast to 2026, Int. Energy Agency Publ. Int. (2021) 167. www.iea.org/t&c/%0Ahttps://webstore.iea.org/download/direct/4329.

[22] Z. Abada, M. Bouharkat, Study of management strategy of energy resources in Algeria, Energy Reports. 4 (2018) 1–7. https://doi.org/10.1016/j.egyr.2017.09.004.

[23] M. Bouznit, M. del P. Pablo-Romero, A. Sánchez-Braza, Measures to promote renewable energy for electricity generation in Algeria, Sustain. 12 (2020) 1–17. https://doi.org/10.3390/su12041468.

[24] Y. Zahraoui, Current Status, Scenario, and Prospective of Renewable Energy in Algeria: A Review, 14 (2021). https://doi.org/10.3390/en14092354.

[25] Messaoud Zoubeidi, Amélioration de la sécurité des systèmes électriques à travers l'approche de sensibilité pour l'emplacement optimal des dispositifs FACTS,These de doctorat,Université Djillali Liabes de Sidi Bel Abbes, 2021.

[26] H. Tebani, Production de l ' Energie Electrique, 2020.

[27] M.L.H. and R. Bouaroudj, Electrical Energy Transmission by High-voltage Direct Current (HVDC) and Prospects for an Electrical Market, Beryl Park. (2014). www.sonelgaz.dz Electrical Energy Transmission by HVDC Networks and Prospects for an Electrical Market.

[28] A. Chabani, S. Makhloufi, S. Lachtar, Overview and impact of the renewable energy plants connected to the electrical network in southwest Algeria, EAI Endorsed Trans. Energy Web. 8 (2021) 1–15. https://doi.org/10.4108/eai.29-3-2021.169168.

[29] Sonelgaz - Production de l'Electricité, (2022). https://www.spe.dz/page/17.

[30] Sonelgaz, Liste des centrales électriques en Algérie — Wikipédia, (n.d.). https://fr.wikipedia.org/wiki/Liste_des_centrales_électriques_en_Algérie.

[31] Djedidi Imen, Optimisation Des Performances Du Réseau Électrique de Distribution Par Des Méthodes Évolutionnaires,These de doctorat, Université Mohamed Khider Biskra, 2023.

[32] R. Del Ciello, C. Camporeale, Efficiency and Renewable, 2020. https://doi.org/at: https://www.researchgate.net/publication/341900356 Country.

[33] Ministère de l'Energie et des Mines, Energies Nouvelles, Renouvelables et Maitrise de l'Energie; Algerian Ministry of Energy: Algiers, Algeria, (n.d.). https://www.energy.gov.dz/?rubrique=energies-nouvellesrenouvelables-et-maitrise-de-lrenergie.

[34] H. Saadat, Power Analysis System Third Edition,2010.

[35] Dr Ouahiba Guerri, L'Énergie éolienne en Algérie : Un bref aperçu, 2011.

[36] Wind Turbine Parts and Functions, (n.d.). https://stock.adobe.com/ca/images/wind-turbine-work-principle-with-mechanical-inner-structure-outline-diagram-labeled-educational-technical-explanation-for-electricity-generator-from-air-vector-illustration-green-energy-power-scheme/469320874.

[37] Aysar Yasin, Distributed Generation Systems based on Hybrid Wind/Photovoltaic/Fuel Cell Structures, Università degli Studi di Catania, n.d.

[38] M.S. Syed, S. V. Chintalapudi, S. Sirigir, Optimal Power Flow Solution in the Presence of Renewable Energy Sources, Iran. J. Sci. Technol. Trans. Electr. Eng. 0123456789 (2020). https://doi.org/10.1007/s40998-020-00339-z.

[39] Mouassa Souhil, Optimal power flow solution with non-conventional methods in smart grids,doctoral thesis, University Ferhat Abbas Setif,2019.

[40] D. Naimi,A. Salhi,Optimisation Multiobjectif Appliqeé a un Reseau Algerien de Transport d'Electricité Contenantune Source Eolienne, (n.d.) 67–72.

[41] Bikash Paland, Xiao-Ping Zhang, Christian Rehtanz, Flexible AC Transmission Systems: Modelling and Control, Springer, New York, 2012. https://doi.org/10.1007/978-3-642-28241-6.

[42] R. Kouadri, L. Slimani, T. Bouktir, Slime Mould Algorithm for Practical Optimal Power Flow Solutions Incorporating Stochastic Wind Power and Static Var Compensator Device, Electr. Eng. Electromechanics. (2020) 45–54. https://doi.org/10.20998/2074-272X.2020.6.07.

[43] S.S. Rao, Engineering optimization: Theory and practice, 2019. https://doi.org/10.1002/9781119454816.

[44] S.A.-H.S.A.-A.H. Mantawy, Modern, Modern Optimization Techniques with Applications in Electric Power Systems, Springer is part of Sp(Springer Science+Business Media, LLC, 233 Spring Street, New York, NY 10013, USA, New York, n.d. https://doi.org/DOI 10.1007/978-1-4614-1752-1.

[45] M.E.C. EL-HAWARY, Optimal Economic Operation of Electric Power Systems, 1979.

[46] Berrouk Fateh, Repartition Optimale des Flux Energetiques et Impact sur la Performance d'un Système Electrique HT,These de doctorat,Université 8 Mai 1945 Guelma, 2019.

[47] Salhi Souheil, Contribution to power flow optimization by enhanced artificial intelligence methods,doctoral thesis, University Mohamed Khider Biskra, 2023.

[48] M. Lin, J. Tsai, C. Yu, A Review of Deterministic Optimization Methods in Engineering and Management, 2012 (2012). https://doi.org/10.1155/2012/756023.

[49] M. Cavazzuti, Optimization methods : from theory to design, Springer Heidelberg New York Dordrecht London, 2015. https://doi.org/10.1007/978-3-642-31187-1.

[50] R.A. James A.Momoh, M. E. El-Hawary, Optimal Power Ftow Literature to 1993 Part I: NonLinear and Quadratic Programming Approaches, IEEE Trans. Power Syst. Vol. 14, No. 1,. 14 (1999) 96–104.

[51] R.A. James A.Momoh,M. E. El-Hawary, A Review of Selected Optimal Power Flow Literature to 1993 Part 11: Newton, Linear Programming and Interior Point Methods., IEEE Trans. Power Syst. Vol. 14, No. 1, Febr. 1999 A. 14 (1999) 105–111.

[52] N. Djemai, Optimisation de l'intégration des ressources énergétiques décentralisées (RED) aux réseaux de distribution dans un marché de l'électricité dérégulé,These de doctorat, Université Mohamed Khider – Biskra Faculté, n.d.

[53] Hachimi Hanaâ, Hybridations d'Algorithmes Metaheuristiques en Optimisation Globale et Leurs Applications,Thèse de doctorat, Université Mohammed V - Agdal, Rabat, 2013.

[54] J.S. Arora, Review Paper Global optimisation m e t h o d s for engineering applications : a review, (1995) 137–159.

[55] Betka Abir Estimation de mouvement par les techniques métaheuristiques,These de doctorat, Université Mohamed Khider - Biskra Faculté, 2019.

[56] F.A. Hashim, E.H. Houssein, M.S. Mabrouk, W. Al-Atabany, S. Mirjalili, Henry gas solubility optimization: A novel physics-based algorithm, Futur. Gener. Comput. Syst. 101 (2019) 646–667. https://doi.org/10.1016/j.future.2019.07.015.

[57] Salhi Ahmed, Contribution a l' Optimisationde l'Ecoulement de Puissance en Utilisant la Logique Floue Associee aux Reseaux de Neurones (Neuro-Flou),These de doctorat, Université Mohamed Khider Biskra Faculté, 2015.

[58] A. Alanazi, M. Alanazi, Z.A. Memon, A. Mosavi, Determining Optimal Power Flow Solutions Using New Adaptive Gaussian TLBO Method, Appl. Sci. 12 (2022). https://doi.org/10.3390/app12167959.

[59] A.K. Khamees, A. El-Rafei, N.M. Badra, A.Y. Abdelaziz, Solution of optimal power flow using evolutionary-based algorithms, Int. J. Eng. Sci. Technol. 9 (2017) 55–68. https://doi.org/10.4314/ijest.v9i1.5.

[60] L.S. and T. Bouktir, Application of Differential Evolution Algorithm to Optimal Power

Flow incorporating FACTS : a case study, J. Adv. Sci. Appl. Eng. . Vol. 01, N (2014) 8–15.

[61] G. Chen, X. Yi, Z. Zhang, S. Qiu, Solving optimal power flow using cuckoo search algorithm with feedback control and local search mechanism, IAENG Int. J. Comput. Sci. 46 (2019) 321–331.

[62] M.A. Taher, S. Kamel, F. Jurado, M. Ebeed, An improved moth-flame optimization algorithm for solving optimal power flow problem, Int. Trans. Electr. Energy Syst. 29 (2019) 1–28. https://doi.org/10.1002/etep.2743.

[63] R. Kouadri, I. Musirin, L. Slimani, T. Bouktir, OPF for large scale power system using ant lion optimization: A case study of the algerian electrical network, IAES Int. J. Artif. Intell. 9 (2020) 252–260. https://doi.org/10.11591/ijai.v9.i2.pp252-260.

[64] M.A. Taher, S. Kamel, F. Jurado, M. Ebeed, Modified grasshopper optimization framework for optimal power flow solution, Electr. Eng. 101 (2019) 121–148. https://doi.org/10.1007/s00202-019-00762-4.

[65] R. Kouadri, I. Musirin, L. Slimani, T. Bouktir, M.M. Othman, Optimal power flow control variables using slime mould algorithm for generator fuel cost and loss minimization with voltage profile enhancement solution, Int. J. Emerg. Trends Eng. Res. 8 (2020) 36–44. https://doi.org/10.30534/ijeter/2020/0681.12020.

[66] O. Akdag, A. Ates, C. Yeroglu, Modification of Harris hawks optimization algorithm with random distribution functions for optimum power flow problem, Neural Comput. Appl. 33 (2021) 1959–1985. https://doi.org/10.1007/s00521-020-05073-5.

[67] B. Mahdad, S. Kamel, New strategy based modified Salp swarm algorithm for optimal reactive power planning: A case study of the Algerian electrical system (114 bus), IET Gener. Transm. Distrib. 13 (2019) 4523–4540. https://doi.org/10.1049/iet-gtd.2018.5772.

[68] H. Hardiansyah, A novel bat algorithm for solving optimal power flow problem, Eng. Rev. 41 (2021) 41–53. https://doi.org/10.30765/ER.1465.

[69] R.A. El Sehiemy, F. Selim, B. Bentouati, M.A. Abido, A novel multi-objective hybrid particle swarm and salp optimization algorithm for technical-economical-environmental operation in power systems, Energy. 193 (2020). https://doi.org/10.1016/j.energy.2019.116817.

[70] A.A.A. Mohamed, Y.S. Mohamed, A.A.M. El-Gaafary, A.M. Hemeida, Optimal power flow using moth swarm algorithm, Electr. Power Syst. Res. 142 (2017) 190–206. https://doi.org/10.1016/j.epsr.2016.09.025.

[71] C. Mayouf, A. Salhi, F. Haidara, F.Z. Aroua, R.A. El-sehiemy, D. Naimi, C. Aya, C. Sidi, E. Kane, Solving Optimal Power Flow Using New Efficient Hybrid Jellyfish Search and Moth Flame Optimization Algorithms, (2024) 1–25.

[72] David H. Wolpert, No Free Lunch Theorems for Optimization, GECCO'08 Proc. 10th Annu. Conf. Genet. Evol. Comput. 2008. (2008) 811–818. https://doi.org/10.1145/1389095.1389254.

[73] M.A. Akbari, M. Zare, R. Azizipanah-abarghooee, S. Mirjalili, M. Deriche, The

cheetah optimizer: a nature-inspired metaheuristic algorithm for large-scale optimization problems, Sci. Rep. 12 (2022) 1–20. https://doi.org/10.1038/s41598-022-14338-z.

[74] O. Herbadji, L. Slimani, T. Bouktir, Optimal power flow with four conflicting objective functions using multiobjective ant lion algorithm: A case study of the algerian electrical network, Iran. J. Electr. Electron. Eng. 15 (2019) 94–113. https://doi.org/10.22068/IJEEE.15.1.94.

[75] F.Z. Aroua, A. Salhi, C. Mayouf, D. Naimi, A Novel Nature-Inspired Meta-heuristic Algorithm for Solving the Economic and Environmental Dispatch Problems in Power System, Prz. Elektrotechniczny. (2024) 280–285. https://doi.org/10.15199/48.2024.07.55.

[76] F.Z. Aroua, A. Salhi, S. Salhi, D. Naimi, A New Efficient Meta-heuristic Method for Solving the Optimal Power Flow Problem in Power System, (2023).The 2nd Electrical Engineering International Conference (EEIC'23), December 05-06, 2023. Bejaia

[77] S. Mouassa, A. Althobaiti, S.S.M. Ghoneim, S. Member, Novel Design of Slim Mould Optimizer for the Solution of Optimal Power Flow Problems Incorporating Intermittent Sources : A Case Study of Algerian Electricity Grid, IEEE Access. 10 (2022) 22646–22661. https://doi.org/10.1109/ACCESS.2022.3152557.

[78] L. Slimani, T. Bouktir, Application of Differential Evolution Algorithm to Optimal Power Flow with High Wind Energy Penetration, 53 (2012) 59–68.

[79] S. Haddi, O. Bouketir, T. Bouktir, Improved optimal power flow for a power system incorporating wind power generation by using Grey Wolf Optimizer algorithm, Adv. Electr. Electron. Eng. 16 (2018) 471–488. https://doi.org/10.15598/aeee.v16i4.2883.

[80] A. Salhi, D. Naimi, T. Bouktir, Resolution of Economic Dispatch problem considering wind power penetration planning, Proc. 2014 Int. Renew. Sustain. Energy Conf. IRSEC 2014. (2014) 395–400. https://doi.org/10.1109/IRSEC.2014.7059911.

[81] R. Christie, Power Systems Test Case Archive - UWEE - University of Washington/ 30 Bus Power Flow Test Case, (n.d.). Data in Common Data Format (file ieee30cdf.txt) / https://labs.ece.uw.edu/pstca/pf30/ieee30cdf.txt.

[82] Christie, Power Systems Test Case Archive - UWEE - University of Washington/ 57 Bus Power Flow Test Case, (n.d.). Data in Common Data Format (file ieee57cdf.txt)/ https://labs.ece.uw.edu/pstca/pf57/ieee57cdf.txt%0A•%09%0A.